UCLouvain

École polytechnique de Louvain

Mechanical properties measurements on alumina/aluminum nanolaminates

Nanoindentation, lab on-chip and tensile test on polymer

Author: **Audrey Weverbergh**
Supervisor: **Thomas Pardoen**
Readers: **Thomas Pardoen, Michaël Coulombier, Morgan Rusinowicz, Laurent Delannay**
Academic year 2022-2023
Master [120] in Chemical and Materials Engineering

Summary

Introduction **5**

1 State of the art **7**
1.1 Mechanical testing techniques . . . 7
1.1.1 Freestanding thin films . . . 7
1.1.2 On substrate . . . 8
1.1.3 Lab on-chip . . . 8
1.2 Mechanical properties of nanolaminates Al_2O_3 - Al . . . 9
1.2.1 Alumina . . . 9
1.2.2 Aluminium . . . 9
1.2.3 Multilayer . . . 9
1.2.4 Lab on-chip, push-to-pull tests results and main purpose of the work . . . 10

2 Experimental methods **13**
2.1 Nanoindentation . . . 13
2.1.1 Nanoindentation technique . . . 13
2.1.2 Limitations of the technique . . . 14
2.1.3 Determination of the Young's modulus, the hardness and the strain rate sensitivity . . . 14
2.1.4 Some information about the nanoindentation testing . . . 17
2.1.5 Paul Baral's Method and strain rate sensitivity coefficient . . . 17
2.2 Lab on-chip technique . . . 18
2.2.1 Concept . . . 18
2.2.2 Fabrication of a one elementary tensile test structure . . . 19
2.2.3 Detailed steps of the realised process in the cleanroom WINFAB . . . 19
Spin coating of AZMIR 701 . . . 21
Exposure with UltraViolet radiation (UV) . . . 21
Etching of Si_3N_4 . . . 21
Developer . . . 21
Cutting of the wafer . . . 21
Deposition of a nanolaminate . . . 22
Lift-off to take off the photoresist and the deposition of the nanolaminate over it . . . 22
Thickness of the specimen beams . . . 23

XeF_2 release . . . 23
Thickness of the silicon nitride . . . 23
SEM measurements . . . 23
2.2.4 General information about the structures . . . 24
Specimen beam length . . . 24
Specimen beam width . . . 24
Dogbone . . . 24
2.2.5 Calculations to obtain the true stress-strain curve . . . 24
2.2.6 Behavioural line . . . 25
2.2.7 Calculation of the mismatch of the sample . . . 27
2.2.8 Propagation of the errors . . . 28
Specimen beam mismatch . . . 28
Specimen beam section . . . 28
Displacement . . . 29
2.2.9 Advantages and disadvantages of the lab on-chip technique . . . 29
2.3 Tensile test on polymer . . . 30
2.3.1 Preparation . . . 30
2.3.2 Experimental conditions . . . 30
2.3.3 Stress-strain curve and fracture toughness determination . . . 30

3 Preparation of the samples, experiments and results 33
3.1 Nanoindentation . . . 33
3.1.1 Deposition of a nanolaminate 100 nm Al_2O_3 10 nm Al x5 . . . 33
3.1.2 Thickness . . . 33
3.1.3 Constant strain rate : test 1 and quasi-static mode . . . 34
Observations . . . 34
Results . . . 35
3.1.4 Constant strain rate : test 2 . . . 38
Results . . . 38
3.1.5 Constant strain rate : test 3 . . . 40
Results . . . 40
3.1.6 Paul Baral's Method : test 1 . . . 42
Results . . . 42
3.1.7 Paul Baral's Method : test 2 . . . 43
Results . . . 43
3.1.8 Conclusion about the nanoindentation tests . . . 45
3.2 Lab on-chip . . . 46
3.2.1 Sample 85-10 nm x5 . . . 46
Choice of the thickness and deposition of the nanolaminate . . . 46
Release . . . 46
Observations . . . 47
Results . . . 47
3.2.2 Sample 46-10 nm x5 . . . 50
Choice of the thickness and deposition of the nanolaminate . . . 50
Release . . . 50
Observations . . . 50

Results . . . 51
Solutions . . . 52
3.2.3 Sample 70-12 nm x5 . . . 53
Choice of the thickness and deposition of the nanolaminate . . . 53
Indium deposition . . . 53
Lift-off and thickness measurements . . . 53
FIB cutting of cursors . . . 53
Release . . . 53
Observations . . . 54
Results . . . 55
3.2.4 Sample 70-12 nm x5 - release by FIB cutting of the cursors . . . 56
Cutting with FIB to release other structures . . . 56
Results . . . 57
DIC pictures . . . 59
3.2.5 Conclusion about the lab on-chip tests . . . 60
3.3 Tensile test on polymer . . . 62
3.3.1 Choice of the thickness and deposition of the nanolaminate . . . 62
3.3.2 Observations . . . 62
3.3.3 Results . . . 64
Stress-strain curve . . . 65
Fracture toughness . . . 65

4 Discussion **67**
4.1 Mechanical properties . . . 67
4.1.1 Young's modulus . . . 68
4.1.2 Hardness . . . 69
4.1.3 Maximum strain . . . 69
4.1.4 Plasticity . . . 70
4.1.5 Fracture . . . 70
4.1.6 Fracture toughness . . . 70
4.2 Relaxation and strain rate sensitivity coefficient . . . 71
4.3 Future research and improvements . . . 72

Conclusion **72**

Appendices **77**
A Correction of the contact depth . . . 77
B SEM : steps to follow to use the machine . . . 79
C Standard cleaning and drying . . . 79
D Aja Machine : Steps to follow to use the machine . . . 80
E XeF2 etching to release the structures . . . 84
Introduction of the sample into the machine . . . 84
Release . . . 84
Remove the sample from the machine . . . 85
F Lab on-chip : Nanolaminates deposited by Sahar Jaddi . . . 86
F.1 Lab on-chip : Sample 50-20 nm x3 . . . 86

Thickness of the nanolaminate and release 86
Observations and results 86
F.2 Lab on-chip : Sample 50-20 nm x5 87
Thickness of the nanolaminate and release 87
Observations 87
Results 87
G Errors contribution 90

List of Figures

1.1 Stress versus strain curve from a PTP test on a nanolaminate alumina-aluminium 120-10 nm *Private communication - Thomas Pardoen* . . . 11
1.2 Stress versus strain curve on aluminum (LOC tensile test) *Private communication - Thomas Pardoen* . . . 11
1.3 Stress versus strain curve on alumina (LOC and PTP tensile tests) *Private communication - Thomas Pardoen* . . . 11

2.1 Load-displacement curve during nanoindentation . . . 14
2.2 Berkovich tip scheme . . . 14
2.3 (a) Scheme of a pile-up effect (b) Sheme of a sink-in effect . . . 14
2.4 Load versus penetration depth curve . . . 15
2.5 Dimensions of a nanoindentation test . . . 16
2.6 One elementary tensile test structure : (a) before release, (b) after release . . . 18
2.7 Scheme of the force equilibrium between the actuator (spring representation) and the specimen beam: (a) before release, (b) after release . . . 19
2.8 Fabrication of one elementary tensile test structure . . . 19
2.9 Process lab on-chip . . . 20
2.10 Process lab on-chip . . . 20
2.11 Sputtering method : variation of the thickness as a function of the width of the specimen beam (the illustrated sample is the first lab on-chip studied sample of this work) . . . 22
2.12 Cursors with a displacement u . . . 23
2.13 Force-displacement evolution for an actuator in red and the specimen beam in dark gray . . . 26
2.14 Evolution of the force as a function of the displacement for the actuator and the specimen beam with the equilibrium point reached during the relaxation process 27
2.15 Thickness measurement of one specimen beam . . . 28
2.16 Kapton polymer for the tensile test on polymer (dimensions in mm) . . . 30

3.1 Transverse section of the nanolaminate deposited for the nanoindentation . . . 34
3.2 CSR test on Al_2O_3-Al 138-16 nm x5: Indents 4x4 matrix . . . 35
3.3 CSR test on Al_2O_3-Al 138-16 nm x5 : Zoom of one indent . . . 35
3.4 CSR test at 0.05 s^{-1} on Al_2O_3-Al 138-16 nm x5: Apparent Young's modulus as a function of the contact depth . . . 35

3.5 CSR test at 0.05 s^{-1} on Al_2O_3-Al 138-16 nm x5: Film Young's modulus as a function of the contact depth . . . 35
3.6 CSR test at 0.05 s^{-1} on Al_2O_3-Al 138-16 nm x5: Hardness as a function of the contact depth . . . 36
3.7 CSR test at 0.05 s^{-1} on Al_2O_3-Al 138-16 nm x5: Strain rate as a function of the contact depth . . . 36
3.8 QS test on Al_2O_3-Al 138-16 nm x5: Load as a function of the time . . . 36
3.9 QS test on Al_2O_3-Al 138-16 nm x5: Load as a function of the time : zoom of the third unload . . . 36
3.10 QS test on Al_2O_3-Al 138-16 nm x5: Young's modulus as a function of the contact depth . . . 37
3.11 Load-displacement curve. (a) purely elastic; (b1) and (b2) elasto-plastic behavior with no change of hysteresis with strain rate; (c) viscous-elastic behavior; (d) viscous-elasto-plastic behavior . . . 37
3.12 CSR test at different strain rates on Al_2O_3-Al 138-16 nm x5: Strain rate as a function of the contact depth . . . 38
3.13 CSR test at different strain rates on Al_2O_3-Al 138-16 nm x5: Hardness as a function of the contact depth . . . 38
3.14 CSR test at different strain rates on Al_2O_3-Al 138-16 nm x5: Apparent Young's modulus as a function of the contact depth . . . 38
3.15 CSR test at different strain rates on Al_2O_3-Al 138-16 nm x5: Film Young's modulus as a function of the contact depth . . . 38
3.16 CSR test at different strain rates on Al_2O_3-Al 138-16 nm x5: Hardness as a function of the strain rate . . . 39
3.17 CSR test at different strain rates on Al_2O_3-Al 138-16 nm x5: Strain rate as a function of the contact depth . . . 40
3.18 CSR test at different strain rates on Al_2O_3-Al 138-16 nm x5: Hardness as a function of the contact depth . . . 40
3.19 CSR test at different strain rates on Al_2O_3-Al 138-16 nm x5: Apparent Young's modulus as a function of the contact depth . . . 40
3.20 CSR test at different strain rates on Al_2O_3-Al 138-16 nm x5: Film Young's modulus as a function of the contact depth . . . 40
3.21 CSR test at different strain rates on Al_2O_3-Al 138-16 nm x5: Hardness versus strain rate curve in a log-log scale (all tests) . . . 41
3.22 Baral's method on Al_2O_3-Al 138-16 nm x5: Load as a function of the time . . . 42
3.23 Baral's method on Al_2O_3-Al 138-16 nm x5: Load as a function of the time in a log scale . . . 42
3.24 Baral's method on Al_2O_3-Al 138-16 nm x5: Representative stress versus representative strain rate curve in a log-log scale . . . 43
3.25 Baral's method on Al_2O_3-Al 138-16 nm x5: Load as a function of the time . . . 44
3.26 Baral's method on Al_2O_3-Al 138-16 nm x5: Load as a function of the time in a log scale . . . 44
3.27 Baral's method on Al_2O_3-Al 138-16 nm x5: Representative stress versus representative strain rate curve in a log-log scale . . . 44
3.28 LOC test on Al_2O_3-Al 85-10 nm x5: Broken structures and strange cursors . . . 47
3.29 LOC test on Al_2O_3-Al 85-10 nm x5: True stress versus true strain curve . . . 48

3.30 LOC test on Al_2O_3-Al 85-10 nm x5: True stress versus true strain curve - Relaxation 4 days and 13 days . . . 49
3.31 LOC test on Al_2O_3-Al 46-10 nm x5: Broken structures and broken at the overlap 51
3.32 LOC test on Al_2O_3-Al 46-10 nm x5: True stress versus true strain curve . . . 52
3.33 FIB cutting of the deposited nanolaminate Al_2O_3-Al 70-12 nm x5 . . . 54
3.34 One structure and the overlap: Al_2O_3-Al 70-12 nm x5 sample . . . 54
3.35 Reference specimen beam of width 0.6 µm . . . 55
3.36 Reference specimen beam of width 0.7 µm . . . 55
3.37 Reference specimen beams to observe their quality . . . 55
3.38 Fracture of a specimen beam: Al_2O_3-Al 70-12 nm x5 sample . . . 55
3.39 LOC test on Al_2O_3-Al 70-12 nm x5: True stress versus true strain curve . . . 56
3.40 Cursors with FIB cutting . . . 56
3.41 LOC test on Al_2O_3-Al 70-12 nm x5: True stress versus true strain curve - FIB cutting . . . 57
3.42 LOC test on Al_2O_3-Al 70-12 nm x5: True stress versus true strain curve - Relaxation 1 hour, 5 hours and 8 days . . . 58
3.43 Behavioural law . . . 58
3.44 Pictures for the DIC analysis: Al_2O_3-Al 70-12 nm x5 sample . . . 59
3.45 LOC test on Al_2O_3-Al 85-10 nm x5, 46-10 nm x5 and 70-12 nm x5: True stress versus true strain curve . . . 60
3.46 Sample 1 Al_2O_3-Al 100-10 nm x5: before tensile test . . . 62
3.47 Sample 2 Al_2O_3-Al 100-10 nm x5: before tensile test . . . 62
3.48 Sample 3 Al_2O_3-Al 100-10 nm x5: before tensile test . . . 63
3.49 Sample 3 Al_2O_3-Al 100-10 nm x5: before tensile test . . . 63
3.50 Sample 3 Al_2O_3-Al 100-10 nm x5: before tensile test . . . 63
3.51 Sample 1 Al_2O_3-Al 100-10 nm x5: after tensile test . . . 64
3.52 Sample 2 Al_2O_3-Al 100-10 nm x5: after tensile test . . . 64
3.53 Sample 1 Al_2O_3-Al 100-10 nm x5: after tensile test . . . 64
3.54 Sample 1 Al_2O_3-Al 100-10 nm x5: after tensile test - zoom . . . 64
3.55 Tensile test of Al_2O_3-Al 100-10 nm x5 on polymer: Force versus displacement for the polymer and the deposited sample . . . 65
3.56 Tensile test of Al_2O_3-Al 100-10 nm x5 on polymer: Force versus displacement for the polymer . . . 65
3.57 Tensile test of Al_2O_3-Al 100-10 nm x5 on polymer: Force versus displacement for the deposited sample . . . 65
3.58 Tensile test of Al_2O_3-Al 100-10 nm x5 on polymer: True stress versus true strain curve for the deposited sample . . . 65

4.1 Results from the nanoindentation tests, LOC tests and tensile tests on polymer 68
4.2 Film Young's modulus-content of alumina curve *(Private communication - Paul Baral)* . . . 69
4.3 Hardness-content of alumina curve *(Private communication - Paul Baral)* . . . 69
4.4 Shape of one indent from nanoindentation . . . 70
4.5 LOC : fracture of one specimen beam . . . 70
4.6 Sharp cracks from tensile test . . . 70

4.7 Baral's method on Al_2O_3-Al 138-16 nm x5: Representative stress versus representative strain rate curve in a log-log scale . . . 71
4.8 Representative strain rate as a function of the hardness (*Private communication - Paul Baral*) . . . 71
4.9 CSR test at different strain rates on Al_2O_3-Al 138-16 nm x5: Strain rate as a function of the contact depth . . . 77
4.10 CSR test at different strain rates on Al_2O_3-Al 138-16 nm x5: Hardness as a function of the contact depth . . . 78
4.11 CSR test at different strain rates on Al_2O_3-Al 138-16 nm x5: Apparent Young's modulus as a function of the contact depth . . . 78
4.12 Vacuum level in the chamber (green arrow) . . . 80
4.13 Venting/pumping button (blue arrow) and rotation buttons (green arrow) . . . 80
4.14 Stopping the loadlock pumping system (blue arrow) . . . 80
4.15 Levels of the chamber holder position . . . 81
4.16 Interface to realise the deposition . . . 82
4.17 Interface to realise the deposition . . . 82
4.18 Xactix machine software . . . 84
4.19 Actuator structures for the release . . . 85
4.20 One structure after release . . . 85
4.21 Broken at the overlap . . . 86
4.22 Overlap . . . 86
4.23 LOC test on Al_2O_3-Al 50-20 nm x3: True stress versus true strain curve . . . 86
4.24 Broken specimen beam . . . 87
4.25 Zoom of the broken specimen beam . . . 87
4.26 LOC test on Al_2O_3-Al 50-20 nm x5: True stress versus true strain curve . . . 88
4.27 LOC test on Al_2O_3-Al 50-20 nm x5: True stress versus true strain curve - Relaxation 2 hours, 13 days, 19 days and 25 days . . . 88
4.28 0.75 µm W - 10 µm L structures . . . 89
4.29 1.5 µm W - 100 µm L structures . . . 89
4.30 1.5 µm W - 400 µm L structures . . . 89
4.31 1.5 µm W - 400 µm L structures . . . 89
4.32 LOC test on Al_2O_3-Al 85-10 nm x5: True stress versus true strain curve . . . 90
4.33 LOC test on Al_2O_3-Al 46-10 nm x5: True stress versus true strain curve . . . 90
4.34 LOC test on Al_2O_3-Al 70-12 nm x5: True stress versus true strain curve . . . 90

List of abbreviations

CSM Continuous Stiffness Measurement. 14, 33, 36

CSR Constant Strain Rate. vii, viii, x, 15, 35, 36, 38–43, 45, 68, 71, 72, 77, 78

DIC Digital Image Correlation. v, ix, 53, 59, 62, 72, 73

FIB Focused Ion Beam. v, ix, 8, 22, 29, 53, 54, 56, 57, 60, 61, 68, 70, 72

HMDS HexaMethylDiSilazane. 21

LOC Lab On-Chip. vii–x, 1, 7, 10, 11, 24, 28, 46–49, 51–53, 56–58, 60, 68–73, 86, 88, 90

LPCVD Low Pressure Chemical Vapor Deposition. 19

MEMS Microelectromechanical system-based devices. 5, 73

PTP Push-To-Pull. vii, 7, 10, 11

QS Quasi-Static. viii, 14, 33, 36, 37

SEM Scanning Electrons Microscope. iv, v, 16, 23, 29, 33, 34, 47, 50, 54, 56, 57, 59, 61, 63, 64, 70, 72, 73, 79

TEM Transmission Electrons Microscope. 10, 34, 37

UV UltraViolet Radiation. iii, 21

WEC Wedge Error Compensation. 21

WINFAB Wallonia Infrastructure Nano Fabrication. iii, 19

Abstract

Nowadays, the characterisation of thin films is very important for all kinds of applications, in electronics or coating. This research work is carried out with the aim of determining the mechanical properties of nanolaminates composed of alumina and aluminium. To this end, nanoindentation tests are carried out in the first instance, but also Lab On-Chip tests (LOC), a technique developed by UCLouvain, and tensile tests on polymer. First, a Young's modulus of 145 GPa and a hardness of 7.5 GPa are found, but also variations in Young's modulus and hardness as a function of the strain rate showing a viscoelastic and viscoplastic character. Continuous stiffness measurements at different strain rates are used to obtain a strain rate sensitivity coefficient of 0.04 at higher strain rates and Paul Baral's method is used for the strain rate sensitivity coefficient of 0.24 at lower strain rates. A strain up to 3.4 % is achieved using the lab on-chip technique and even up to 4.7 % after some relaxation. Plastic strain is reached. Relaxation of the material also allows to determine a strain rate sensitivity coefficient between 0.01 and 0.03. Finally, nanoindentation deforms plastically the nanolaminate while the LOC tests seem to show a brittle fracture and the tensile tests on polymer give very sharp cracks with a rapid propagation.

Remerciements

Tout d'abord, je souhaite remercier mon promoteur, le Professeur Thomas Pardoen, pour m'avoir proposé ce sujet de mémoire malgré mon changement tardif de mémoire. Vous m'avez tout de suite prêté certaines thèses que j'ai aussitôt commencé à feuilleter pour me plonger dans le monde des nanolaminés et du lab on-chip. Toujours bienveillant envers vos étudiants, c'était un plaisir de vous croiser dans les couloirs du bâtiment Stevin pendant ce semestre, merci pour votre confiance.

Je tiens également à remercier le Professeur Laurent Delannay d'avoir accepté de lire mon mémoire et de faire partir du jury, tout comme le Professeur Pardoen, Michaël Colombier et Morgan Rusinowicz.

J'ai eu la chance d'être encadrée par Michaël Coulombier et Morgan Rusinowicz. Je tiens à vous remercier énormément pour m'avoir accompagnée et épaulée tout au long du mémoire. Merci Michaël, maître du lab on-chip, pour ton efficacité, tes explications, ainsi que ta disponibilité. Tu as toujours su te rendre disponible pour avancer dans le process en salle blanche, m'apprendre à réaliser les mesures au profilomètre, à l'ellipsomètre, et m'apprendre à réaliser certaines étapes du process par moi-même, comme la gravure au XeF2.

Merci Morgan, maître de la nanoindentation, pour ton temps, ta pédagogie et tous les conseils que tu m'as apportés. Tu m'as expliqué et appris beaucoup, toujours avec attention. C'était sympas d'apprendre ensemble les techniques et machines des laboratoires de l'UCLouvain. Merci aussi de m'avoir proposé de t'accompagner à Grenoble, ta ville de thèse et ma ville d'Erasmus (programme FAME+), pour découvrir la nanoindentation couplant les propriétés électriques et mécaniques des matériaux.

Un grand merci à vous deux pour avoir eu la patience de répondre à mes nombreuses questions; cela m'a permis de progresser d'apprendre tant aussi vite. Je vous remercie également pour nos échanges autant scientifiques que personnelles à propos du fameux doctorat et de la vie future.

Je tiens également à remercier Marie-Stéphane Colla, pour ta disponibilité et ton aide dans l'élaboration des tests de traction sur polymère. Tu as pris le temps de me montrer le test et m'a expliquée comment traiter les résultats. Merci aussi à Audrey Favache et Laurence Reylandt pour les formations à la nanoindentation et au microscope à balayage électronique.

Je remercie aussi tout le personnel des salles blanches, présent en cas de petit soucis, et en particulier à Sébastien Faniel qui m'a permis de devenir autonome pour le dépôt des nanolaminés.

Enfin, un immense merci à mes proches, et ma famille pour m'avoir soutenue au long de ce mémoire, court mais intense. Merci Julie, ma sœur adorée qui m'a toujours soutenue, encouragée, malgré la distance, tu es toujours là quand ça ne va pas. Merci à Julien, Diego, Damien, Léo, Marie, Emma, Alexis, Nathan et Livia pour vos encouragements et votre écoute. Merci à la danse, qui me permet de m'évader et vivre ces moments où je ne pense plus à rien, ni les cours, ni les projets, ni les petits soucis quotidiens. Et merci à mes parents qui m'ont toujours soutenue et appris à me donner à fond dans tout ce que je fais.

A vous tous, je vous présente mes remerciements ainsi que ma gratitude.

Introduction

Nowadays thin films, films ranging from a few nanometres to a few micrometres in thickness, and 2D materials, consisting of a single atomic layer, are at the heart of many applications. Indeed, first of all, electronics is trying to continuously minimise the size of electronic components and Microelectromechanical system-based devices (MEMS) are more and more used and developed. In addition, some applications require certain electronic systems to be more flexible. Finally, thin films are used to protect a material against the environment, corrosion, abrasion, erosion or to make it functional and thus give it a particular property [25] [28].

For all these applications, the materials must respect certain mechanical properties in order to be reliable. But the mechanical properties of these nanometals are not necessarily the same as those of macroscopic materials. Indeed, size effects occur due to the large surface-to-volume ratio and the fine microstructure. Thin films often require good mechanical properties such as high strength, hardness, large ductility but also high fracture toughness to avoid initiation and propagation of cracks [12]. Thus, for future applications in microelectronics, it is important to determine the mechanical properties and to understand and analyse the behaviour of materials at the nanoscale. [18] [16]

Therefore, a technique has been developed by UCLouvain. It is the lab on-chip technique which allows to obtain a stress-strain curve. This work is based on this technique, as well as on nanoindentation, a technique that is often used to obtain Young's modulus and hardness, and also on tensile tests on a polymer.

In addition, a new type of material has caught attention in recent years because of its electronic, magnetic, thermal, mechanical or optical properties [19]. These are nanolaminates, i.e. materials composed of several layers with different properties. The nanolaminate studied here is the nanolaminate composed of alumina and aluminium.

This work starts with a state of the art that gives a short history of the techniques and results on nanolaminates so far. Then, the experimental methods are presented in details, followed by a chapter about the sample preparation and the results. Finally, a general discussion is presented, followed by a conclusion. Appendices are also provided for more information.

Chapter 1

State of the art

This section begins with a brief history of existing mechanical tests to determine the mechanical properties of thin films. First, for techniques for freestanding thin films, then for thin films deposited on a substrate and finally the technique developed by UCLouvain, the lab on-chip technique. Mechanical properties of nanolaminates composed by alumina and aluminium are then presented with some previous results from LOC and push-to-pull (PTP) techniques.

1.1 Mechanical testing techniques

As mentioned in the previous section, thin films require good mechanical properties. But these properties are different from those of solid materials because of size effects and strain and fracture mechanisms which are not always the same [14]. Several techniques therefore exist and allow mechanical properties to be determined, when the film is freestanding or deposited on a substrate [25].

1.1.1 Freestanding thin films

To obtain the Young's Modulus of the film, a bending test can be performed thanks to a nanoindenter which gives the stiffness as the slope of the load-deflection curve [23] [25]:

$$k = \frac{E\omega}{4(1-\nu^2)}\left(\frac{t}{l}\right)^3 \tag{1.1}$$

Where k is the stiffness of the beam, E the Young's modulus, ω the width of the beam, ν the Poisson ratio of the film, t the thickness of the beam and l the distance between the anchor of the beam and the contact point with the nanoindentator.

Another possible test is the bulge test where a pressurised fluid allows the deflection of the film. From the evolution of the pressure as a function of the deflection, one can obtain the stress and the strain in the middle of the film [3] [25]. But this technique can give compressive residual stresses which can lead to buckling.

A lot of other techniques are related to tensile tests realised by microfabrication [25]. Firstly, Read et al. deposited on a silicon wafer the specimen attached to a frame from both sides which allows the extension by inserting a hook into one side on the frame by pulling on it [5]. Secondly, Sharpe et al. used load cell on a piezoelectric actuator to measure the load and interferometry for the strain [22]. Another one was proposed by Tsuchiya et al. who used an electrostatic force to pull, by piezoelectric actuator, on the free end of the film [21].

However, the determination of mechanical properties at the sub-micron scale remains very complicated. Indeed, sample preparation, handling, mechanical testing, application of small forces and exact stress and strain measurements require high precision. Furthermore, perfect alignment for uniaxial tension are quite complicated to ensure.

1.1.2 On substrate

The wafer curvature test is used to determine the internal stresses of the film based on the change in curvature of the substrate, for example after deposition. The Stoney equation gives [25]:

$$\sigma = \frac{1}{6}\frac{E_s}{1-\nu_s}\frac{t_s^2}{t_f}\left(\frac{1}{R_{post}} - \frac{1}{R_{pre}}\right) \tag{1.2}$$

With σ, the stress in the film, $\frac{E_s}{1-\nu_s}$ the biaxial modulus of the substrate, t_s the thickness of the substrate, t_f the thickness of the film, $\frac{1}{R_{pre}}$ the initial curvature of the substrate and $\frac{1}{R_{post}}$ the final curvature of the substrate.

Regarding the compression methods, a flat nanoindenter tip is used to compress a micropillar cut by Focused Ion Beam (FIB). But the FIB step can induce some defects in the material which can modify its properties [4].

Tensile testing of thin films on a substrate prevents the observation of the mechanical properties of the film itself. Several options are then possible, such as removing the contribution of the substrate in the stress-strain curve or in-situ measurements to measure the interatomic displacement in the film [8].

Nanoindentation is also a technique often used to determine the Young's modulus and hardness of materials. It is easier to perform, but substrate effects are difficult to avoid for films thinner than 100-200 nm.

1.1.3 Lab on-chip

Thus, for avoiding the substrate effects and the difficulties to perform a test on a freestanding thin film, a new technique has been developed at UCLouvain to evaluate the mechanical properties of thin films. This is the lab on-chip technique, which corresponds to a nanomechanical test platform on a chip based on the use of internal stresses in one material to deform a second, attached to the first one. This technique makes it possible to carry out mechanical tests on thin films, on thousands of structures at a time, and to obtain mechanical properties such as Young's modulus, hardness, strain rate sensitivity coefficient, as well as fracture properties and strain hardening [20] [18].

This technique is explained in details in the section 2.2 and has already been proven with several materials already tested such as silicon nanowires, polysilicon films [18], aluminium films, palladium films [11], and metallic glass films [20]. 15 % strain below 500 nm is achieved for ZrNi films [10] and up to 10 % for palladium [20], aluminium [18] and polysilicon [18].

Moreover, the crack on-chip technique also exists based on the same principle as the lab on-chip. The idea relies on a crack arrest measurement, based on a precrack. Indeed, generating atomically sharp precracks in micro-specimens is quite complicated [17].

1.2 Mechanical properties of nanolaminates Al_2O_3 - Al

The objective of the work is to obtain the mechanical properties of nanolaminates composed of alumina and aluminium with the future aim of better understanding the deformation and damage mechanisms at the nanoscopic scale to further optimise this system.

As already mentioned in chapter , a nanolaminate is a material with a thickness of no more than a few micrometers, composed of several layers alternating different constituents with different properties. Previous research at UCLouvain has found that nanolaminates composed of amorphous alumina and aluminium exhibit very interesting mechanical properties. Indeed, they have high strength, high ductility and high fracture toughness at the same time.

1.2.1 Alumina

The compound most present in the nanolaminate is amorphous alumina. Indeed, it is chosen for its high hardness (10-12 GPa [26]) and its large strength (240 MPa [26]). To make a material harder, the idea is to decrease the size of the sample, 'smaller is stronger'. Alumina also has resistance to oxidation. Moreover, this material can reach a ductility up to 0.12-0.15 when its thickness is smaller than 100 nm whereas ceramics are mostly brittle due to their low strain hardening which prevents a certain ductility [12].

1.2.2 Aluminium

Aluminium is less hard (240 MPa [30]) and less strong (90 MPa [30]). However, its main purpose is to interrupt alumina and thus stop the propagation of cracks [19]. Moreover, aluminium is tough. Indeed, for an alumina layer thickness below 100 nm, the toughness of the nanolaminate reaches up to 350 J/m^2 ($K_{Ic} = 7.5$ MPa$\sqrt{m}$), two orders of magnitude higher than bulk alumina.

But aluminium also serves to stabilise the deformation process and dissipate energy since it deforms plastically; due to its good ductility and good strain rate hardening.

1.2.3 Multilayer

Moreover, multilayering also makes it possible to avoid the spread of shear bands throughout the material. Indeed, the plasticity mechanisms, controlled by dislocations or twins in crystalline materials, are confined to the aluminium, whereas shear banding is in amorphous materials [12]. The presence of interfaces is thus really advantageous [7].

1.2.4 Lab on-chip, push-to-pull tests results and main purpose of the work

Previous works show that the hardness and fracture strain of this kind of nanolaminates are over 9 GPa and 7 % respectively for a thickness combination of 50-10 nm x3 for alumina/aluminium. The associated Young's modulus is 160 GPa and the toughness 350 J/m^2. The alumina concerned is processed by sputtering; it is fully amorphous. [12]

Thus, the best performance can be achieved when the alumina thickness is below 100 nm and the aluminium thickness between 10 and 20 nm [12]. The very good mechanical properties of nanolaminates come mainly from the interfaces between the layers, which are very good here because there is a good compatibility between the two materials.

The hardness and the Young's modulus are determined by nanoindentation. Push-to-pull tensile tests show a strain of up to 7 %, with a 730 nm thick nanolaminate composed of layers of 10 nm aluminium and 120 nm alumina, as shown in Fig. 1.1. The modulus obtained is about 100 GPa.

In addition, some PTP tests have been carried out under Transmission Electronic Microscope (TEM) to visualise the deformation mechanisms. This showed that the electron beam influences the kinetics of the deformation mechanisms. Indeed, the interaction of the electrons with the material allows for more homogeneous deformation and increases the ductility.

But only the PTP technique has made it possible to observe such levels of strain within the nanolaminate, but it is not the case of LOC test. Actually, the lab on-chip allowed the determination of a Young's modulus of the aluminium and alumina as shown in Fig. 1.2 and 1.3. Moreover, these Young's moduli of 70 GPa and 185 GPa respectively seem to be consistent with the literature data which corresponds to 70 GPa for aluminium [30] and about 200 GPa for alumina for small thicknesses [31]. On the other hand, Fig. 1.3 also shows that the Young's modulus given by the PTP tests seems to be lower. Furthermore, the LOC test of the aluminium allowed the determination of a stress-strain curve with strain corresponding to plastic strain as shown in Fig. 1.2. But the lab on-chip tests on alumina do not show plastic strain whereas the push-to-pull tests do.

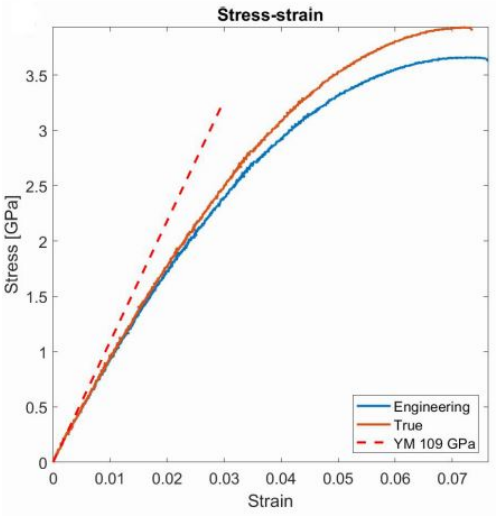

Figure 1.1: Stress versus strain curve from a PTP test on a nanolaminate alumina-aluminium 120-10 nm
Private communication - Thomas Pardoen

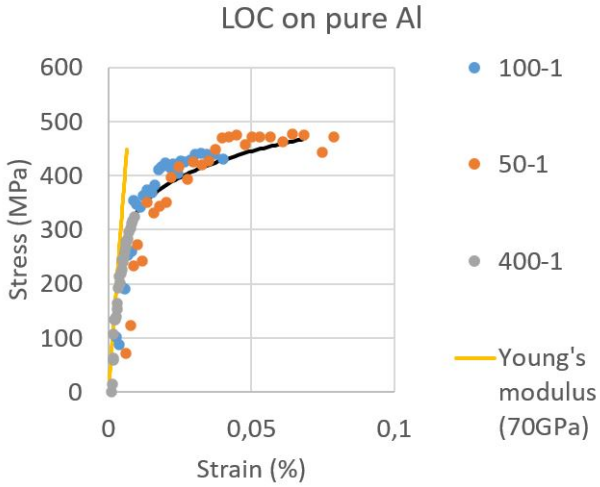

Figure 1.2: Stress versus strain curve on aluminum (LOC tensile test)
Private communication - Thomas Pardoen

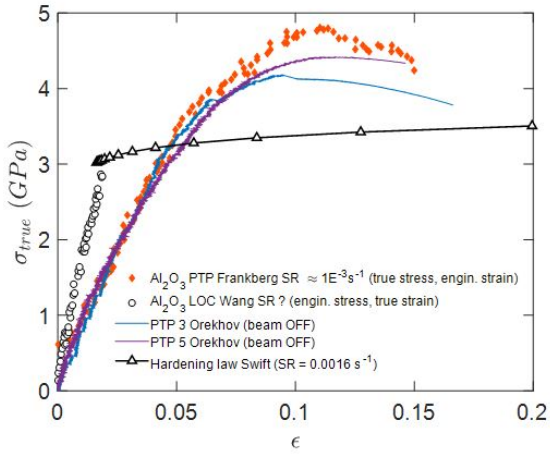

Figure 1.3: Stress versus strain curve on alumina (LOC and PTP tensile tests)
Private communication - Thomas Pardoen

The aim of the thesis is therefore to achieve plastic strain with the LOC technique. The nanolaminates studied have a desired thickness smaller than 100 nm for the alumina layer and between 10 nm and 20 nm for the aluminium layer.

Chapter 2

Experimental methods

This section presents the experimental methods. The nanoindentation is first described, with its limitations, the calculations in order to obtain certain mechanical properties such as the hardness, the Young's modulus and the strain rate sensitivity coefficient, and the Paul Baral's method which will also be used.

Then the lab on-chip method is detailed, starting with the concept, the process steps, the advantages and disadvantages, then the calculations to obtain a stress-strain curve, the mismatch of the sample and the propagation of errors.

Finally, the tensile tests on polymer are presented with the preparation of the test as well as the determination of a stress-strain curve and the fracture toughness.

2.1 Nanoindentation

2.1.1 Nanoindentation technique

First of all, this technique allows to determine the Young's modulus, the hardness of thin films but also their strain rate sensitivity.

A single crystal diamond tip is driven into the material at constant force or constant displacement. The hardness of diamond is well known and is equal to 40 GPa and its elastic modulus is 1141 GPa [32]. The applied load is recorded as a function of the penetration depth of this crystal into the material. The raw data of a nanoindentation test are the applied force and the penetration depth as shown in Fig. 2.1. The force is of the order of a few tens of mN and the depth can go up to 1000 nm. There are different types of tips: conical, spherical, Vickers type and the most used is the Berkovich type because it is the easiest to manufacture; it is represented on Fig. 2.2 [25]. For this type of tip, the face angle is 65.27°, which corresponds to a conical tip with a semi-angle of 70.32°. These tips are self-similar, which means that their radius is proportional to their height; the stress and strain fields are geometrically similar [32].

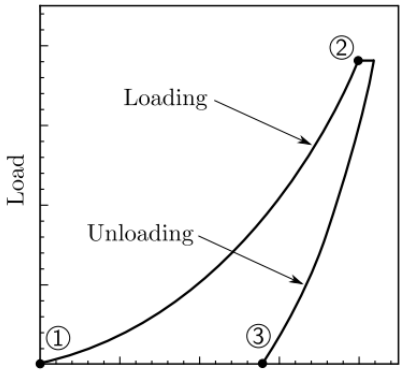

[25]

Figure 2.1: Load-displacement curve during nanoindentation

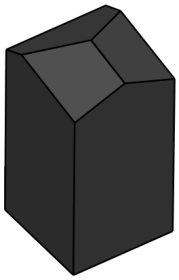

[32]

Figure 2.2: Berkovich tip scheme

2.1.2 Limitations of the technique

First, for nanofilms, one must be careful about the effects due to the substrate. The analysis of ductile films is more complicated because there is a strain gradient plasticity [18]. In addition, there may be pile-up and sink-in effects as shown in Fig. 2.3 in rigid-plastic and elastic materials respectively [32]. And the fracture toughness cannot be obtained easily [18].

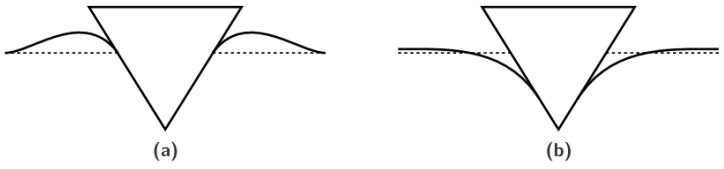

[25]

Figure 2.3: (a) Scheme of a pile-up effect (b) Sheme of a sink-in effect

2.1.3 Determination of the Young's modulus, the hardness and the strain rate sensitivity

First, Meyer defined the hardness H by the Eq. 2.1 [29] [32]:

$$H = \frac{F}{A_c} \tag{2.1}$$

Where F is the measured applied load and A_c the indenter/material contact area, which is the projected area of the tip surface in contact with the sample surface.

To determine the Young's modulus, several steps are necessary. In fact, the stiffness S is measured during the test as the slope of the curve at the beginning of the discharge as shown in Fig. 2.4. Two modes are possible: the Quasi-Static mode (QS) or the Continuous Stiffness Measurement mode (CSM). The first one performs several discharges at regular intervals. The

loading rate $\dot{F}$ is kept constant. The second one allows to obtain continuously the stiffness, which allows to have the Young's modulus in a continuous way since these two quantities are linked as explained below. This is possible thanks to the superposition of a harmonic force on the nominal increasing force (shown in Fig. 2.4); at each discharge, the stiffness is measured. In this case, the loading rate $\frac{\dot{F}}{F}$ is kept constant and the strain rate $\frac{\dot{h}}{h}$ is equal to half $\frac{\dot{F}}{F}$. These tests are called Constant Strain Rate (CSR) tests.

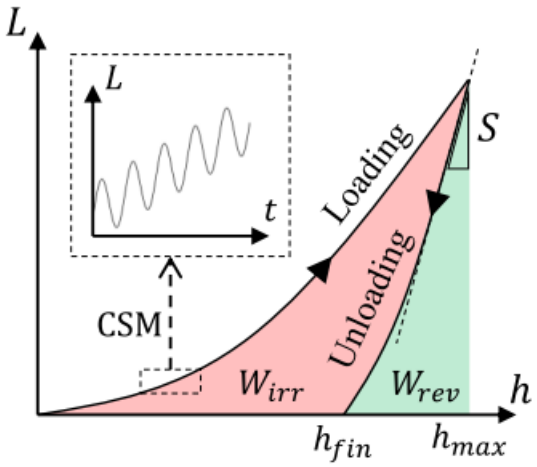

[32]

Figure 2.4: Load versus penetration depth curve

Sneddon's equation Eq. 2.2 allows to relate the contact stiffness S, the contact area A_c and the reduced Young's modulus E^* [29].

$$S = 2E^* \sqrt{\frac{A_c}{\pi}} \tag{2.2}$$

Where E^* is the reduces Young's modulus defined by Eq. 2.3 [29]:

$$\frac{1}{E^*} = \frac{1-\nu_{tip}^2}{E_{tip}} + \frac{1-\nu_{app}^2}{E_{app}} \tag{2.3}$$

Where E_{tip} is the Young's modulus of the tip, 1141 GPa, E_{app}, the Young's modulus of the film impacted by the substrate, ν_{tip} the Poisson coefficient of the tip, 0.07 and ν_{app} the Poisson coefficient of the film impacted by the substrate, 0.25.

And by matching the contact area into a circular contact area, the contact radius can be defined as follows:

$$r_c = \sqrt{\frac{A_c}{\pi}} \tag{2.4}$$

By Eq. 2.2, the reduced Young's Modulus is given by Eq. 2.5:

$$E^* = \frac{\sqrt{\pi}}{2} \frac{S}{\sqrt{A_c}} \tag{2.5}$$

And by Eq. 2.3, the apparent Young's modulus can finally be determined.

In order to determine the hardness or Young's modulus, it remains to determine the contact area. For this, post-mortem experiments can be performed with Scanning Electron Microscope (SEM), but models have been created and are often used. These models allow to obtain the contact depth h_c illustrated in Fig. 2.5 from the quantities measured during the test.

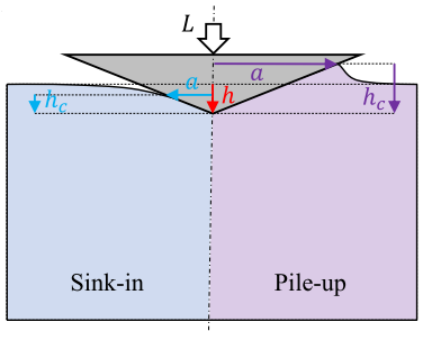

[32]

Figure 2.5: Dimensions of a nanoindentation test

For sink-in configuration, isotropic and bulk materials, the Oliver-Pharr model described by Eq. 2.6 can be applied [29].

$$h = h_c + 0.75\frac{F}{S} \tag{2.6}$$

For pile-up configuration, isotropic and bulk, the Loubet model described by Eq. 2.7 can be applied [6].

$$h_c = 1.2(h - \frac{F}{S} + h_0) \tag{2.7}$$

Where h_0 is the tip default due to usure.

The shape function is a geometrical calibration of the tip, which allows to determine the contact area as a function of the contact depth and which is in the form of Eq. 2.8:

$$A_c(h_c) = m_0 h_c^2 + m_1 h_c + m_2 h_c^{\frac{1}{2}} + m_3 h_c^{\frac{1}{4}} + ... \tag{2.8}$$

To obtain it, a fused silica nanoindentation is performed. This material is used because its deformation is isotropic, and its properties are well known ($E = 72$ GPa and $\nu = 0.2$) [29].

Once the contact area is obtained, it is possible to determine the apparent Young's modulus and the hardness by Eq. 2.1 and 2.5, respectively. The Young's modulus of the film is determined by the Hay and Crawford model which is not demonstrated here [27].

Once the hardness and strain are determined for different strain rates, it is possible to determine the strain rate sensitivity coefficient by Eq. 2.9 [14].

$$m = \frac{\partial \ln H}{\partial \ln \dot{\epsilon_r}} \tag{2.9}$$

2.1.4 Some information about the nanoindentation testing

The machine used is the G200 nanoindenter of the laboratory which is equipped with a dynamic contact module II head with 50 nN and 0.01 nm of force and vertical displacement resolution, respectively. A Berkovich diamond tip is used and the contact area calibration is well done with a fused silica reference. To verify that the silica calibration is correct, the Young's modulus should be equal to 72 GPa and that the ratio $\frac{S^2}{L}$ is constant as a function of the depth of penetration because silica is an almost isotropic material.

The tests are performed at room temperature with the load-control mode with an exponential loading to have a constant indentation loading rate $\frac{\dot{F}}{F}$. For each of the tests, several indents are performed for statistical analysis. More specific conditions such as thermal drift and indentation depth are described for each test as these parameters vary from one experiment to another one.

To determine the hardness, the Young's modulus and the strain rate sensitivity coefficient, these values are taken for a penetration depth of usually 10 % of the total thickness of the thin film. This gives a good compromise to minimise the substrate and tip rounding effect [31]. The first tests are performed with the continuous stiffness measurement mode to obtain a continuous hardness and Young's modulus as a function of the penetration depth. A test in quasi-static condition and finally two tests with the Baral's method are also carried out.

2.1.5 Paul Baral's Method and strain rate sensitivity coefficient

This method consists in imposing a constant stiffness and to see the variation of force with time and allows to obtain a strain rate sensitivity coefficient. In this case, the hardness, the representative strain rate and the representative stress are given by Eq. 2.10, Eq. 2.11 and Eq. 2.12 [14] [13].

$$H = \frac{F}{A_c} = \frac{4F}{\pi}\left(\frac{E^*}{S}\right)^2 \tag{2.10}$$

$$|\dot{\epsilon_r}| = \frac{|\dot{\sigma_r}|}{E_{app}} \tag{2.11}$$

$$\sigma_r = \frac{H}{c} = \frac{\zeta_3 \cot(\theta) H}{\zeta_1 \cot(\theta) - (1-\zeta_2)\frac{H}{E^*}} \tag{2.12}$$

With c is equal to around 2.2 usually and equal to 2.3 in this case (calculated by numerical simulations by Morgan Rusinowicz), $\zeta_1 = 0.66$, $\zeta_2 = 0.216$, $\zeta_3 = 0.24$ and $\theta = 70.32°$ for a cone of half-included angle as for the Berkovich tip.

Once the stress and strain are determined for different strain rates, it is possible to determine the strain rate sensitivity coefficient by Eq. 2.13 [14].

$$m = \frac{\partial \ln \sigma_r}{\partial \ln \dot{\epsilon_r}} \tag{2.13}$$

In order to neglect the experimental noise, the Baral's method proposes to scale the time in log and to make classes to average the stress.

2.2 Lab on-chip technique

2.2.1 Concept

This technique is based on a stress relaxation principle and allows the determination of a Young's modulus, by a stress-strain curve. The idea is to use to internal tensile stress into an actuator material to create uniaxial tension.

The studied structures are produced using microfabrication techniques such as cleaning, deposition, lithography and release [9]. A schematic of a lab on-chip structure is shown in Fig. 2.6 and consists of an actuator made of Si_3N_4 and the specimen beam made of the deposited sample deposited on a sacrificial layer. The overlap of the specimen on the actuator must be large enough for good adhesion. The principle of the tensile test is to actually remove the sacrificial layer in order to release the actuator, which has internal tensile stresses of 1 GPa from its deposition [2]. Thus, the actuator that is attached to the specimen beam can pull on it and a force balance takes place as shown in Fig. 2.7.

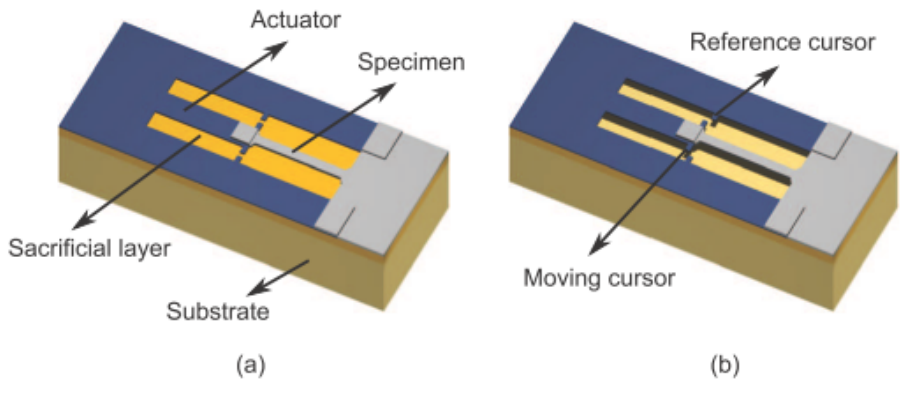

Figure 2.6: One elementary tensile test structure : (a) before release, (b) after release

By knowing the Young's modulus and the mismatch of the actuator, it is possible to find the stress and strain applied to the specimen as explained in section 2.2.5 [18]. These calculations are based on measurements of the displacement u shown in Fig. 2.7, corresponding to the release of the actuator [20]. A structure thus allows to find one point of the stress-strain curve. For this reason, a certain set of structures consists of tens of structures where the specimen has always the same length but the actuator is of different length, which allows different strain levels to be reached.

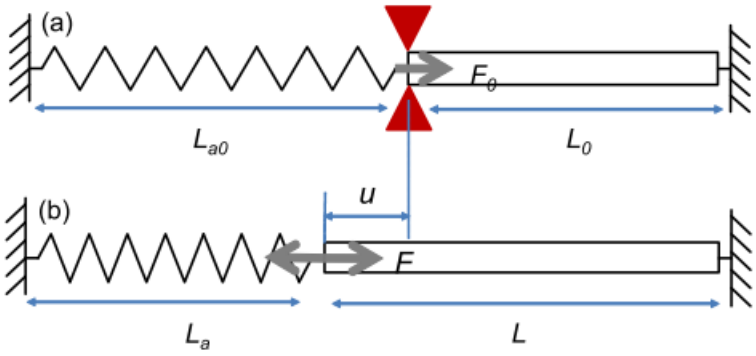

[20]

Figure 2.7: Scheme of the force equilibrium between the actuator (spring representation) and the specimen beam: (a) before release, (b) after release

2.2.2 Fabrication of a one elementary tensile test structure

As explained in Fig. 2.8, the fabrication of these tensile test structures is performed in several steps. In this work the sacrificial layer is the silicon substrate. The silicon nitride is first deposited by Low Pressure Chemical Vapour Deposition (LPCVD) at 790 °C to obtain 1 GPa of internal stress. Then, in order to obtain their desired shape, a positive photoresist is deposited and the silicon nitride is etched by CHF_3. Then, a negative photoresist is deposited, followed by the deposition of the sample by sputtering. A lift-off is then necessary to obtain the specimen beams of the desired shape. It should be noted that the specimen must overlay the actuator sufficiently to ensure good adhesion [20] [31]. The next step is the etching of the sacrificial layer with XeF_2. Thus, the actuator pulls on the specimen beams and they deform until the forces between the actuator and the specimen beams are balanced. [9] [16]

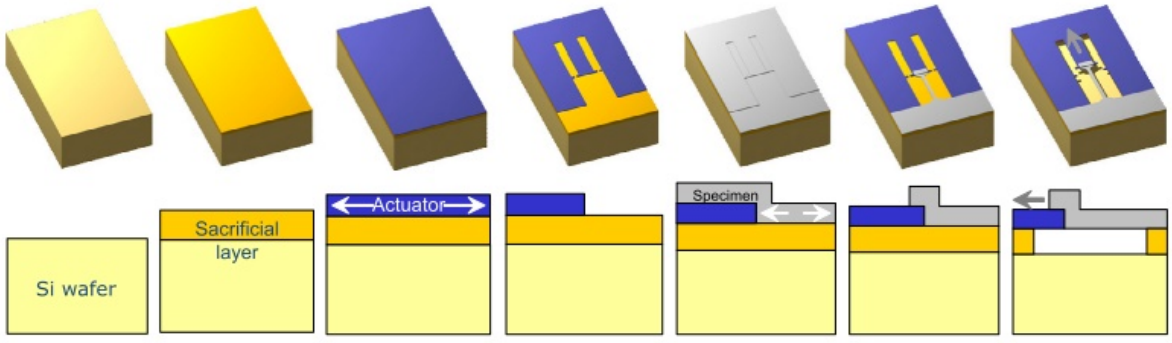

[20]

Figure 2.8: Fabrication of one elementary tensile test structure

2.2.3 Detailed steps of the realised process in the cleanroom WINFAB

The whole process is well described in tables 2.9 and 2.10.

1	STEP	MACHINE	GOAL	COMMENTS
2	Cleaning standard (with HF)	Cleaning benches	Clean wafer before entering a furnace	We used old wafers so this part was already done
3	Si3N4 LPCVD deposition	Koyo furnace	Deposition of actuator material	
4	Check ellipsometer	Ellipsometry	Measure thickness of SiN	
5	Cleaning standard (without HF)	Cleaning benches	Clean wafer but no HF as it etches Si3N4	
6	Degasing 800°C under N2	Furnace Tempress	Dry wafer to remove any water for further adhesion of photoresist	
7	HMDS for adherence promotion	LPIII	Functionnalisation of substrate surface for photoresist to have good adherence	
8	Spin coating of AZMIR 701 4000 rpm	Suss gamma 80	Deposition of positive photoresist with ~1µm thickness	
9	Soft bake 90°C 90s	Suss gamma 80	Harden the photoresist a bit	
10	Exposure with UV lignt 365 nm, dose 170 mJ/cm2, vaccum contact	Mask aligner (SUSS MA6)	Breaks polymer chains of unexposed photoresist	Lithography
11	Post exposure bake 110°C 90s	Suss gamma 80	Hardens unexposed photoresist	
12	Developer (60s)	Suss gamma 80	Dissolves exposed photoresist	
13	CHF3 etching of Si3N4	Oxford plasma	Etch anisotropically SiN using photoresist as a mask	Ecthing actuator layer
14	Check ellipsometer	Ellipsometry	Check that SiN if fully etched	We prefer a little overetch vs underetch
15	Aceton cleaning	Any wet bench	Remove the photoresist	

Figure 2.9: Process lab on-chip

16	Cleaning standard (with HF)	Cleaning benches	Remove all photoresit properly and make sure no oxide on Si	
17	Degasing 800°C under N2	Furnace Tempress	Dry wafer to remove any water for further adhesion of photoresist	In the case of the 3 wafers with SiN thickness = 140 nm we have to avoid this as Si susbtrate is doped (==> oxidation)
18	HMDS for adherence promotion	LPIII	Functionnalisation of substrate surface for photoresist to have good adherence	
19	Spin coating of AZ5010 3000 rpm	Suss gamma 80	Deposition of negative photoresist with ~1µm thickness	
20	Soft bake 90°C 60s	Suss gamma 80	Harden the photoresist a bit	Lithography
21	Exposure with UV lignt 365 nm, dose 120 mJ/cm2, vaccum contact	Mask aligner (SUSS MA6)	Polymerize exposed photoresist	
22	Post exposure bake 105°C 60s	Suss gamma 80	Hardens exposed photoresist	
23	Developer (60s or may be less)	Suss gamma 80	Dissolves unexposed photoresist	
24	Cutting wafers to test multiple thickness of nanolaminates			Only on one wafer
25	Deposition of nanolaminates	AJA	Deposition of specimen material	
26	Lift off : aceton with ultrasonic	Al wet bench	Lift off of unwanted parts of specimen material	
27	Thickness measaurement	Profilometry	Measure thickness of NL	
28	XeF2 etching	Xactix XeF2	Release test structures	Release step
29	Check ellipsometer	Ellipsometry	Measure thickness of SiN	
30	SEM	FIB/SEM	Measure displacements of cursors	

Figure 2.10: Process lab on-chip

For this work, the first two steps are already done because old wafers are used. Six old wafers are used to start with, three with a silicon nitride thickness of 90 nm and three with a thickness of 150 nm. Then the process sheet is followed. Here are some notes and important points about some of the process steps.

Spin coating of AZMIR 701

All six wafers are coated with positive AZIR 701 resin (line 8 in Table 2.9), but the three 90 nm nitride wafers are not coated with HMDS for adhesion promotion, as a matter of time saving. Resin deposition on these three wafers is not as good, and "comets" are visible on the surface; this is probably due to dirt, the resin or the non-use of HMDS. The next steps of the process only involve one wafer with 90 nm silicon nitride and one with 150 nm of silicon nitride.

Exposure with UltraViolet radiation (UV)

Then, before exposure to UV (line 10 in Table 2.9), the mask must be cleaned well so that there are no particles between the mask and the sample. It can be cleaned with ultrasound for about ten minutes, at 37 Hz at maximum power, then put under acetone, methanol and dry. For the exposure, the Wedge Error Compensation (WEC) allows the mask and the sample to be well parallel. It puts a distance of 30 microns between the two and makes them parallel then vacuum contact is applied and the exposure allows to break the polymer chains of the positive resist.

Etching of Si_3N_4

In order to etch the silicon nitride with the Oxford machine (line 13 of Table 2.9), CHF_3 (100 SCCM) and O_2 (10 SCCM) are used. This operation is performed in the etching chamber. It is first important to purge the C_4F_8 since it is this gas that is usually used by this machine. It is also important to activate the cooling system because the plasma is heating up. The turbo-pump must also be activated. One uses O_2 to prevent the etching from stopping because of fluorine. The etching speed is 17 nm/min at 20 mTorr and 20 °C; 100 Watt are used to accelerate the ions through the sample. For information, etching is faster in the centre of the wafer. Ellipsometry gives 92.5 nm and 141 nm for both wafers. The 141 nm wafer will not be used in the end but the idea is to locally thin the silicon nitride at the overlap for a better coverage.

Developer

After the development (line 23 in Table 2.10) of about 40 seconds (to develop too much would risk to give structures too wide), the optical microscope shows that the structures 0.7 are just opened. It is nice because one has to deposit up to 0.75 microns wide (these are the least wide structures to deposit).

Cutting of the wafer

This cutting must take place under water so that the dirt does not come to stick. The cutting takes place very easily because silicon is a crystal; the propagation is thus carried out along the atomic planes.

Deposition of a nanolaminate

The deposition of nanolaminates is performed with the AJA machine. It is a sputtering deposition at ambient temperature. The aluminium target is initially 6 mm thick. Moreover, the sample rotates during the deposition, which allows a lower pressure and thus less porosity during the deposition. The deposition rate varies according to the vacuum and the cleanliness and wear of the target. The deposition pressure is 1.5 mTorr and the power is equal to 300 W. The gas mixture is made of argon 25 SCCM for the aluminum layer deposition and it is made of argon 22 SCCM and oxygen 3 SCCM. These information are important to note because there influence the properties of the deposited material [31].

The deposition time is chosen by the user to obtain the desired thickness. The last depositions realised in the clean room indicate a speed of 11.3 nm/min and aluminum of 7.7 nm/min. These deposition rates and therefore the deposition time is adjusted for the second deposition because the first deposition shows that the rates are not those indicated. As already mentioned in the section 1.2, the deposited nanolaminates are both alumina and aluminum layers and the nanolaminate has an alumina layer at both ends. It is therefore important to note that after the deposition of an alumina layer, it is necessary to wait a little until the target surface is clean again before depositing the aluminum. All the technical steps necessary to deposit a nanolaminate are explained in details in the appendix D.

Moreover, with the sputtering technique, the thickness depends on the width; this is due to shading effects because of the sputtering angle. This is illustrated in Fig. 2.11.

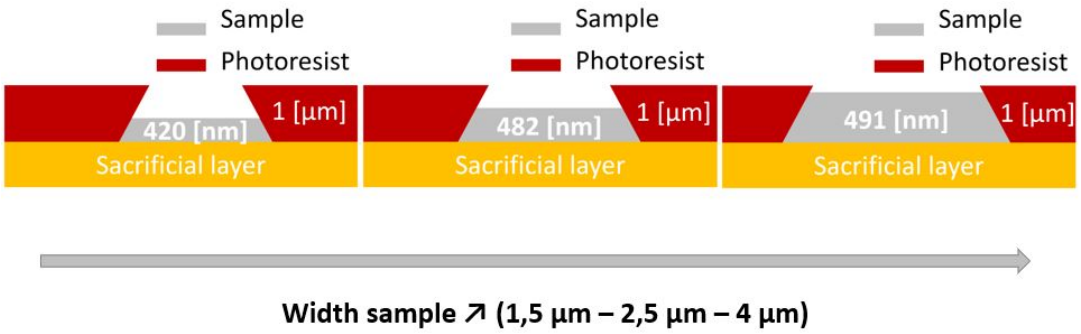

Figure 2.11: Sputtering method : variation of the thickness as a function of the width of the specimen beam (the illustrated sample is the first lab on-chip studied sample of this work)

It is however important to note that the depositions are made with a power of 300 W when a current of 300 mA is required. This may have distorted the deposited thicknesses but the FIB image (presented in Fig. 3.33 in section 3.2.3) shows that this error did not have much impact on our depositions, fortunately.

Lift-off to take off the photoresist and the deposition of the nanolaminate over it

The sample must be cleaned with acetone and then placed in a beaker with 200 mL of acetone, placed in the ultrasound at 37 Hz, maximum power for about ten minutes. To remove the sample from the beaker, it is necessary to leave it continuously under acetone and methanol

until it is dried with nitrogen gun.

Thickness of the specimen beams

The thickness of the specimen beam is important to know for the stress calculations (see section 2.2.5). It is measured by profilometry since it is a non-transparent material [9].

XeF_2 release

The release allows to etch the silicon and to remove the sacrificial layer under the specimen beams and the actuators to allow the tensile test. A first big pulse of XeF_2 is done to start the etching everywhere and make it homogeneous and then small pulses are done to avoid over etching. The technical steps to perform a release are explained in details in the appendix E.

Moreover, one can note that it is better to over-etch than to under-etch because under-etching is the same as not releasing the structures but in both cases, the length of the actuator is modified which can alter the calculations afterwards.

Thickness of the silicon nitride

The thickness of the silicon nitride is also important to know for the stress calculations (see section 2.2.5). It is measured by ellipsometry since it is a transparent material [9].

SEM measurements

To obtain the evolution of the stress with the strain, it is necessary to measure the displacement of the 2 µm wide cursors connected to the specimen beams as shown in Fig. 2.12.

SEM pictures are taken with 2 keV, x10k magnification, a working distance of 5 mm and 1024x768 image resolution. It should be noted that the displacement measurement is not perfect. One pixel represents 11 nm and there may be some error due to the pixels, the way of calculating the displacement, the quality of the cursors; this is taken into account in the propagation of the errors explained in section 2.2.8.

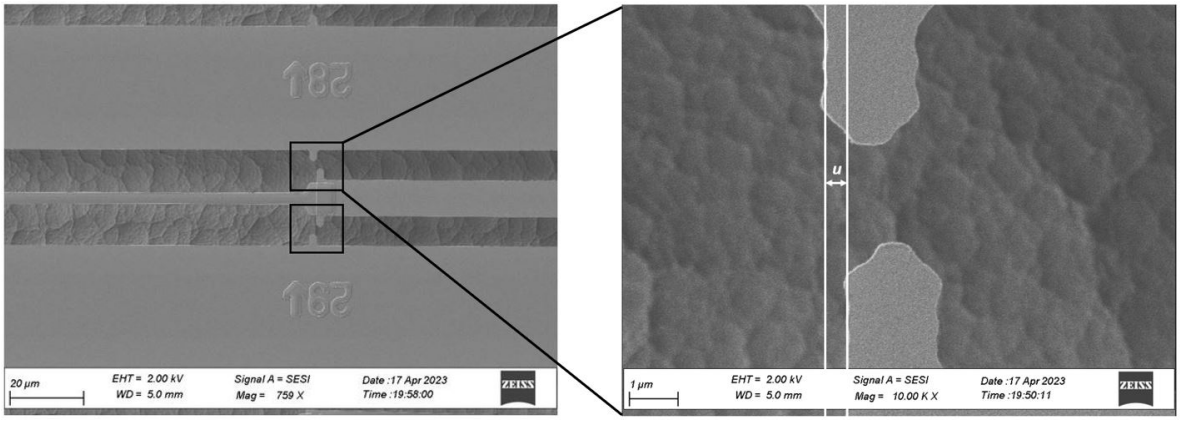

Figure 2.12: Cursors with a displacement u

Finally, since each sample has a different thickness and release start because a big pulse is not always enough to start the etching, these are presented for each sample in section 3.

2.2.4 General information about the structures

Each set of structures is described according to a certain nomenclature: "BX Y Z", where X is the width of the actuator in µm, Y the width of the specimen beam in µm and Z the length of the specimen beam in µm.

Specimen beam length

Concerning the size of the specimen beams, the shortest samples are those where the strain is the greatest because they have fewer defects. It is important to be careful with these specimen beams because the dogbone is much more important. Indeed, since the dogbone is not taken into account in the calculations, the calculated stress and strain are not the most correct because the deformation also takes place in the dogbone and the specimen beams are actually longer. However, the deformation in this dogbone is lower because it is wider and thicker by the sputtering deposition because it is wider.

The longest specimen beams are used to have the lowest strains and thus the elastic behavior. These are the 400 and 800 micron structures.

For the same type of structure, all specimen beams have the same length; it is the size of the actuator that varies. A structure with a longer actuator therefore results in bigger displacements.

Specimen beam width

The wider structures for the same length give more accurate points for stress because the error on the width (presented in section 2.2.8) is smaller. In addition, the wider structures can sustain more stress than the narrower ones, so the narrower ones are more interesting because the stress concentration is bigger, which can cause failure in the specimen beam and not at the overlap.

Dogbone

The dogbone is 8 microns wide for all structures except the 0.75 µm wide structures where it is 4 microns wide. The presence of the dogbone favours uniaxial tension but also reduces the stress concentration at the overlap between the specimen beam and the actuator [16]. It is important to note that the calculations described in section 2.2.5 do not take into account the dogbone and consider the specimen beam as a perfect rectangle. The effects of the dogbone are more important for structures smaller in length.

2.2.5 Calculations to obtain the true stress-strain curve

The raw data from LOC tensile tests are the displacement measurements of the cursors. Here are the different steps to obtain the true stress and strain within the beam specimen.

First, the total strain equation into the specimen beam can be written by Eq. 2.14 [25].

$$\epsilon_{tot} = \ln\left(\frac{L_s + u}{L_s}\right) = \epsilon_{mech} + \epsilon_{mis_s} \tag{2.14}$$

Where ϵ_{tot} is the total strain in the specimen beam, ϵ_{mech} is the mechanical strain and ϵ_{mis_s} is the strain due to the mismatch of the sample.

The true mechanical strain is therefore given by Eq. 2.15.

$$\epsilon_{true} = \ln\left(\frac{L_s + u}{L_s}\right) - \epsilon_{mis_s} \tag{2.15}$$

Where u is the displacement of the cursors and L_s the length of the specimen beam.

For the stress, one has to divide the force in the actuator by the cross-section of the specimen beam.

$$\sigma_{eng} = \frac{F}{S_s} \tag{2.16}$$

$$= \frac{\sigma_{eng_a} S_a}{S_s} \tag{2.17}$$

$$= \frac{E_a S_a}{S_s}\left(\frac{-u}{L_a} - \epsilon_{mis_a}\right) \tag{2.18}$$

$$\sigma_{true} = \frac{E_a S_a}{S_s}\left(\frac{-u}{L_a} - \epsilon_{mis_a}\right) * e^{\epsilon_{true}} \tag{2.19}$$

Where u is the displacement of the cursors, E_a is the Young's modulus of the actuator material, S_a the section of the actuator material, L_a the length of the actuator material, S_s the section of the specimen beam. The mismatch is defined as positive if the sample is in compression and negative in tension.

The numerical values related to the material actuator are in Table 2.1 :

Material	**Young's modulus [GPa]**	**Internal stress [GPa]**	**Mismatch [-]**
Si_3N_4	250	1	$3.3 * 10^{-3}$

Table 2.1: Mechanical properties about the silicon nitride

Thickness and width measurements and mismatch of the deposited sample are necessary to determine the stress and strain. But all these values are sources of measurement errors. An error propagation study is therefore performed and presented in the section 2.2.8.

2.2.6 Behavioural line

It is also interesting to represent the force-displacement evolution during the release, corresponding to the actuator and the specimen beam.

First, concerning the actuator, the Eq. 2.20 defines the free displacement of the actuator due to its mismatch and the Eq. 2.21 gives the initial force in the actuator, also due to the mismatch [25].

$$u_{free} = \frac{L_a}{\epsilon_{mis_a}} \tag{2.20}$$

$$F_0 = E_a S_a \epsilon_{mis_a} \tag{2.21}$$

For the sample, its initial force is due to internal stresses and given by Eq. 2.22. Assuming a purely elastic behavior, its maximum force is related by its maximum strain by Hooke's law and is given by Eq. 2.23. The maximum strain is given by Eq. 2.24. Finally, the maximum displacement is given by Eq. 2.25.

$$F_{0_s} = \sigma_{int} S_s \tag{2.22}$$

$$F_{max_s} = E_s S_a \epsilon_{max} \tag{2.23}$$

$$\epsilon_{max} = \frac{\sigma_y}{E_s} \tag{2.24}$$

$$u_{max} = (\epsilon_{max} + \epsilon_{mis_s}) * L_s \tag{2.25}$$

Thus, a typical graph of the evolution of displacement force is shown in Fig. 2.13.

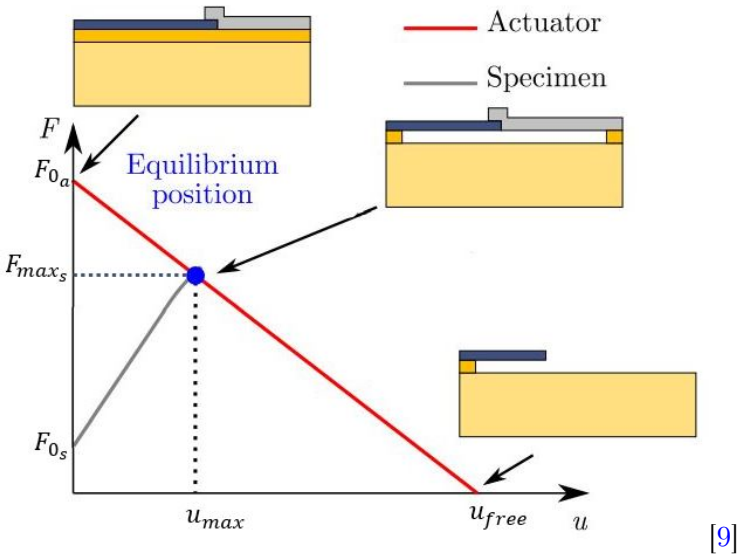

[9]

Figure 2.13: Force-displacement evolution for an actuator in red and the specimen beam in dark gray

If a relaxation process takes place, the evolution of force versus displacement for the actuator and specimen beam is shown in Fig. 2.14. A long as relaxation occurs, the force decreases and the displacement increases.

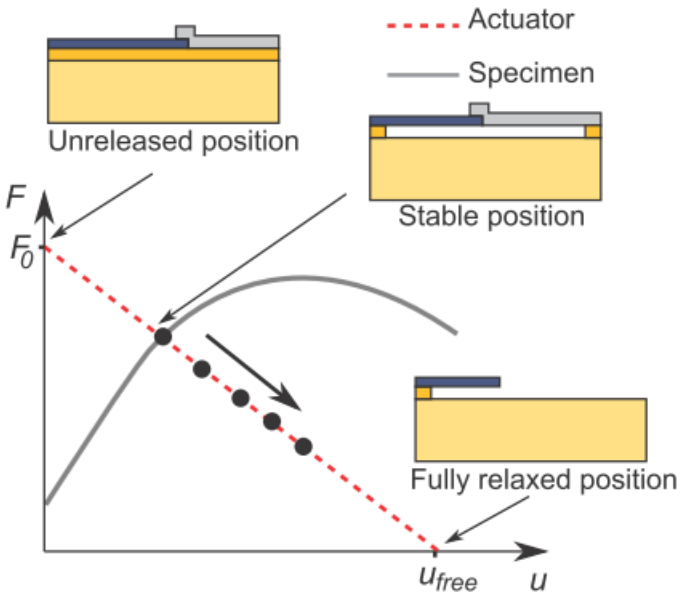

[9]

Figure 2.14: Evolution of the force as a function of the displacement for the actuator and the specimen beam with the equilibrium point reached during the relaxation process

2.2.7 Calculation of the mismatch of the sample

Some structures allow to calculate the mismatch. Indeed, these structures are composed of actuators and specimen beams composed of the deposited nanolaminate. It is therefore possible to obtain the mismatch of the nitride and the nanolaminate. The silicon nitride is well known in the laboratory and its mismatch is also well known, as noted in the Table 2.1. These structures are therefore used to know the mismatch of the nanolaminate.

Assuming a purely elastic strain, one can express the force in the specimen beam by Eq. 2.26.

$$F = S_s E_s \left(\ln \left(\frac{L_s + u}{L_s} \right) - \epsilon_{mis_s} \right) \tag{2.26}$$

For the actuator, one has Eq. 2.27.

$$F = S_a E_a \left(\ln \left(\frac{L_a - u}{L_a} \right) - \epsilon_{mis_a} \right) \tag{2.27}$$

Combining Eq. 2.26 and Eq. 2.27, and equating the Young's modulus of the specimen material and the actuator material, one has the expression of the mismatch ϵ_{mis_s} by Eq. 2.28 [25].

$$\epsilon_{mis_s} = \frac{S_s \ln \left(\frac{L_s+u}{L_s} \right) - S_a \ln \left(\frac{L_a-u}{L_a} \right)}{S_s - S_a} \tag{2.28}$$

On the other hand, the thickness of the actuator and the specimen are not calculated, only the width is taken into account in the section. However, as the thickness is not the same

for the actuator and for the specimen beam due to the sputtering of the nanolaminate, this simplification of calculation is not completely correct.

Therefore, another method is used. It is also possible to take a structure where the actuator has broken. Indeed, in this case, the mismatch is calculated as follows:

$$\epsilon_{mis_s} = \frac{u}{L_s}$$

But care must be taken with these measurements, if the cursors are no longer in the same plane, the displacement measurement is wrong and so is the mismatch.

2.2.8 Propagation of the errors

In the calculations used to obtain the stress-strain curve of the LOC, several variables are sources of error. These are the displacement measurements of the cursors, the thickness, the width and the mismatch. The equations Eq. 2.29 and 2.30 allow to obtain the error bar on the stress and strain:

$$\Delta\epsilon_{true} = \frac{\Delta u}{L_s} + \Delta\epsilon_{mis_s} \tag{2.29}$$

$$\frac{\Delta\sigma_{true}}{<\sigma>} = \frac{\Delta u}{<u>} + \frac{\Delta w_s}{<w_s>} + \frac{\Delta t_s}{<t_s>} \tag{2.30}$$

Where Δx represents the standard deviations of x and $< x >$ the mean of x.

Specimen beam mismatch

As explained in the section 2.2.7, the sample mismatch is calculated using 3 structures where the actuator broke. The mean and standard deviation are therefore simply calculated based on the 3 calculated values.

Specimen beam section

The sputtering gives a dome-shaped section. It is therefore difficult to measure this section. According to the profilometer measurements, a standard deviation of 5 nm is chosen for the thickness. For the width, the two limits are represented in Fig. 2.15b:

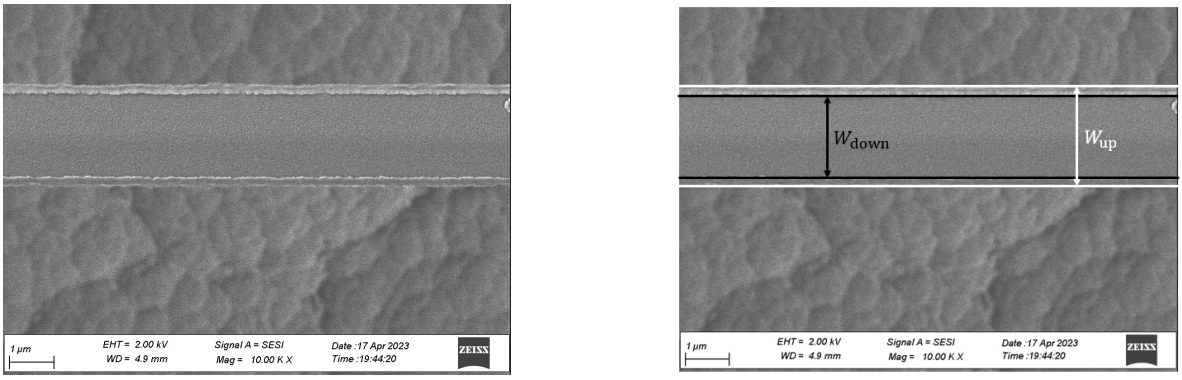

(a) Thickness of one specimen beam

(b) Bounds for the thickness

Figure 2.15: Thickness measurement of one specimen beam

To correct the error on the section, which is huge, one has to make a nice FIB cut and calculate the perfect section.

Displacement

This error takes into account both the quality of the SEM images and the fact that one user or another could take two different measurements depending on how they measure this displacement. A standard deviation of 33 nm is chosen, which corresponds to an error of three pixels. The average of the measurements is the average between the two displacement measurements of the cursors on both sides of the specimen beam as shown in Fig. 2.12.

These error bars are represented in each of the graphs. They cause an error of about 30 % on the Young's modulus.

In appendix G, the contributions of the error sources related to the SEM measurements and the section are shown separately to see the impact of each of them. The error bars represent the error on the SEM measurements and the coloured areas represent the error on the section.

2.2.9 Advantages and disadvantages of the lab on-chip technique

Firstly, this technique avoids misalignment and thus has a pure uniaxial tension since no external loading is required. Moreover, large strains are possible [20] [18]. It also allows the testing of a lot of specimens providing a statistical information and to deform for a long time without monopolising any external loading device. Furthermore, it allows to reach strain rates lower than 10^{-6} s^{-1} [9].

The displacement measurement is carried out using a SEM, which brings errors in accuracy because of the resolution of the pictures or the resolution of the lithography for the cursors shape. In addition, the measurement is not immediate after release but only after about one hour. This can be a problem if the material tends to relax. Furthermore, during etching, the selectivity must be high enough to maintain the dimensions of the specimen beams and the actuator. The adhesion between these two beams must also be sufficient for the measurement to proceed properly [20]. The mismatch of the sample and the cross-section of each set of structures is also not so easy to obtain accurately, which adds an error on the final results.

2.3 Tensile test on polymer

This test allows to obtain a stress-strain curve of the thin film but also the fracture toughness.

2.3.1 Preparation

The polymer used for this tensile test is kapton. It has a Young's modulus of 3.5 GPa and a thickness of 13 µm *(Private communication - Marie-Stéphane Colla)*. The polymer sheet is cut with a punch, to obtain the following geometry. Dimensions are indicated in mm:

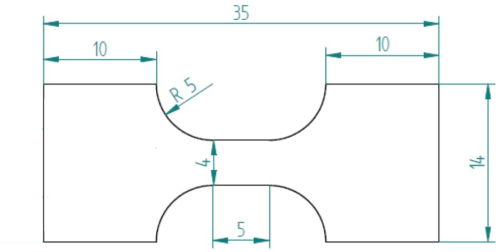

Figure 2.16: Kapton polymer for the tensile test on polymer (dimensions in mm)

The dogbone is chosen to take the forces in the jaws of the traction machine. Four samples are deposited on a wafer with sticky kapton paper.

The deposited sample is described in the section 3.3.1.

2.3.2 Experimental conditions

The test is performed at room temperature, with the Gatan micro testing machine. The maximum force is 2 kN and the displacement speed is set at 0.1 mm/min. During the test, the raw data are the displacement between the jaws and the force. The test is performed under an optical microscope, which allows to obtain a video of the test. This allows to obtain the real displacement within the material and not just between the jaws, by measuring the distance between 2 fixed points of the sample, every 10 seconds. The resolution of the microscope is 2880x2160 pixels with a magnification of x100.

2.3.3 Stress-strain curve and fracture toughness determination

The stress-strain curve of the polymer and the sample is obtained as follows, after subtracting the initial force within the jaws.

$$\epsilon_{true} = \ln \frac{L}{L_0} \tag{2.31}$$

$$\sigma_{true} = \sigma_{eng}(1 + \epsilon_{eng}) \tag{2.32}$$

With

$$\sigma_{eng} = \frac{F}{S} \tag{2.33}$$

$$\epsilon_{eng} = \frac{L - L_0}{L_0} \tag{2.34}$$

Where σ is the stress, ϵ the strain, F the force, L the length and L_0 the initial length.

To know the contribution of the thin film only, the force-displacement curves of the polymer and the polymer with the sample are plotted. The polymer curve is subtracted and then the stress is obtained by dividing the force by the thin film section.

The toughness can be obtained by knowing the stress and the strain corresponding to the propagation of the first crack. Actually, thanks to the video from the optical microscope, the fracture stress and the fracture strain can be obtained. Then, assuming the film behaves as linear elastic, the toughness is determined by Eq. 2.35 and 2.36 :

$$G_c = Z\frac{\sigma_f^2 t_f}{E'_f} \tag{2.35}$$

$$G_c = Z\epsilon_f^2 t_f E'_f \tag{2.36}$$

Where Z is a coefficient depending on two Dundurs parameters α and β, E'_f is equal to $\frac{E_f}{1-\nu^2}$, with E_f the Young's Modulus of the film extracted by nanoindentation, ν is the Poisson ratio, ϵ_f is the fracture strain, σ_f is the fracture stress and t_f is the thickness of the film [1] [15]. But this formula assumes an infinite substrate with stationary cracking, which is not the case here. One should know the initial crack length but it is not the case. This formula is therefore not the best for having toughness [33].

Chapter 3

Preparation of the samples, experiments and results

This chapter covers all the experiments carried out in this work. The first sample analysed is reserved for the nanoindentation tests. The sample preparation is presented, followed by the tests performed with the CSM method, the QS method and the Paul Baral's method, with their experimental conditions and results.

Then, three lab on-chip tests are detailed. For each of them, the choice of the sample thickness is explained, followed by the way the release is carried out. A few words about the structures studied are given and finally the results are presented.

Finally, the tensile tests on polymer are presented with first the choice of the nanolaminate thickness, the observations before and after the test and the results.

3.1 Nanoindentation

3.1.1 Deposition of a nanolaminate 100 nm Al_2O_3 10 nm Al x5

As mentioned in section 1.2, the most tough, ductile and hard materials are the nanolaminated materials 100 nm Al_2O_3 10 nm Al . To keep the effect of multilayer and a thin film at the same time, one deposits 4 bi-layers of 100 nm of alumina and 10 nm of aluminum followed by a last layer of alumina. The last layer of alumina is there to keep an alumina sample; the goal of the aluminum being rather to interrupt the alumina. The deposition times are 9 min for alumina and 1.5 min for aluminum.

3.1.2 Thickness

In order to deposit the next nanolaminates, it is better to know it deposits the desired thickness. Therefore, a cross section of the nanolaminate is observed with the SEM. This gives a thickness of 750 nm but it is not very accurate, while the total thickness should be 540 nm. Based on this information, for the next sample to deposit, the speed of deposition and the time of deposition

are taken as a ratio of about 2/3 to the previously used. The precise times are indicated for each sample in the following sections.

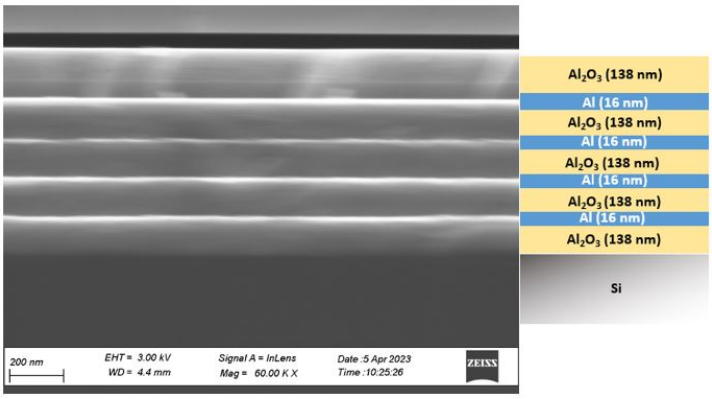

Figure 3.1: Transverse section of the nanolaminate deposited for the nanoindentation

3.1.3 Constant strain rate : test 1 and quasi-static mode

The constant strain rate test is performed on a 4x4 indents array, spaced 50 µm apart, with a penetration depth of 500 nm and at a loading strain rate $\dot{F}/F$ of 0.05 s^{-1}. The maximum allowed thermal drift is set to 0.05 nm/s, the approach speed to 10 nm/s and the detection limit to 100 N/m.

For the quasi-static mode, the test is performed on a 4x4 indents array, spaced 50 µm apart, with a penetration depth of 500 nm. The maximum allowed thermal drift is set to 0.05 nm/s, the approach speed to 10 nm/s and there are five times to load.

Moreover, as mentioned in section 1.2.4, laboratory experiments show that electron beam irradiation in dynamics changes the mechanical response of a material. Indeed, the push-to-pull method is performed with a TEM (200 keV) for in-situ tensile tests and it is observed that the mechanical response of the material changed, depending on whether or not the electron beam is used to observe the sample in the TEM. Exposure to the beam would accelerate the kinetics of the material and thus allow it to reach larger strains. Thus, the goal of this experiment is to determine if static irradiation already has an impact on the material properties. These nanoindentation tests are thus carried out on a part of non-irradiated sample and irradiated by 30 keV at SEM.

Observations

Here are the observations of the indents made in the SEM, with an electron beam of 3 keV, a working distance of 10 mm and a magnification of x1k and x10k. In the calculations, the Oliver-Pharr method (Eq. 2.6 explained in the section 2.1.3) is used. Indeed, since the edges of the trace are straight, it is more likely to be a sink-in phenomenon. Moreover, the imprint is nice and does not show any cracks, as can be seen in Fig. 3.3.

Figure 3.2: CSR test on Al_2O_3-Al 138-16 nm x5: Indents 4x4 matrix

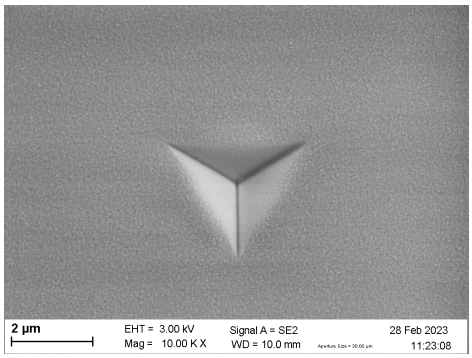

Figure 3.3: CSR test on Al_2O_3-Al 138-16 nm x5 : Zoom of one indent

Results

Here are the results obtained using the formulas in section 2.1.3. Firstly, one can say that there is nearly no difference between the irradiated and non-irradiated indents. These results show for $h_c = 50$ nm, a film Young's modulus of 142 GPa, an apparent Young's modulus of 152 GPa and a hardness of about 7 GPa. The strain rate $\frac{\dot{h}}{h}$ is also illustrated in Fig. 3.7.

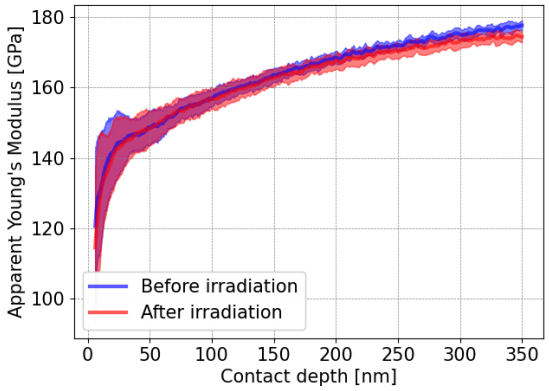

Figure 3.4: CSR test at 0.05 s^{-1} on Al_2O_3-Al 138-16 nm x5: Apparent Young's modulus as a function of the contact depth

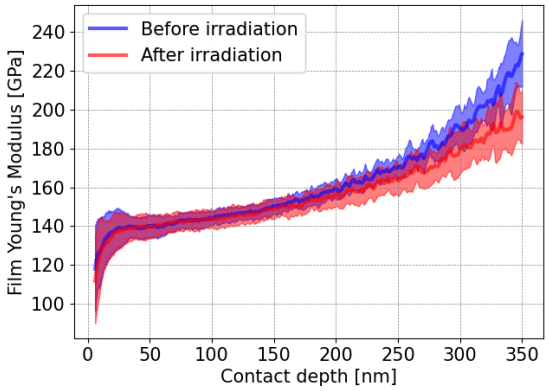

Figure 3.5: CSR test at 0.05 s^{-1} on Al_2O_3-Al 138-16 nm x5: Film Young's modulus as a function of the contact depth

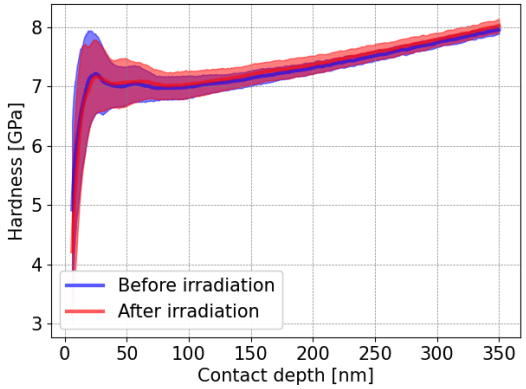

Figure 3.6: CSR test at 0.05 s^{-1} on Al_2O_3-Al 138-16 nm x5: Hardness as a function of the contact depth

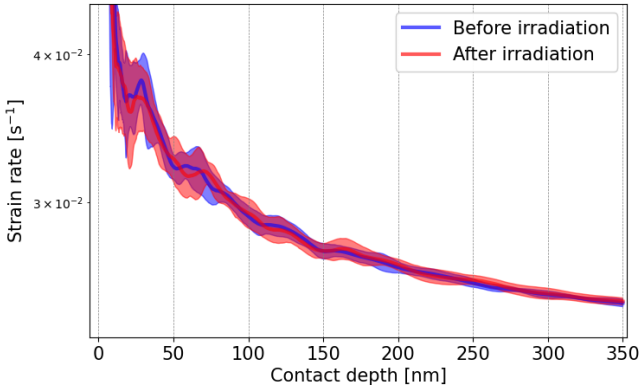

Figure 3.7: CSR test at 0.05 s^{-1} on Al_2O_3-Al 138-16 nm x5: Strain rate as a function of the contact depth

Regarding the quasi-static mode, Fig. 3.8, 3.9 and 3.10 present the results. Fig. 3.10 shows the Young's modulus as a function of the contact depth. The values found vary very strongly up to 300 GPa, which is not possible. In fact, thermal drift and viscoplastic phenomena could explain these distorted values. Indeed, in quasi-static mode, the strain rate is lower, which allows the material to evolve. The slope does not only correspond to an elastic response as in CSM mode, but also to a plastic response or/and a relaxation. The CSM method is therefore better for determining a modulus for example.

On the other hand, these results show that some things happen when the strain rate is slower. These errors in the modulus can be explained by the possible viscoplastic and viscoelastic behavior of the material. Indeed, Fig. 3.11 (d) schematises the load as a function of displacement if the material has viscous-elasto-plastic behavior and this is also observable in Fig. 3.9.

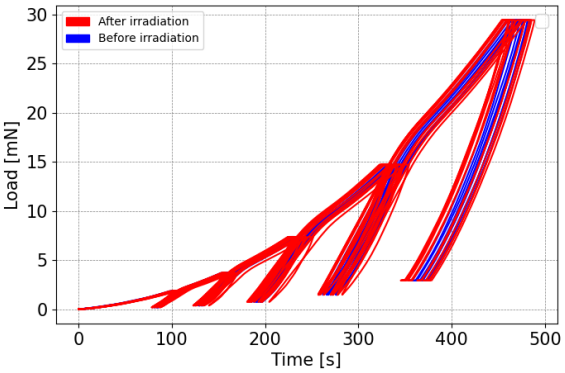

Figure 3.8: QS test on Al_2O_3-Al 138-16 nm x5: Load as a function of the time

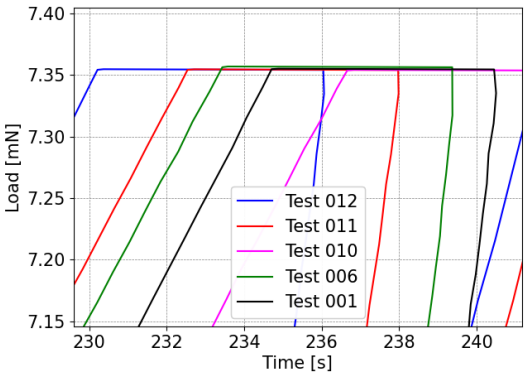

Figure 3.9: QS test on Al_2O_3-Al 138-16 nm x5: Load as a function of the time : zoom of the third unload

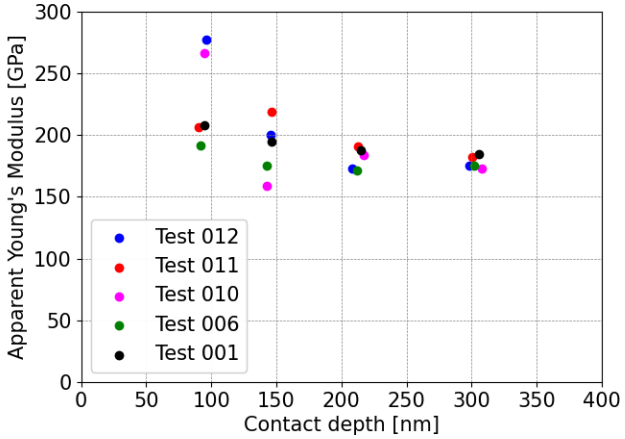

Figure 3.10: QS test on Al_2O_3-Al 138-16 nm x5: Young's modulus as a function of the contact depth

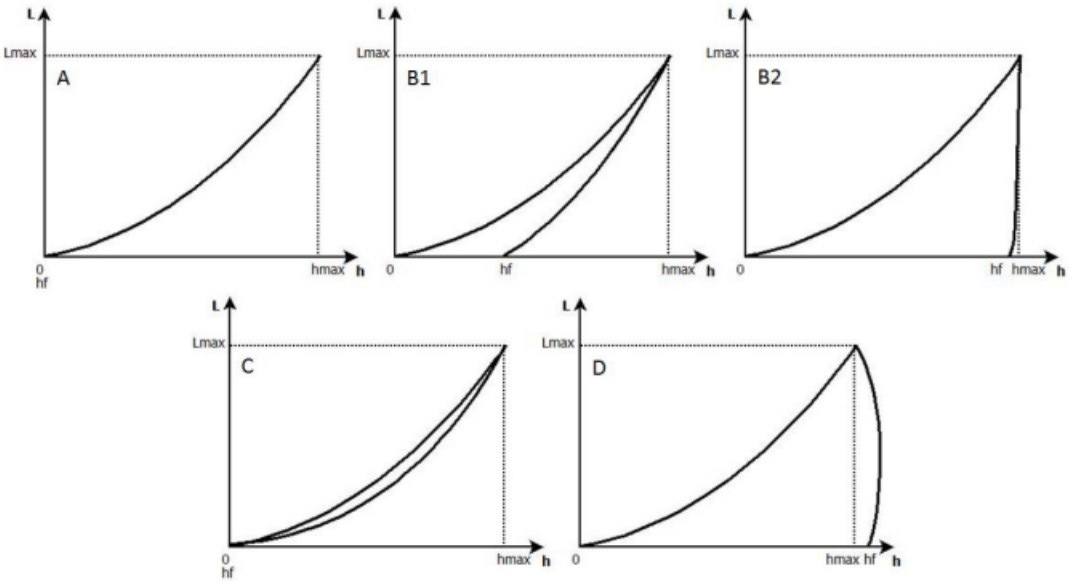

[24]

Figure 3.11: Load-displacement curve. (a) purely elastic; (b1) and (b2) elasto-plastic behavior with no change of hysteresis with strain rate; (c) viscous-elastic behavior; (d) viscous-elasto-plastic behavior

This is why relaxation tests are interesting to realise. Paul Baral's method is therefore performed as explained in the section 2.1.5.

Again, concerning the influence of irradiation, the results seem to show no change on the values of Young's modulus, hardness or strain rate. It should also be taken into account that the sample analysed is 500 nm thick while the samples analysed by TEM are only 30 nm thick.

3.1.4 Constant strain rate : test 2

The nanoindentation test is carried out on a matrix of 3x3 indents spaced 2 µm apart, with a penetration depth of 100 nm, for the following loading strain rates $\dot{F}/F$: 0.2, 0.1, 0.05, 0.02, 0.01, 0.005, 0.002 s^{-1}. The maximum allowed thermal drift is set to 0.05 nm/s. The approach speed is set to 10 nm/s and the detection limit is set to 100 N/m.

Results

Fig. 3.12, 3.13, 3.14 and 3.15 present respectively the evolution of the strain rate, the hardness, the apparent Young's modulus and the film Young's modulus as a function of the contact depth.

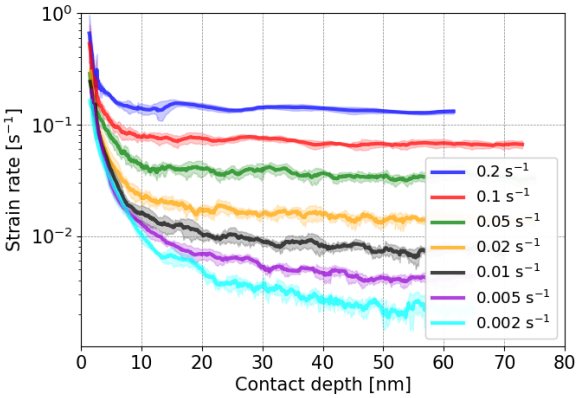

Figure 3.12: CSR test at different strain rates on Al_2O_3-Al 138-16 nm x5: Strain rate as a function of the contact depth

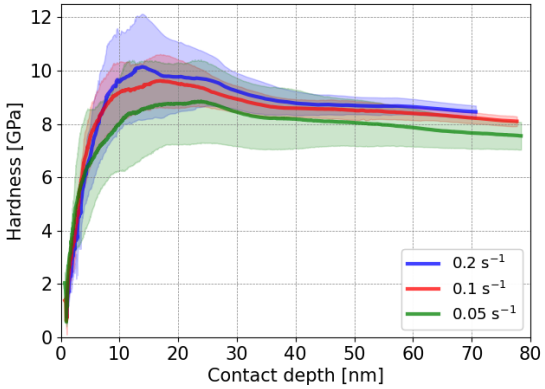

Figure 3.13: CSR test at different strain rates on Al_2O_3-Al 138-16 nm x5: Hardness as a function of the contact depth

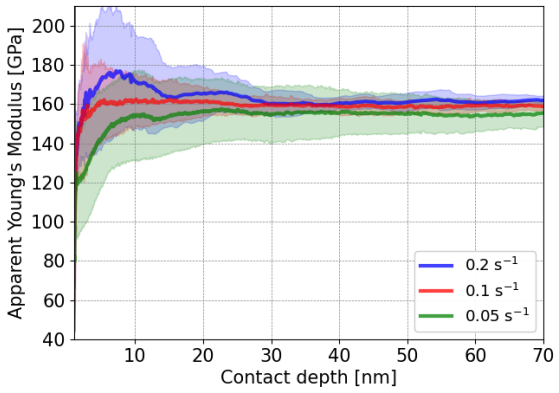

Figure 3.14: CSR test at different strain rates on Al_2O_3-Al 138-16 nm x5: Apparent Young's modulus as a function of the contact depth

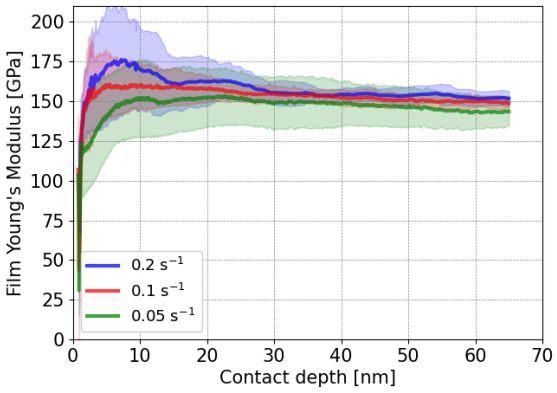

Figure 3.15: CSR test at different strain rates on Al_2O_3-Al 138-16 nm x5: Film Young's modulus as a function of the contact depth

In view of the Fig. 3.12, very low strain rates have difficulty in stabilising. Thus, it is decided to keep only the strain rates of 0.4, 0.2 and 0.05 s^{-1} as consistent results. These curves are

made on the basis of the calculations explained in section 2.1.3. Moreover, a correction of the contact area is made using the calibration given by the software. This correction is explained in the appendix A and shows that it is not necessary for the strain rates considered hereafter and in the following experiments.

For a contact depth of 50 nm, the hardness obtained is about 8 GPa, for 0.05 s^{-1}, the Young's modulus obtained is 155 GPa and the film modulus is 145 GPa.

Moreover, the hardness and Young's modulus change as a function of the strain rate; this shows a viscoplastic and viscoelastic character respectively.

It is also interesting to plot the hardness as a function of the strain rate as shown in Fig. 3.16. Considering the three strain rates studied, the slope of this graph represents the strain rate sensitivity as explained by Eq. 2.9 in section 2.1.3. The strain rate sensitivity coefficient m found is 0.06.

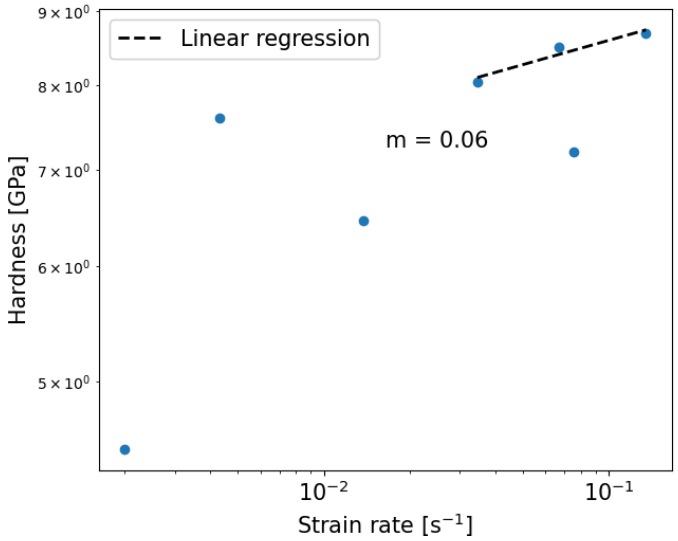

Figure 3.16: CSR test at different strain rates on Al_2O_3-Al 138-16 nm x5: Hardness as a function of the strain rate

However, Fig. 3.13 shows that the hardness does not seem to remain constant with depth and the Young's moduli have two plateaus instead of one. The tests are performed on 100 nm of nanoindentation, which is not enough. Indeed, the hardness probably decreases due to a tip defect (Oliver-Pharr by Eq. 2.6 underestimates the contact area, and therefore the hardness and the moduli are overestimated). It should be seen to stabilise and then rise again because of the substrate effect (the hardness of the silicon is higher than that of the film). A second test is therefore carried out with a penetration depth of 200 nm.

3.1.5 Constant strain rate : test 3

An array of 4x4 indents, spaced 2 µm apart with a penetration depth of 200 nm is made, for the following loading strain rates $\frac{\dot{F}}{F}$: 0.4, 0.2, 0.1, 0.05, 0.03 s^{-1}. These strain rates are not too low to limit thermal drift problems and they are sufficiently numerous for the linear regression to obtain a strain rate sensitivity coefficient.

The maximum thermal drift allowed is set at 0.03 nm/s to obtain better results than the previous one. The approach speed is set at 5 nm/s. It may have been too high (10 nm/s), which could cause or increase overshoot of the load and thus distort the hardness. This may also stabilise the strain rate which was not stabilised quickly. The detection limit is set to 200 N/m while it was set to 100 N/m to make sure that the material to indent is well detected.

Results

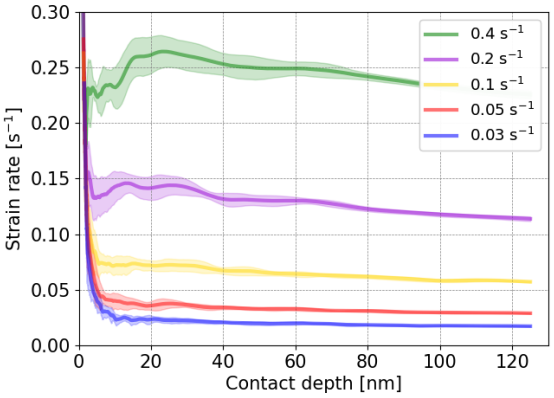

Figure 3.17: CSR test at different strain rates on Al_2O_3-Al 138-16 nm x5: Strain rate as a function of the contact depth

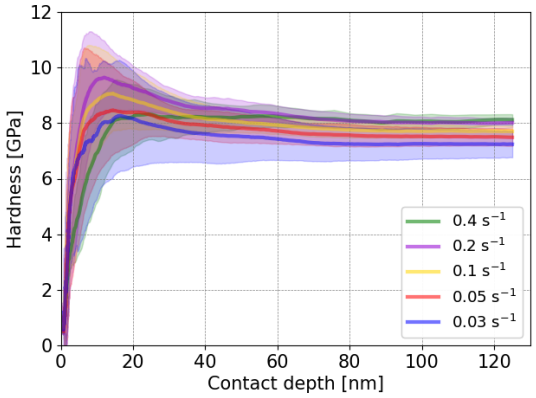

Figure 3.18: CSR test at different strain rates on Al_2O_3-Al 138-16 nm x5: Hardness as a function of the contact depth

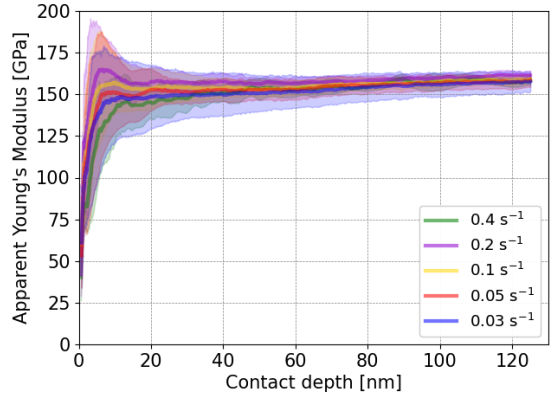

Figure 3.19: CSR test at different strain rates on Al_2O_3-Al 138-16 nm x5: Apparent Young's modulus as a function of the contact depth

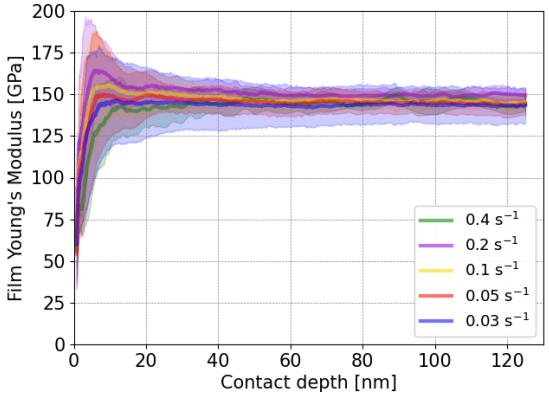

Figure 3.20: CSR test at different strain rates on Al_2O_3-Al 138-16 nm x5: Film Young's modulus as a function of the contact depth

Results are presented in Fig. 3.17, 3.18, 3.19 and 3.20.

For a contact depth of 100 nm, the apparent Young's modulus is 157 GPa, the film modulus is 147 GPa and the hardness is 7.5 GPa. The contact depth is taken at 100 nm because this is where the hardness starts to stabilise well. Before that, it has a peak, probably due to the tip defect in part which underestimates the contact area and therefore overestimates the hardness and Young's modulus.

As with the previous experiment, for the different loading strain rates, the Young's modulus increases as the strain rate increases; this corresponds to a slight viscoelastic effect. Also, the hardness increases with increasing strain rate; this corresponds to a viscoplastic effect.

Plotting the hardness versus the strain rate in Fig. 3.21, the strain rate sensitivity coefficient is 0.04.

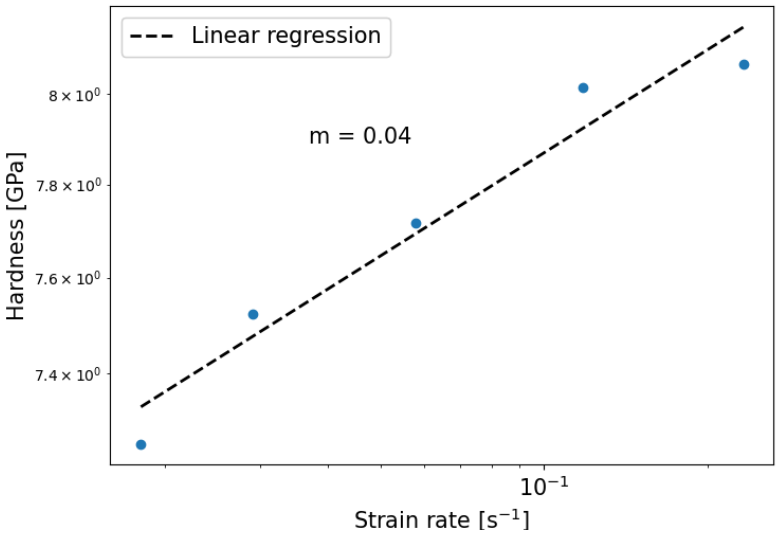

Figure 3.21: CSR test at different strain rates on Al_2O_3-Al 138-16 nm x5: Hardness versus strain rate curve in a log-log scale (all tests)

Moreover, from this test which is the most reliable test in the continuous stiffness mode, it is also possible to find the strain at which the material would plasticize ϵ_{pl} by Eq. 3.1:

$$\epsilon_{pl} = \frac{\sigma_y}{E} \tag{3.1}$$

With

$$\sigma_y = \frac{H}{2.3} \tag{3.2}$$

With a hardness of 7.5 GPa, a modulus of 147 GPa, one has a plastic strain of 2.3%.

3.1.6 Paul Baral's Method : test 1

As the previous tests have shown, the material seems to be sensitive to the strain rate. Therefore, the Paul Baral's technique is used. A penetration depth of 50 nm is imposed. The strain rate target $\dot{F}/F$ is set to 0.03 s^{-1}, the stiffness stop to 63500 N/m, the stiffness hold to 65000 N/m for 7200 s, the surface approach to 10 nm/s and the thermal drift to 0.02 nm/s.

Results

The load as a function of the time is shown in Fig. 3.22 and in Fig. 3.23 in a log scale and by separating all the points in several classes to avoid the noise of the measurements as explained in section 2.1.5. Fig. 3.22 shows a decay which would correspond to the relaxation of the material and thus to a time-dependent behaviour. The data are taken up to 1200 seconds because beyond that, the depth (displacement into surface) becomes negative, as if the tip is rising higher than the surface. As explained in the section 2.1.5, by plotting the representative stress versus representative strain rate shown in Fig. 3.24, the strain rate sensitivity coefficient is 0.1. The CSR test which gives a strain rate sensitivity coefficient of 0.04 is also represented.

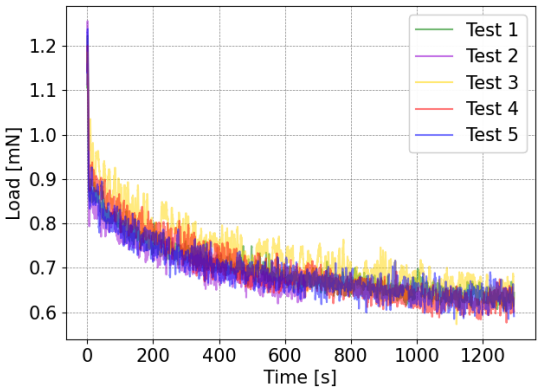

Figure 3.22: Baral's method on Al_2O_3-Al 138-16 nm x5: Load as a function of the time

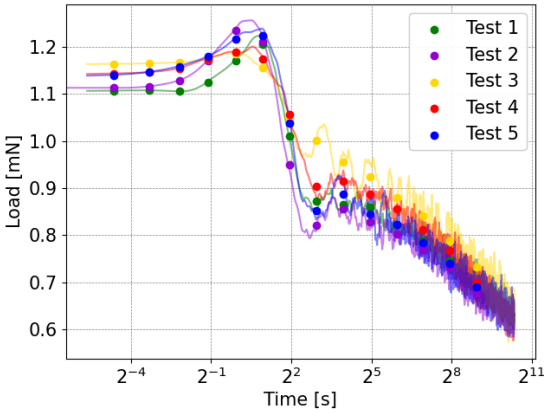

Figure 3.23: Baral's method on Al_2O_3-Al 138-16 nm x5: Load as a function of the time in a log scale

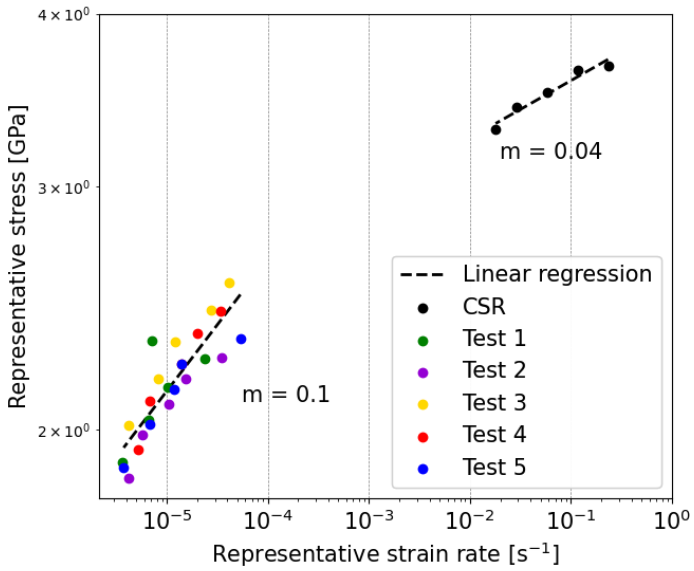

Figure 3.24: Baral's method on Al_2O_3-Al 138-16 nm x5:
Representative stress versus representative strain rate curve in a log-log scale

This first test with Paul Baral's method should be taken with caution, as the load rises again after 1200 seconds and the displacement h becomes negative. Moreover, there is an overshoot of the load at the very beginning, at the contact with the material. Therefore, several other tests are performed.

3.1.7 Paul Baral's Method : test 2

First of all, the tests are performed at night, thinking that there would be less thermal drift. But this does not help. Then, different parameters are modified and finally, a good test is obtained on 5 indents with a space between indents of 4 µm, with the following parameters: the penetration depth is set to 50 nm, the strain rate target $\dot{F}/F$ to 0.01 s^{-1}, the stiffness stop to 119500 N/m, the stiffness hold to 120000 N/m for 7200 seconds, the surface approach to 5 nm/s and the thermal drift to 0.02 nm/s.

Results

The load as a function of the time is shown in Fig. 3.25 and in Fig. 3.26 in a log scale and by separating all the points in several classes to avoid the noise of the measurements as explained in section 2.1.5.

As explained in the section 2.1.5, by plotting the representative stress versus representative strain rate shown in Fig. 3.27, the strain rate sensitivity coefficient is 0.24. The CSR test which gives a strain rate sensitivity coefficient of 0.04 is also represented.

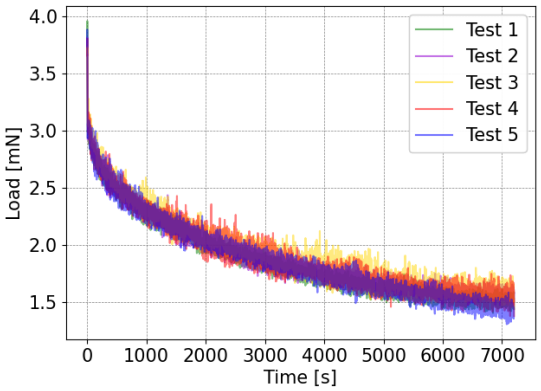

Figure 3.25: Baral's method on Al_2O_3-Al 138-16 nm x5: Load as a function of the time

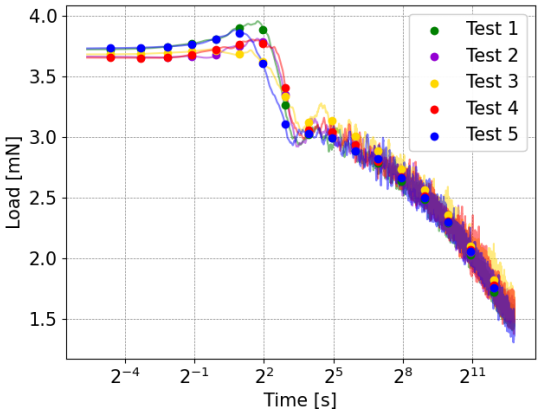

Figure 3.26: Baral's method on Al_2O_3-Al 138-16 nm x5: Load as a function of the time in a log scale

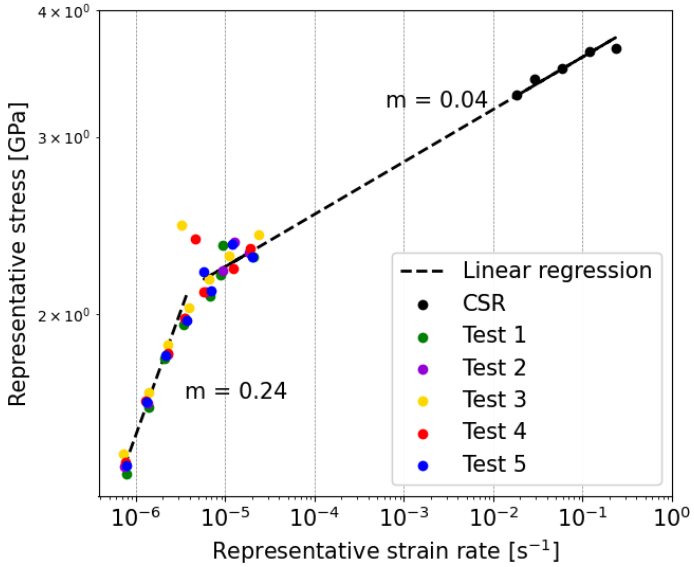

Figure 3.27: Baral's method on Al_2O_3-Al 138-16 nm x5: Representative stress versus representative strain rate curve in a log-log scale

Firstly, one can say that this test is more reliable than the first one since the load continuously decreases as a function of the time, the displacement is not negative anymore and the overshoot of the load is smaller. By Fig. 3.27, one can observe the strain rate sensitivity coefficient for low strain rates equal to 0.24. For higher strain rates, it is rather 0.04, found by the constant strain rate method.

A further test shows that it is the stiffness hold that fixed the problem. If these values are below 100000 N/m, the load always rises.

3.1.8 Conclusion about the nanoindentation tests

The first tests with constant strain rate allowed to determine a hardness, a Young's modulus of the film, the apparent modulus and the strain rate sensitivity coefficient. The values are shown in the following Table 3.1:

Mechanical properties	**CSR 1**	**CSR 2**	**CSR 3**
Apparent Young's modulus [GPa]	152	155	157
Film Young's modulus [GPa]	142	145	147
Hardness [GPa]	7	8	7.5
Strain rate sensitivity coefficient [-]	/	0.06	0.04

Table 3.1: Mechanical properties obtained by the nanoindentation tests

These tests also showed that the strain rate influenced the hardness and the Young's modulus of the material, showing a viscoplastic and viscoelastic character respectively. The quasi-static test also showed this behaviour.

Also tests with the Paul Baral's method are performed to find the strain rate sensitivity coefficient for lower strain rates. However, it is still important to note that the second test is the more reliable as explained in the previous section.

Mechanical properties	**Baral's method 1**	**Baral's method 2**
Strain rate sensitivity coefficient [-]	0.1	0.24

Table 3.2: Mechanical properties obtained by the nanoindentation tests

Moreover, these different tests following the CSR method and Paul Baral's method show different strain rate sensitivity coefficients depending on whether the strain rate is higher or lower.

3.2 Lab on-chip

3.2.1 Sample 85-10 nm x5

Choice of the thickness and deposition of the nanolaminate

As already mentioned in section 1.2, one of the purposes of the LOC tensile tests is to observe plastic strain. The thinner specimen beams are by consequence better to analyse.

However, Sahar Jaddi's samples show that the samples of about 200 nm of thickness (50-20 nm x3) break at the overlap. Actually, some of the structures are studied at the beginning of this work and the results are in the appendix F.1.

A sample of about 350 nm (50-20 nm x5) from Sahar Jaddi is also analysed at the beginning of the work. The results are in appendix F.2 and show that the nanolaminate seems to break in a brittle way and that the sample relaxes with time.

The first sample deposited is of a desired thickness of about 500 nm to prevent it from breaking on the overlap. It is composed of 5 alumina/aluminium bilayers of 85-10 nm respectively. It is deposited according to the conditions cited in the section 2.2.3. The deposition times are 6 minutes for alumina and 1 minute for aluminium.

Then the lift off is performed according to the section 2.2.3. Table 3.3 shows the different thicknesses of the nanolaminate according to the width. Some of them are higher than the deposited thickness, it is probably a question of errors in the measurements, probably due to dross.

Material	Thickness [nm]
Nanolaminate	460
Nanolaminate 8 µm Wide	518
Nanolaminate 4 µm Wide	491
Nanolaminate 2.5 µm Wide	482
Nanolaminate 1.5 µm Wide	420

Table 3.3: Thickness of the specimen beams

Release

The etching does not start after the first pulse of about 10 seconds. A second pulse is necessary, from the remaining 150 Pa and after 2-3 seconds the etching starts. Then the cycles explained in appendix E above can be started. Table 3.4 shows that only 1 nm of nitride is etched during the release at XeF_2, which is good.

Material	Thickness [nm]
Si_3N_4	91 (from 92)

Table 3.4: Thickness of the silicon nitride

Observations

The first measurements are made four days after the release according to the availability of the SEM. The structures have therefore already relaxed as already illustrated for the Sahar Jaddi sample in appendix F.2.

The structures analysed on this sample are the "B11 1.5 100", "B11 1.5 400", "B11 2.5 400" and the "B11 1.5 25" (for this last type of structures, only the most deformed one is represented in the stress-strain graph).

Fig. 3.28 show that some structures "B11 1.5 25" and "B11 2.5 400" break in the actuator only, but only two are broken. Concerning the structures "B11 1.5 100" and "B11 1.5 400", it is broken either in the specimen beam or in the actuator but not at the overlap. Furthermore, it can be seen that the cursors of the "B11 4 400" structures are not clean; the measurements are therefore not carried out for the latter.

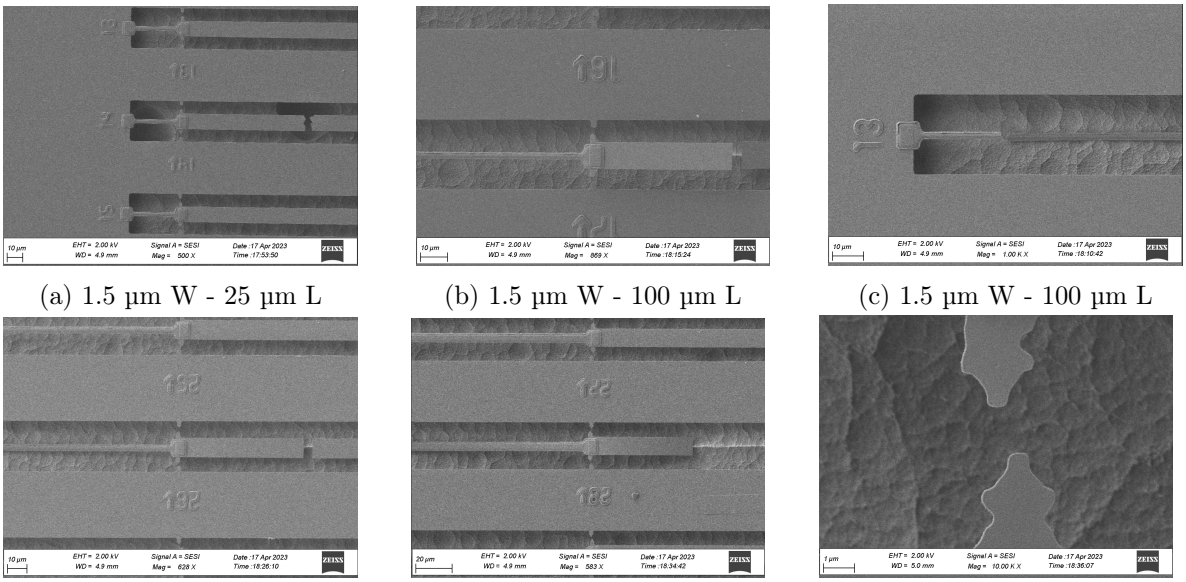

(a) 1.5 µm W - 25 µm L (b) 1.5 µm W - 100 µm L (c) 1.5 µm W - 100 µm L

(d) 2.5 µm W - 400 µm L (e) 4 µm W - 400 µm L (f) 45 µm W - 400 µm L

Figure 3.28: LOC test on Al_2O_3-Al 85-10 nm x5: Broken structures and strange cursors

Results

Fig. 3.29 presents the results in a stress-strain curve. This shows a maximum strain of 1.2% (the volume of considered structure is 23.3 μm^3) and a Young's modulus between 100 GPa and 120 GPa if the 25 µm long structures are considered as not precise enough. This modulus should still be taken with caution as the sample has already relaxed.

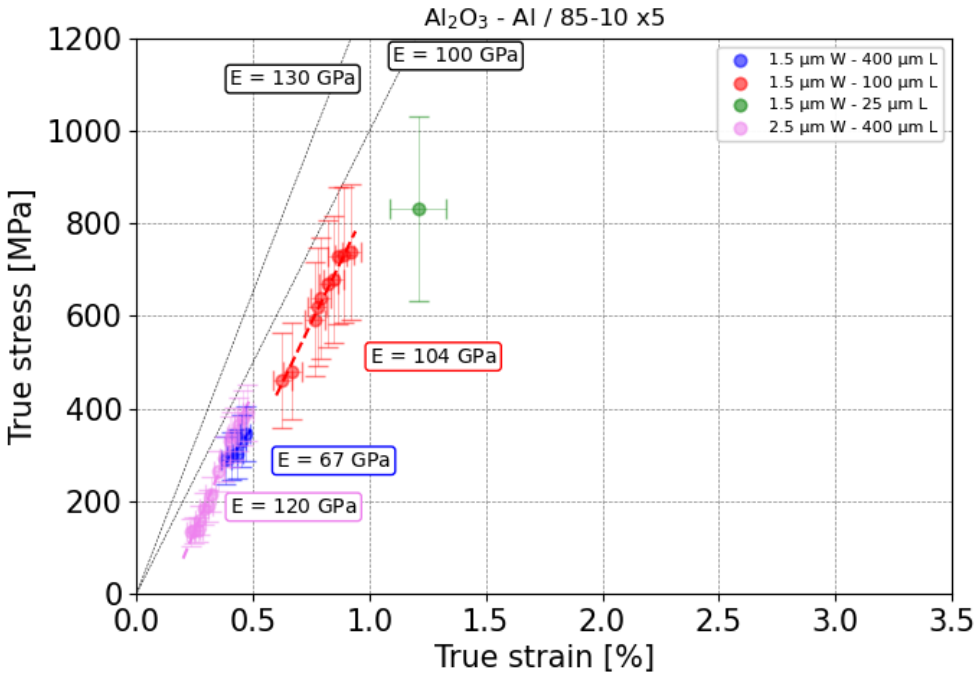

Figure 3.29: LOC test on Al_2O_3-Al 85-10 nm x5: True stress versus true strain curve

Regarding the relaxation, the behaviour of the actuators shown in Fig. 2.13 shows that the most deformed structures relax the most. Thus, some of the more deformed structures are measured after 13 days as shown in Fig. 3.30. The sample relaxes well over time.

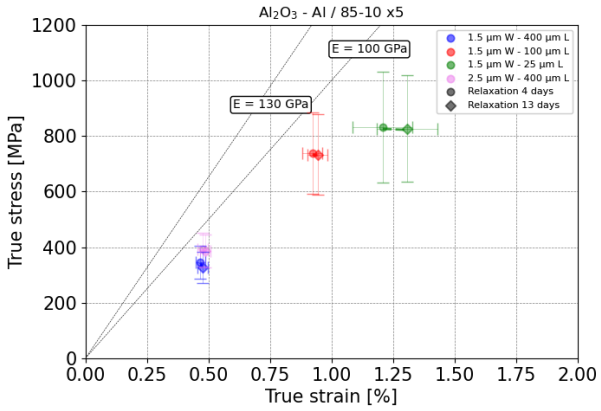

(a) All structures

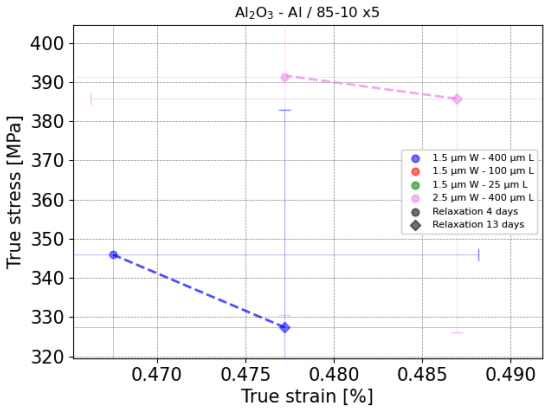

(b) 1.5 µm W - 400 µm L and 2.5 µm W - 400 µm L structures

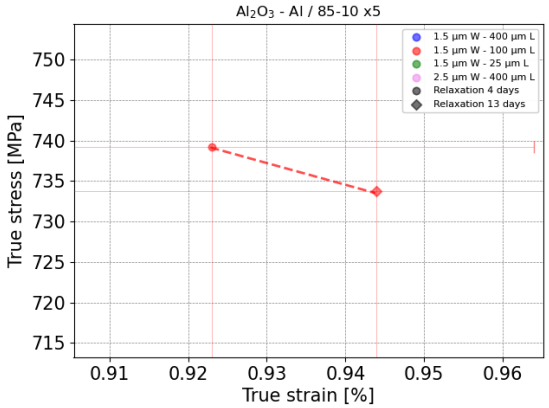

(c) 1.5 µm W - 100 µm L structures

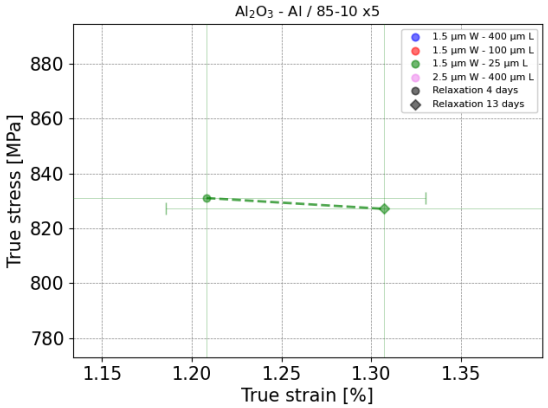

(d) 1.5 µm W - 25 µm L structures

Figure 3.30: LOC test on Al_2O_3-Al 85-10 nm x5:
True stress versus true strain curve - Relaxation 4 days and 13 days

3.2.2 Sample 46-10 nm x5

Choice of the thickness and deposition of the nanolaminate

The 500 nm thick sample does not break at the overlap but does not allow large strains to be achieved. Therefore, the second sample deposited is 300 nm thick and composed of 5 alumina/aluminium bilayers of 46-10 nm. Deposition times are 3 minutes for alumina and 1 minute for aluminum. After the nanolaminate is deposited, the lift off is performed and the thicknesses of the specimen beams are measured and given in Table 3.5.

Material	Thickness [nm]
Nanolaminate	271
Nanolaminate 4 µm Wide	265
Nanolaminate 2.5 µm Wide	260
Nanolaminate 1.5 µm Wide	224

Table 3.5: Thickness of the specimen beams

Release

Three large pulses are required to start etching and this involves etching 12 nm of the silicon nitride as shown in the Table 3.6.

Material	Thickness [nm]
Si_3N_4	80 (from 92)

Table 3.6: Thickness of the silicon nitride

Observations

The measurements are carried out four days after the release following the availability of the SEM. The structures have therefore already relaxed as illustrated for the Sahar Jaddi sample in appendix F.2.

The structures analysed on this sample are the "B11 8 800", "B11 6 800", "B11 4 400", "B11 2.5 400", "B11 1.5 400", "B11 1.5 100" , "B11 1.5 50" (only the most deformed one is represented in the stress-strain graph), "UL 1 10 800" and "UL 1.5 10 800".

Let's start with the shortest structures, which pull the most. The "B11 1.5 25", "B11 2.5 25" and "B11 2.5 50" structures are all broken at the overlap, on one side or the other. This is also the case for the majority of the "B11 1.5 50" structures. Only one of them breaks in the specimen beam.

As already mentioned, the longest structures are the ones that give the lowest strains and therefore break the least. Most of the "B11 1.5 100" structures break at the overlap but also in the specimen beam in a rather brittle way referring to the pictures. The "B11 2.5 100" structures are not analysed because the stress concentration is lower in the specimen beam and they all break at the overlap. This is probably due to the thickness of 300 nm. Longer structures such as "B11 4 400" and "B11 2.5 400" do not break in the specimen beam.

Concerning the 800 µm long structures "B11 8 800" and "B11 6 800", some of them break in the actuator but the others allow to obtain points corresponding to very small strains; these points being more correct than those given by the other structures because they do not have a dogbone (the calculations do not take into account this last one by question of facility).

One analyses the unloaded structures "UL 1 10 800" and "UL 1.5 10 800" which correspond to a discharge (the deposited sample has internal tensile stresses; it is therefore a discharge) of the sample and therefore to a true Young's modulus measurement.

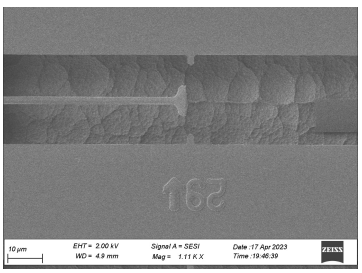

(a) 1.5 µm W - 50 µm L

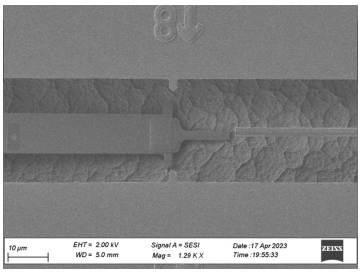

(b) 1.5 µm W - 50 µm L

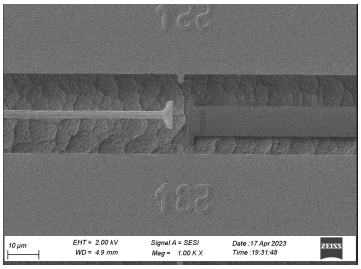

(c) 1.5 µm W - 100 µm L

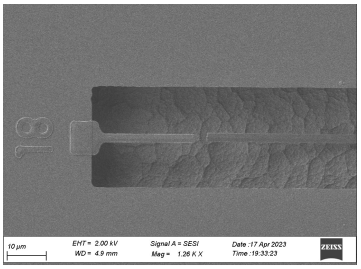

(d) 1.5 µm W - 100 µm L

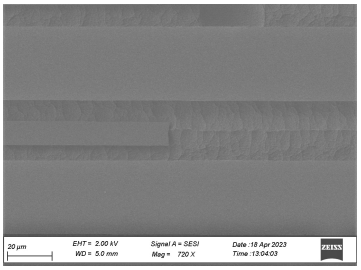

(e) 6 µm W - 800 µm L

Figure 3.31: LOC test on Al_2O_3-Al 46-10 nm x5: Broken structures and broken at the overlap

Results

Fig. 3.32 presents the results in a stress-strain curve. This shows a maximum strain of 1.04 % (the volume of considered structure is 22.7 μm^3) and a Young's modulus between 100 GPa and 120 GPa considering the more reliable structures points. This modulus should still be taken with caution as the sample has already relaxed.

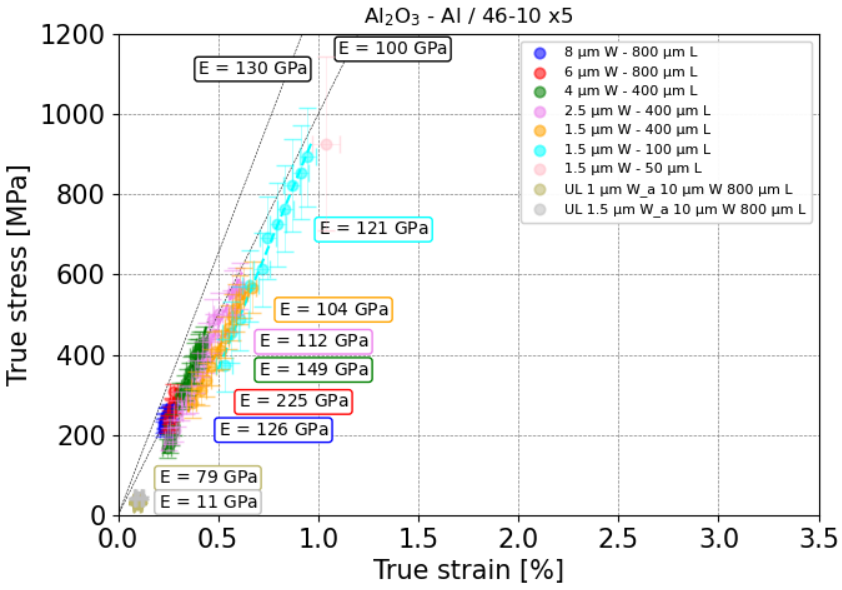

Figure 3.32: LOC test on Al_2O_3-Al 46-10 nm x5: True stress versus true strain curve

Solutions

The maximum strain is not very high because the shorter structures break at the overlap. Several solutions are possible. First of all, to deposit a greater thickness. Secondly, to study narrower structures where the stress concentration would be higher in the specimen, which would prevent breaking at the overlap. A third solution is to thin the silicon nitride because the overlap is not conform as observed in Sahar Jaddi's sample in Fig. 4.22.

3.2.3 Sample 70-12 nm x5

Choice of the thickness and deposition of the nanolaminate

As mentioned in the section 3.2.2, the third sample made is about 400 nm and 5x 70-12 nm alumina/aluminium bilayers. The nanolaminate is deposited with the following deposition times: 5 minutes for alumina and 1 minute for aluminium.

Indium deposition

After this first deposition of the nanolaminate, indium is deposited with the Vacotec machine, by evaporation, with the aim of doing Digital Image Correlation (DIC) to understand the deformation mechanism and to see if the deformation is homogeneous or not. In order to make the vacuum, a primary and then a cryogenic pump are used. The deposition speed is 1 Å/s in a vacuum of 1.3 $*10^{-7}$ mbar. The deposition time is 50 seconds. 5 nm of indium are deposited. If more indium is deposited, the balls are not homogeneous and this makes the DIC more complicated; conversely, if the balls are too small, this is also more complicated for the DIC. It is important that these indium balls are not continuous so as not to influence the tensile test. Unfortunately, the DIC is not carried out in this work due to lack of time.

Lift-off and thickness measurements

After the nanolaminate is deposited, the lift off is performed and the thicknesses of the specimen beams are measured and given in Table 3.7.

Material	Thickness [nm]
Nanolaminate	400
Nanolaminate dogbone	323
Nanolaminate 0.75 µm Wide	165

Table 3.7: Thickness of the specimen beams

These thicknesses are very interesting for the LOC. Indeed, the sample is thin but thicker at the dogbone, which probably can prevent break at the overlap. But the error on the thickness and width is still considerable since the sample is so thin... This error is reflected in the stress.

FIB cutting of cursors

In fact the structures analysed for this sample are the "B6 0.75 10" to observe large strains. But the cursors are still attached to the structures. That is why, before the release, one has to cut out some structures (5-15-25-35-45-55-65-75-85) with the FIB.

Release

Three big pulses are needed to start the release and this involves etching 6 nm of the silicon nitride as shown in Table 3.8.

Material	Thickness [nm]
Si_3N_4	86 (from 92)

Table 3.8: Thickness of the silicon nitride

Observations

SEM measurements are taken 1 hour after the release.

First, here is on Fig. 3.33 a FIB section of the deposited sample with the corresponding layers:

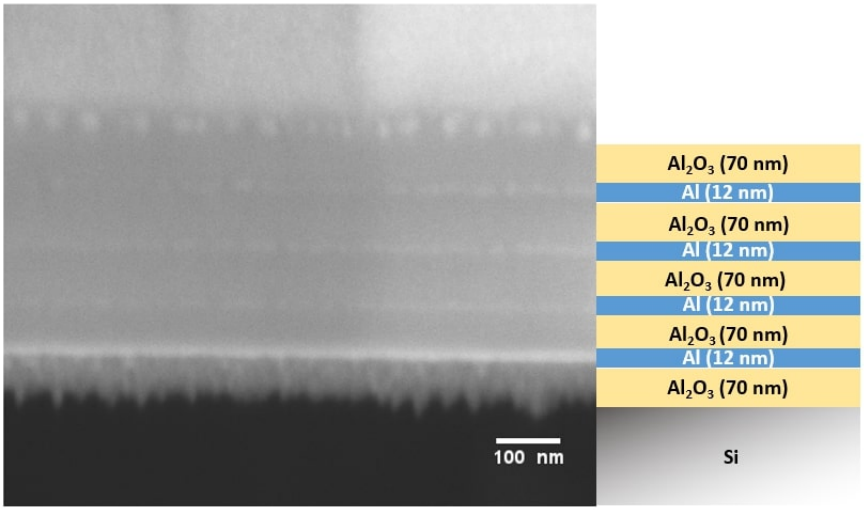

Figure 3.33: FIB cutting of the deposited nanolaminate Al_2O_3-Al 70-12 nm x5

The deposition at the overlap is still not conform despite the greater thickness as Fig. 3.34 shows.

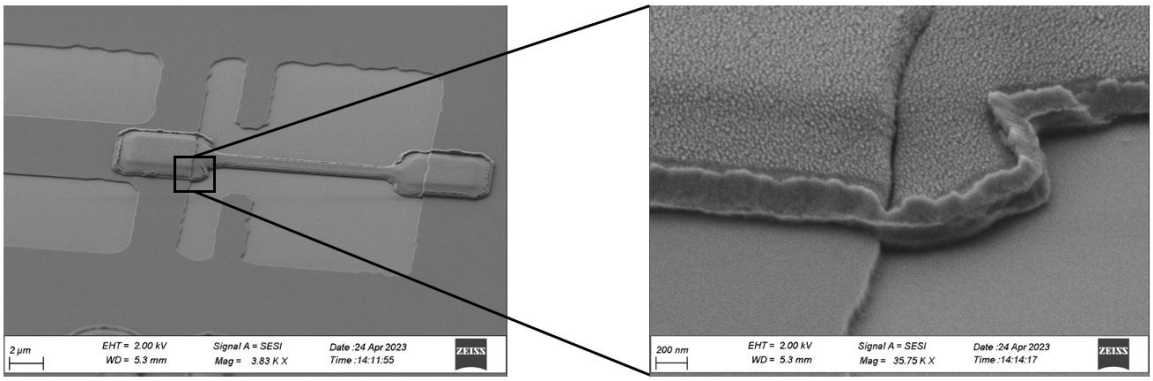

Figure 3.34: One structure and the overlap: Al_2O_3-Al 70-12 nm x5 sample

Furthermore, as can be seen in Fig. 3.37, structures with a width of less than 0.7 microns cannot be studied.

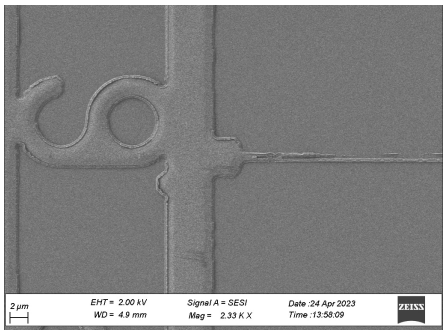

Figure 3.35: Reference specimen beam of width 0.6 µm

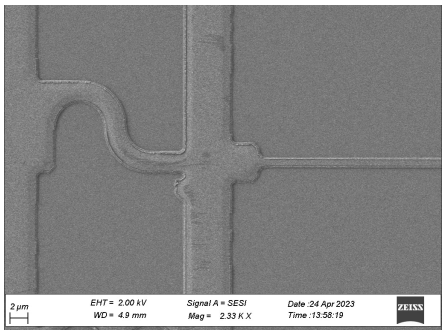

Figure 3.36: Reference specimen beam of width 0.7 µm

Figure 3.37: Reference specimen beams to observe their quality

One can also see that it is in the specimen beam that the fracture takes place, for the most deformed structures (75 and 85 which is represented in Fig. 3.38). It looks brittle as already observed previously.

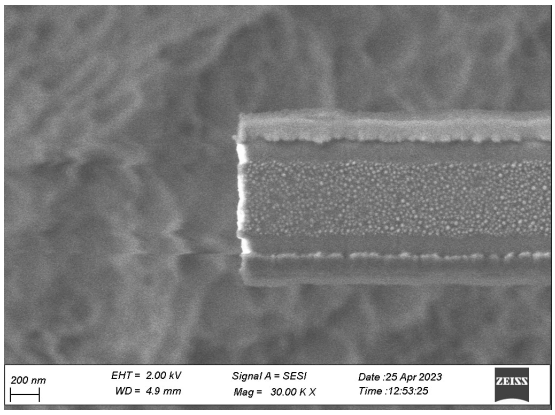

Figure 3.38: Fracture of a specimen beam: Al_2O_3-Al 70-12 nm x5 sample

Results

First, one should remind that the analysed specimen beams are very small. By consequence, the dogbone has an important influence which is not taken into account in the calculations. Fig. 3.39 presents the results in a stress-strain curve. This shows a maximum strain of 2.6 % (the volume of considered structure is 1.6 μm^3). The Young's modulus is not considered because the errors on these points are quite large. The small crosses correspond to structures where the specimen beam has broken.

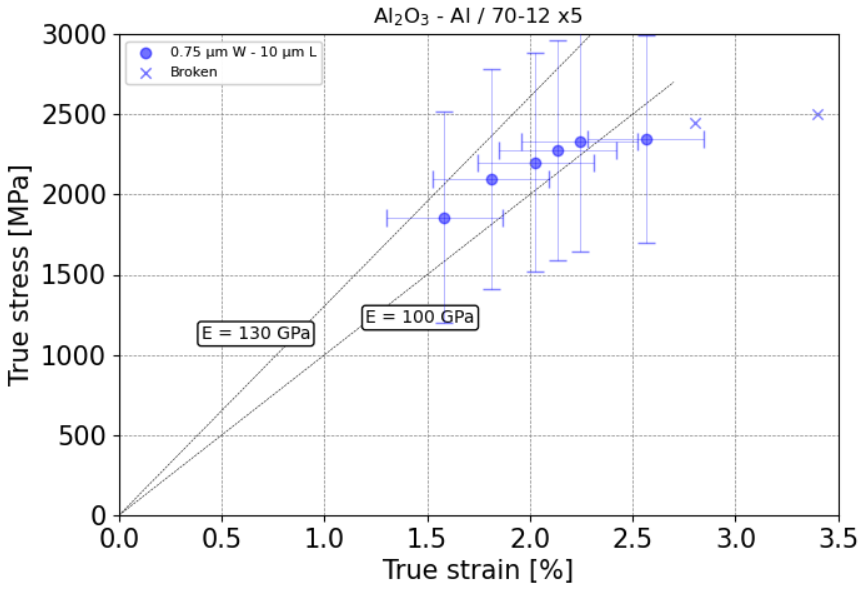

Figure 3.39: LOC test on Al_2O_3-Al 70-12 nm x5: True stress versus true strain curve

3.2.4 Sample 70-12 nm x5 - release by FIB cutting of the cursors

Cutting with FIB to release other structures

The idea here is to cut the cursors directly into the SEM. These cursors are shown in Fig. 3.40. This allows the specimen to be released and then the displacements can be measured with the cut-out cursors only three minutes after release. There would therefore be nearly no relaxation. However, these measurements should not be compared directly with the previous ones: the loading rate is probably not the same as with the classical release and the relaxation time between the release and the measurements is about one hour with the usual release and only three minutes with this release thanks to the FIB cut.

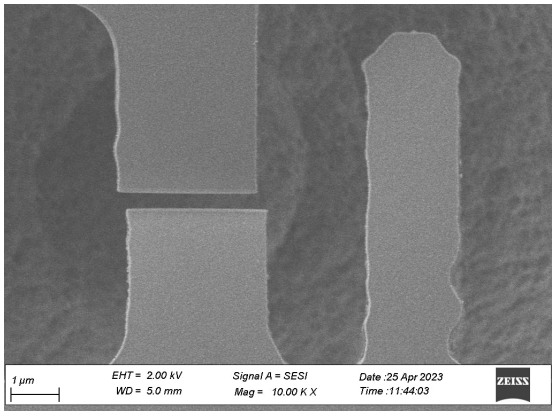

Figure 3.40: Cursors with FIB cutting

Results

Thanks to this release with the FIB cutting of the cursors, structures deform at a level where they had broken with the usual release method, as shown in Fig. 3.41. Indeed, it is the case of the two structures 75 and 85 indicated by small crosses in Fig. 3.39. In contrast, structures 80 and 90 do not break with the FIB release. This makes it possible to achieve higher strains than previously up to almost 3.5 %.

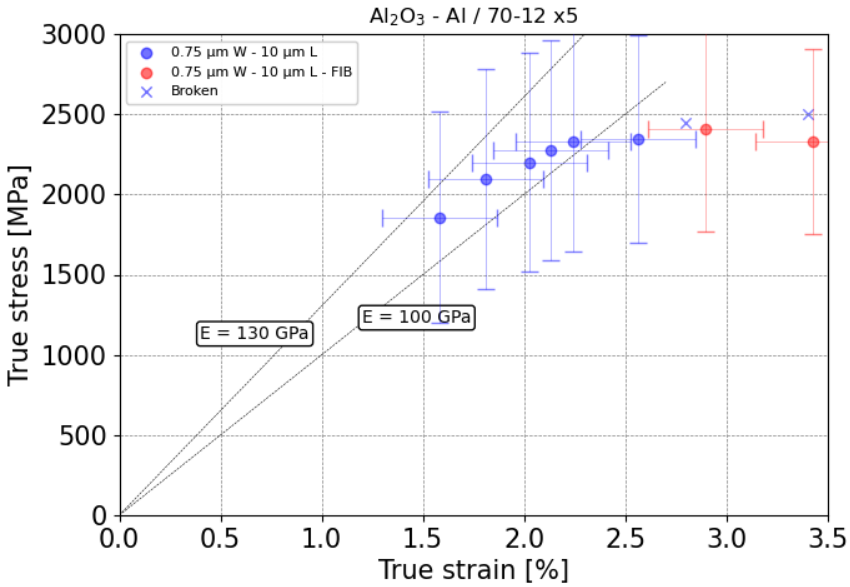

Figure 3.41: LOC test on Al_2O_3-Al 70-12 nm x5: True stress versus true strain curve - FIB cutting

To study the relaxation of the sample, SEM measurements of the cursors are performed 5 hours after the release and 8 days later to observe and characterise the relaxation. The stress-strain curve is shown in Fig. 3.42. Thanks to this relaxation, a strain of 4.7 % is reached.

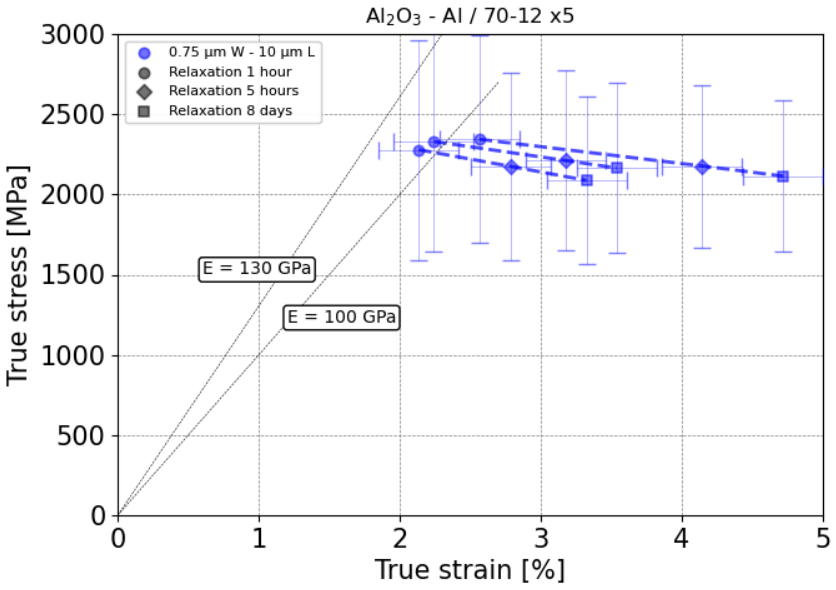

Figure 3.42: LOC test on Al_2O_3-Al 70-12 nm x5: True stress versus true strain curve - Relaxation 1 hour, 5 hours and 8 days

These points have also been represented in Fig. 3.43 in a force-displacement graph as explained in the section 2.2.6.

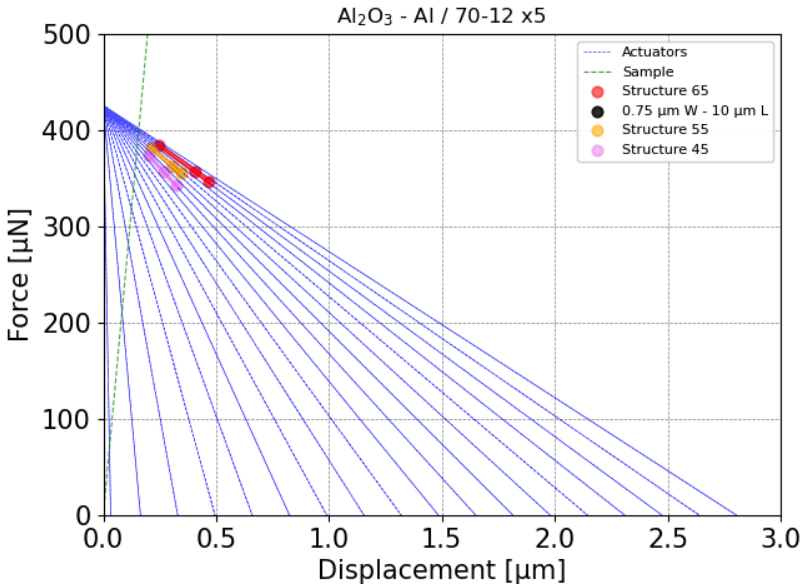

Figure 3.43: Behavioural law

Knowing three different relaxation times, the stress and strain data as well as the time between

these relaxation times, it is possible to calculate the strain rate sensitivity coefficient as follows:

$$m = \frac{d \ln \sigma}{d \ln \dot{\epsilon}}$$

The first strain rate ϵ_1 is calculated by taking the data corresponding to the 1 hour and 5 hours relaxations; the second strain rate, between the 5 hours and 8 days relaxation ($\dot{\epsilon_{2_1}}$) and between 1 hour and 8 days ($\dot{\epsilon_{2_2}}$). Here are the results in Table 3.9:

Structure	$\dot{\epsilon_1}$	$\dot{\epsilon_{2_1}}$	$\dot{\epsilon_{2_2}}$	**m with** $\dot{\epsilon_{2_1}}$	**m with** $\dot{\epsilon_{2_2}}$
65	1.1 * $10^{-}6$	8.6 * $10^{-}9$	3.13 * $10^{-}6$	0.011	0.013
55	1.35 * $10^{-}6$	5.28 * $10^{-}7$	1.88 * $10^{-}6$	0.032	0.039
45	9.5 * $10^{-}7$	7.77 * $10^{-}7$	1.73 * $10^{-}6$	0.03	0.2

Table 3.9: Strain rate and strain rate sensitivity coefficient

However care should be taken because, for the DIC pictures, the electron beam stayed a long time on the specimen beams and this distorted the results a little since the kinetic seems to be accelerated.

DIC pictures

For the DIC, the photos are taken before and after the release, with a good resolution of 3072x2304 to ensure the best possible quality. The structures involved are all multiples of 5 and are taken with 2 keV, a working distance of 5 mm, magnification at x10k, x20k and x50k, a contrast of 30 % and a brightness of 50 %. Fig. 3.44 show SEM pictures of one structure :

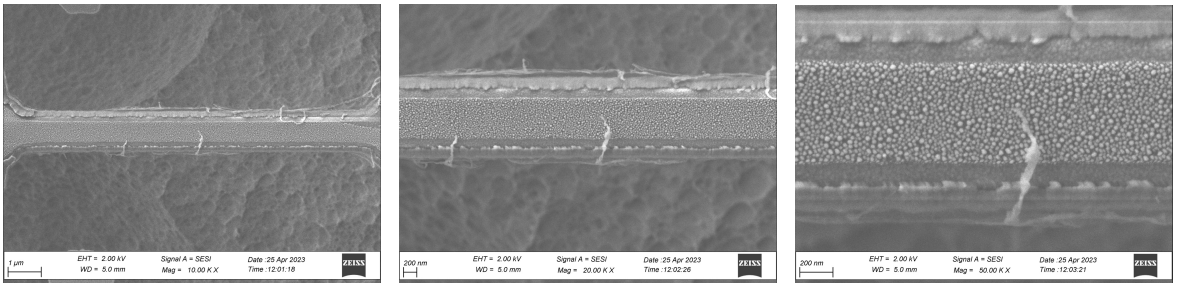

(a) Zoom x10k (b) Zoom x20k (c) Zoom x50k

Figure 3.44: Pictures for the DIC analysis: Al_2O_3-Al 70-12 nm x5 sample

These figures show that the indium particles are not deposited over the whole visible part of the specimen beams in the SEM. In fact, the indium is deposited by evaporation and this makes the deposition strictly vertical. This indium has therefore been deposited on the highest part of the specimen "dome", this dome coming from the fact that the sample is deposited by sputtering as already illustrated in Fig. 2.11.

Taking these pictures allowed to directly see the effect of the electron beam on the samples: the electrons accelerate the kinetics of the samples and they break faster.

3.2.5 Conclusion about the lab on-chip tests

The lab on-chip tests performed on the three deposited samples (85-10 nm x5, 46-10 nm x5 and 70-12 nm x5) are shown in Fig. 3.45. In order to have an alignment between the points of the different samples, a slight lateral shift is performed for the sample 85-10 nm x5 and 46-10 nm x5. Thus, the maximum strains obtained for each of the samples are shown in Table 3.10.

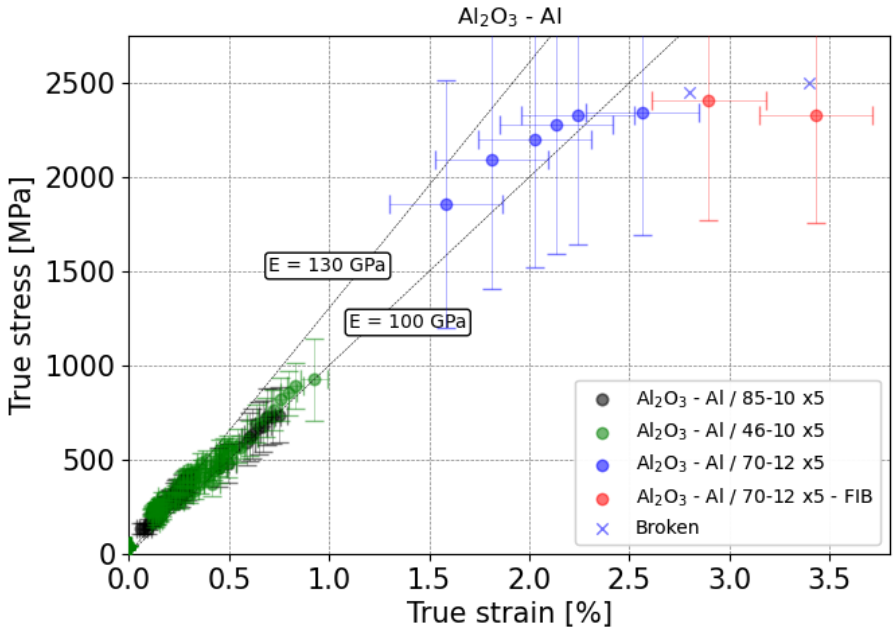

Figure 3.45: LOC test on Al_2O_3-Al 85-10 nm x5, 46-10 nm x5 and 70-12 nm x5: True stress versus true strain curve

Sample	Maximum strain [%]	Volume [µm^3]
85-10 nm x5	0.75	23.3
46-10 nm x5	0.91	22.7
70-12 nm x5	2.6	1.6
70-12 nm x5 - FIB cutting	3.4	1.6
70-12 nm x5 - After relaxation 8 days	4.7	/

Table 3.10: Maximum strain and volume of the most deformed structure

Firstly, although it depends more precisely on the type of structures used, their length and width, the thickest specimen beams give the smallest strains as expected and explained in the section 2.2.4 and the shortest structures of only 10 µm in length give the most significant strains. The fact that these one do not break is probably due to the fact that the specimen beams are so small (the volume of the most deformed structure for each sample is written in Table 3.10): there are fewer defects. This is the case for the push to pull test where the sample of only 2 µm showed a very large strain up to 7 % as mentioned in section 1.2.4.

Moreover, the maximum strain is even greater for the FIB-cut structures and reaches 3.4 %. This is probably due to the loading speed which is different from a normal release. It is also interesting to note that the measurements are taken only three minutes after the release while it is around one hour for a normal release.

Regarding the Young's modulus, it seems to be between 100 and 130 GPa. However, it must be taken into account that the structures probably relax at all levels of strain and that this modulus could therefore be higher.

Moreover, the SEM pictures show a fracture rather brittle in the specimen beam.

3.3 Tensile test on polymer

3.3.1 Choice of the thickness and deposition of the nanolaminate

As with the nanoindentation and lab on-chip samples, the AJA machine is used for deposition. The samples analysed are 1 micron thick so that the effect of the polymer is not too great. To maintain the multilayer effect, 10 alumina/aluminium bilayers (100-10 nm) are deposited. The chosen deposition time is 6 minutes for alumina and 1 minute for aluminium. Of the 4 samples deposited, two are covered with a 5 nm layer of indium deposited by Vacotec. Indeed, as for the lab on-chip, the DIC can be performed to see how the deformation occurs within the material. This DIC experiment is not done in this work due to lack of time.

3.3.2 Observations

Before carrying out the tensile test, it is important to see if there are already cracks in the samples; as a result of mounting, as the film has internal tensile stresses and these relax; or as a result of the samples peeling off the wafer. So one looks at sample 1 without indium under the optical microscope. There appear to be some straight lines. Sample 3 with indium also has some straight lines. Fig. 3.46, Fig. 3.47 and Fig. 3.48 show samples 1, 2 and 3 respectively under the optical microscope.

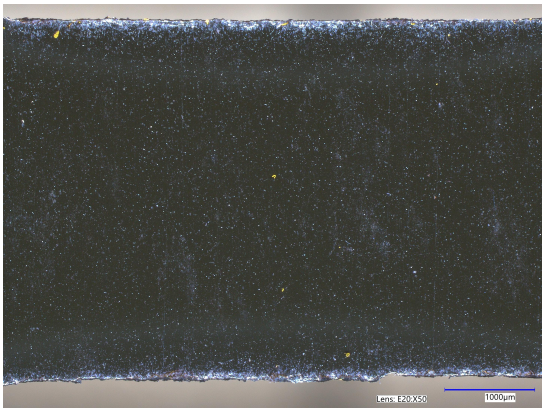

Figure 3.46: Sample 1 Al_2O_3-Al 100-10 nm x5: before tensile test

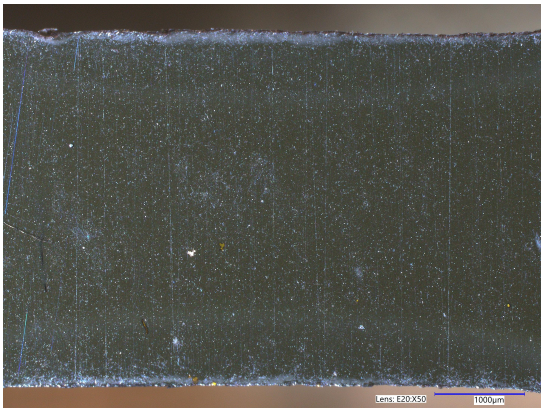

Figure 3.47: Sample 2 Al_2O_3-Al 100-10 nm x5: before tensile test

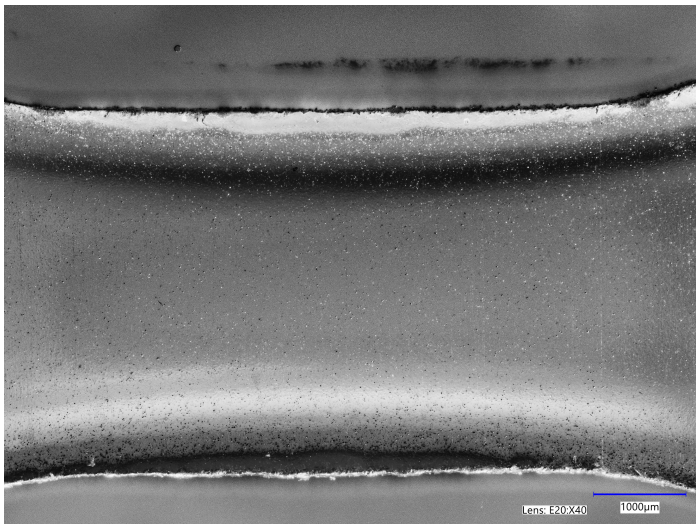

Figure 3.48: Sample 3 Al_2O_3-Al 100-10 nm x5: before tensile test

To be sure whether or not they are cracks, one therefore look at sample 3 with indium in the SEM. These are shown in Fig. 3.49 and in Fig. 3.50. No cracks is observable.

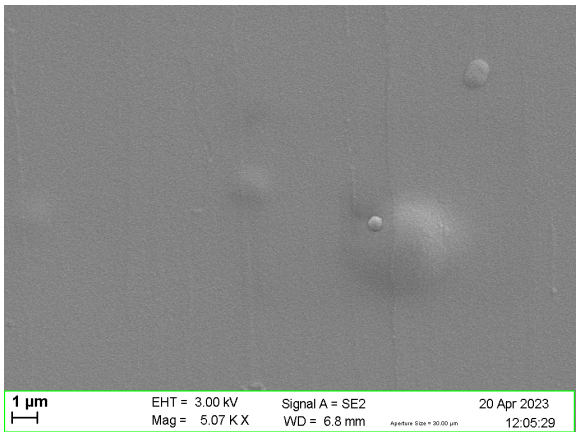

Figure 3.49: Sample 3 Al_2O_3-Al 100-10 nm x5: before tensile test

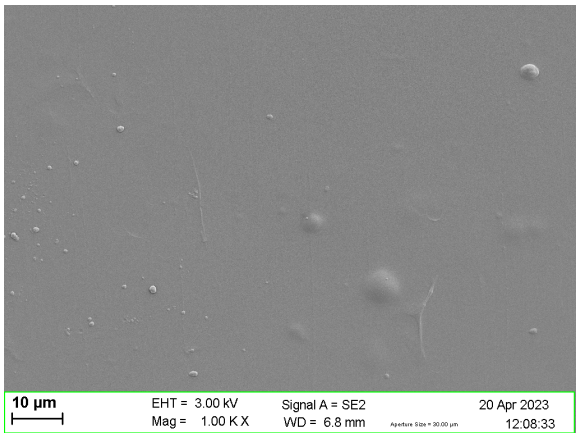

Figure 3.50: Sample 3 Al_2O_3-Al 100-10 nm x5: before tensile test

During the first test, the video from the optical microscope allows to observe the propagation which is really fast. Moreover, it is important to note that there are two small interruptions because the displacement speed controller is not working properly. However, interrupting a test is never good because the sample could have relaxed a little and the fast propagation of the cracks could come from there as mentioned in the article [1]. Moreover, the charge increases faster for the first sample than the second one.

The video under the optical microscope made it possible to locate the first crack which appears after 9.8 seconds for the first sample and after 25.8 seconds for the second one. This is necessary for the toughness calculation.

After the test, samples 1 and 2 are well cracked as shown in Fig. 3.51 and Fig. 3.52 under the optical microscope. Sample 1 is then observed with SEM and Fig. 3.53 and 3.54 show sharp cracks for sample 1.

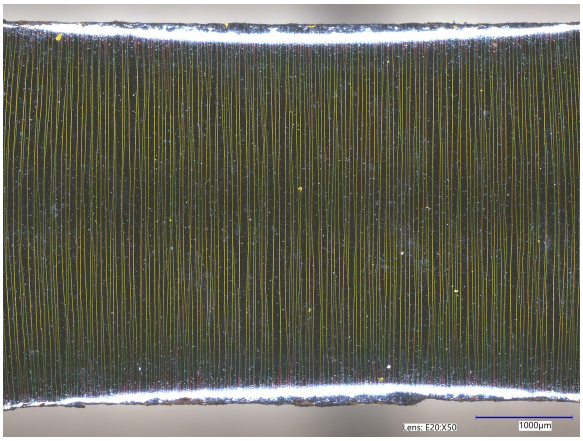

Figure 3.51: Sample 1 Al_2O_3-Al 100-10 nm x5: after tensile test

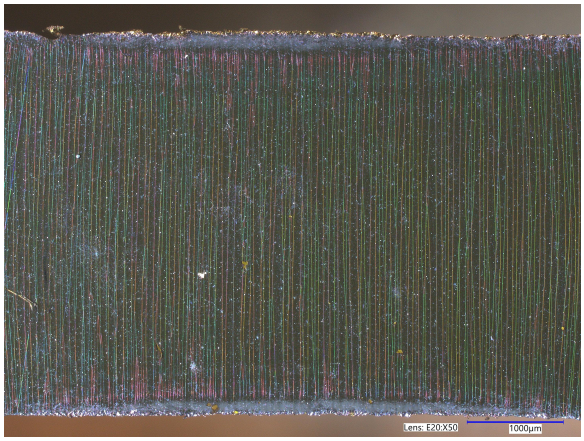

Figure 3.52: Sample 2 Al_2O_3-Al 100-10 nm x5: after tensile test

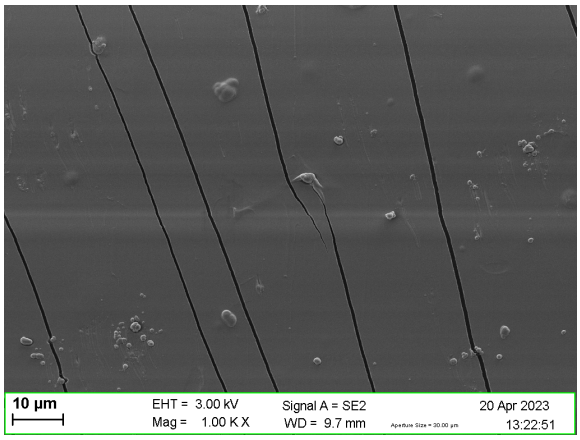

Figure 3.53: Sample 1 Al_2O_3-Al 100-10 nm x5: after tensile test

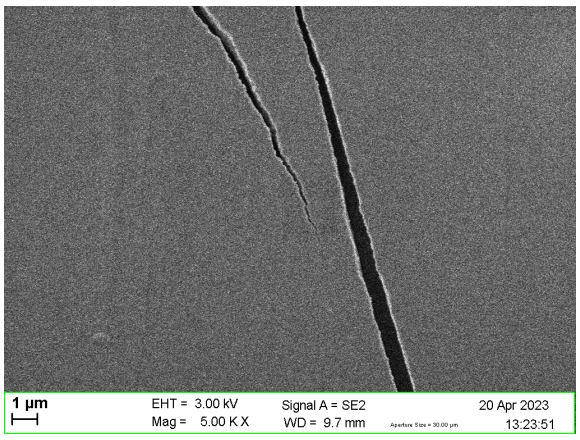

Figure 3.54: Sample 1 Al_2O_3-Al 100-10 nm x5: after tensile test - zoom

3.3.3 Results

Firstly, the initial forces subtracted from the raw data are 1.7 N and 2.7 N for the two samples respectively. The results obtained with the method explained in section 2.3.3 are illustrated below. The Young's modulus appears to be around 145 GPa in this case as shown on Fig. 3.58.

Stress-strain curve

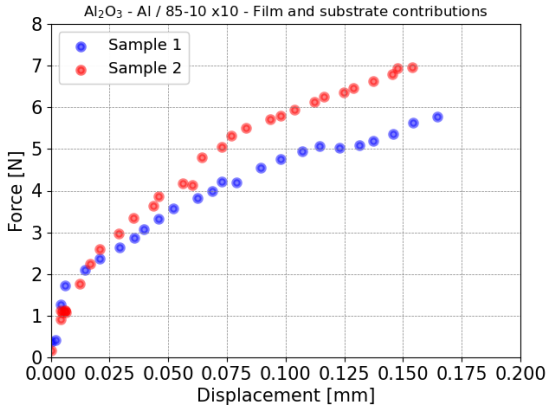

Figure 3.55: Tensile test of Al_2O_3-Al 100-10 nm x5 on polymer: Force versus displacement for the polymer and the deposited sample

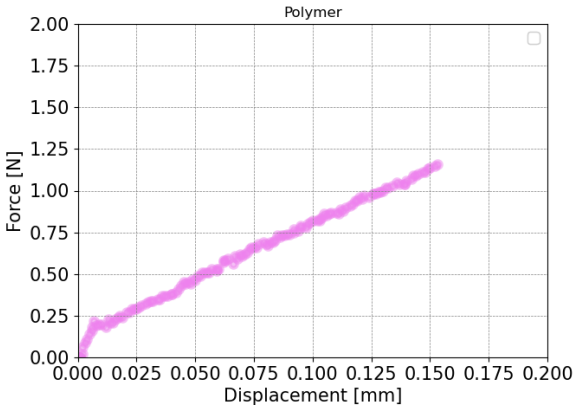

Figure 3.56: Tensile test of Al_2O_3-Al 100-10 nm x5 on polymer: Force versus displacement for the polymer

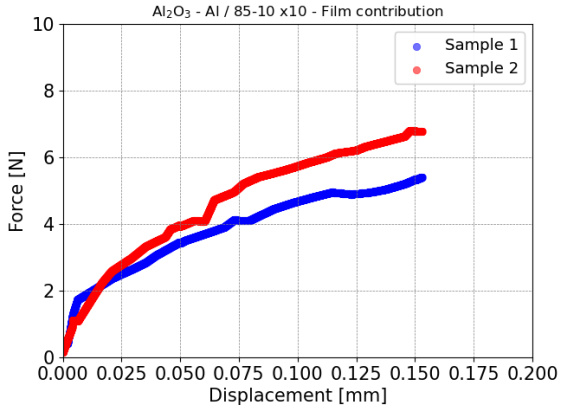

Figure 3.57: Tensile test of Al_2O_3-Al 100-10 nm x5 on polymer: Force versus displacement for the deposited sample

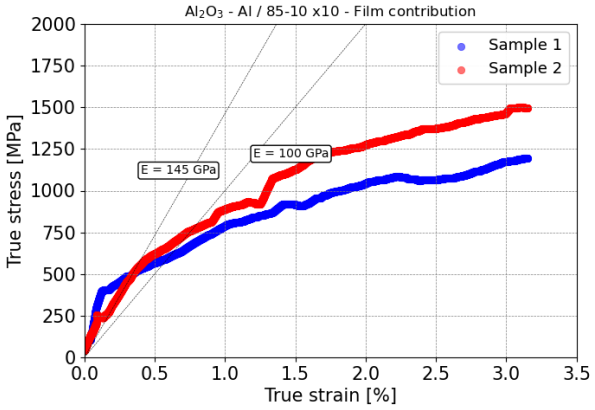

Figure 3.58: Tensile test of Al_2O_3-Al 100-10 nm x5 on polymer: True stress versus true strain curve for the deposited sample

Fracture toughness

The calculations explained in section 2.3.3 give values presented in Fig. 3.11. The value for the Z coefficient is found to be 18 considering a ratio of $\frac{t_{substrate}}{t_{film}} = 13$ and a Dundurs parameter $\alpha = 0.95$ [15] [34].

Sample	ϵ_f [%]	G_c [J/m^2]	σ_f [MPa]	G_c [J/m^2]
1	0.041	0.47	134.7	2.1
2	0.087	2.1	193.5	4.36

Table 3.11: Toughness calculated with the fracture strain and fracture stress

For thin films, the toughness is about 1 to 20 J/m^2 according to the crack on-chip experiments carried out at the laboratory [17]. For more ductile materials, such as steels, the toughness is about 10 kJ/m^2. The values obtained are therefore in the good range for thin films and brittle materials.

It is important to remind that the first test has been interrupted which can lead to an error in the determination of the toughness. Then, regarding the second test, one can consider that the toughness is the mean of the toughness calculated by the fracture stress and the one calculated by the fracture strain, which gives a value of 3.2 J/m^2. This value corresponds to a brittle fracture but it should still be taken with caution as explained in section 2.3.3.

Chapter 4

Discussion

In this work, different tests are carried out in order to determine some properties of the nanolaminates composed of alumina and aluminium and to try to obtain large strains, as it is found by the push-to-pull tests, as mentioned in section 1.2.4. The nanolaminates with thicknesses of less than 100 nm for alumina and between 10 nm and 20 nm for aluminium are chosen because they have high ductility, strength and toughness. Nanoindentation tests, lab on-chip tests and tensile tests on polymer are carried out.

This section presents a discussion of the results. The mechanical properties are first introduced with the Young's modulus, the hardness, the fracture toughness, the maximum strain, the plasticity and finally the fracture. Then the relaxation and the strain rate sensitivity coefficient are presented followed by an opening for future research.

4.1 Mechanical properties

The different nanoindentation tests give a Young's modulus, a hardness as well as a strain rate sensitivity coefficient for higher and lower strain rates thanks to continuous stiffness measurements mode and the Paul Baral's method. Moreover, the lab on-chip tensile tests allow the determination of a Young's modulus in a certain range of values and a maximum strain. And the tensile tests on polymer provide a Young's modulus and a fracture toughness.

For all of them, several tests are performed and the more reliable are illustrated in Fig. 4.1 and the corresponding values are grouped in the Table 4.1, except the strain rate sensitivity coefficients discussed in the section 4.2. Regarding the nanoindentation tests, the more reliable test is the one for which each parameter has been adapted to have the more precise and reliable test. These parameters are the maximum thermal drift allowed, the approach speed, the penetration depth and the detection limit. For the tensile tests on polymer, the values given in Table 4.1 correspond to the second sample test since the first one has been interrupted.

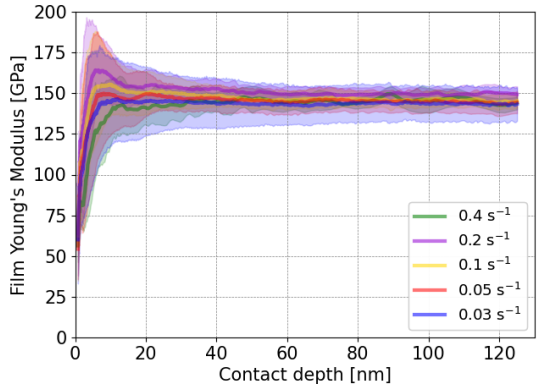

(a) CSR test at at different strain rates on Al_2O_3-Al 138-16 nm x5: Film Young's modulus as a function of the contact depth

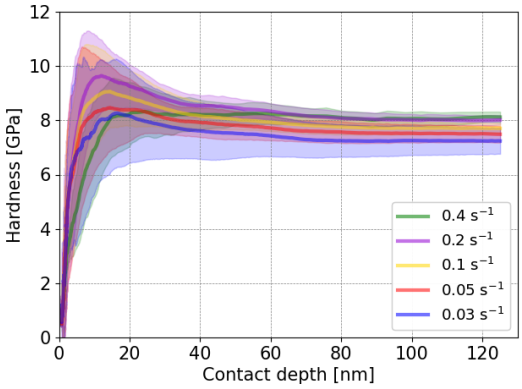

(b) CSR test at different strain rates on Al_2O_3-Al 138-16 nm x5: Hardness as a function of the contact depth

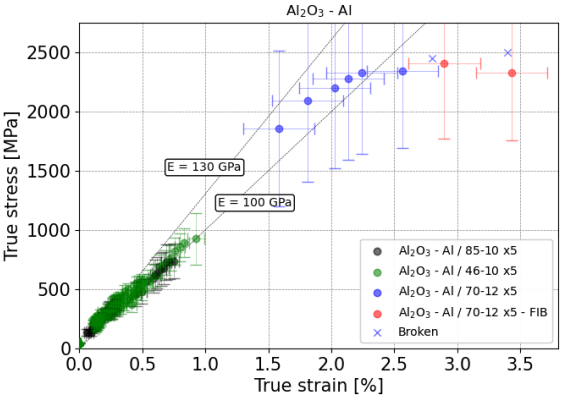

(c) LOC test on Al_2O_3-Al 85-10 nm x5, 46-10 nm x5 and 70-12 nm x5: True stress versus true strain curve

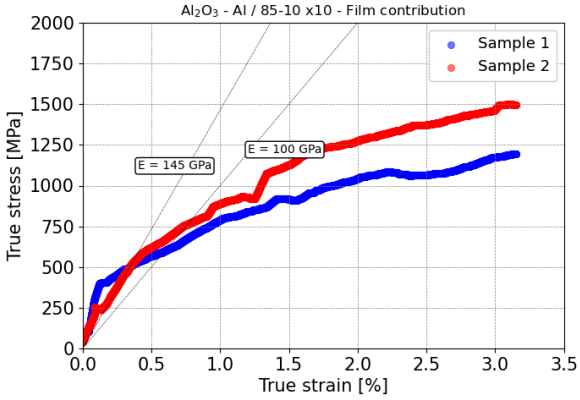

(d) Tensile test of Al_2O_3-Al 100-10 nm x5 on polymer: True stress versus true strain curve for the deposited sample

Figure 4.1: Results from the nanoindentation tests, LOC tests and tensile tests on polymer

Mechanical properties	**Nanoindentation**	**LOC**	**On polymer**
Young's modulus [GPa]	147	100-130	145
Hardness [GPa]	7.5	/	/
Toughness [J/m^2]	/	/	3.2
Maximum strain [%]	/	2.6 and 3.4 - FIB cutting	3.15

Table 4.1: Mechanical properties obtained by the nanoindentation tests, LOC tests and tensile tests on polymer

4.1.1 Young's modulus

First of all, one can see that the Young's modulus is not the same for the three kinds of experiments even if there remain quite close to each other. Regarding the nanoindentation

tests, one can compare this value to the one obtained by Paul Baral *(Private communication)*. Actually, for these materials, he shows that the linear law of mixtures cannot be applied. It would rather be a quadratic law as shown in Fig. 4.2. And based on this graph, for an alumina content of about 10 %, the value of 147 GPa corresponds with the data from Paul Baral.

The value from the lab on-chip tests is lower but this can probably be explained by the following points. First, it is important to remind that the nanolaminates have viscoelastic and viscoplastic behaviour as shown by the continuous stiffness measurement mode and the quasitatic mode in nanoindenation tests. Thus, the structures relax and this can be considered to be the case at all strain levels. The Young's moduli from the lab on-chip tensile tests are therefore lower than the true Young's modulus of the material. Moreover, one must keep in mind that the nanoindentation and the LOC tests are two different tests where the deformation mechanism is not the same which can lead to different Young's moduli. Nanoindentation corresponds more to isostress configuration whereas lab on-chip tests corresponds more to isostrain configuration.

Regarding the tensile test on polymer, this gives a Young's modulus of 145 GPa which corresponds to the nanoindentation test but care should be taken for this since there are only two samples and the decorrelation from the polymer contribution can maybe be improved.

4.1.2 Hardness

As for the Young's modulus, previous studies by Paul Baral proposed a quadratic law for the hardness of nanolaminates composed by alumina and aluminium layers. Indeed, Fig. 4.3 shows a hardness of 7 GPa for a content of 90 % of alumina in the nanolaminate which is similar to the measured one.

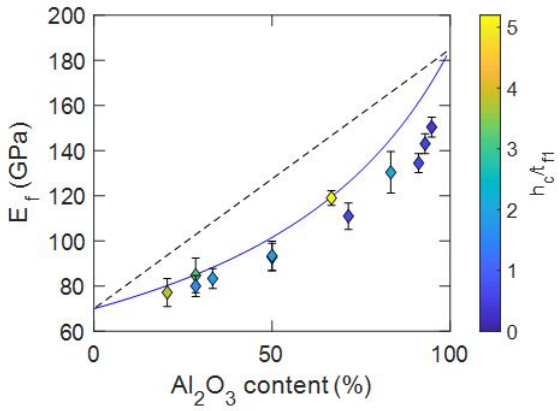

Figure 4.2: Film Young's modulus-content of alumina curve *(Private communication - Paul Baral)*

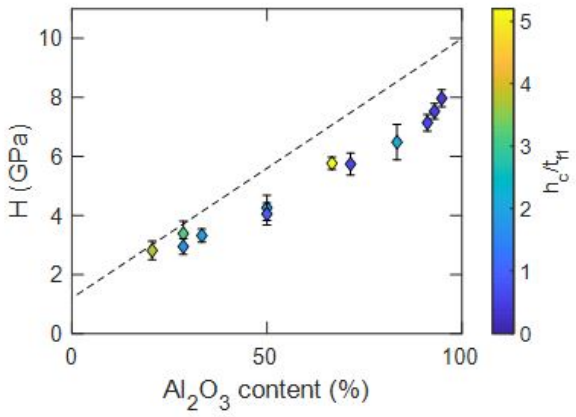

Figure 4.3: Hardness-content of alumina curve *(Private communication - Paul Baral)*

4.1.3 Maximum strain

The lab on-chip tests allowed to obtain a maximum strain of 2.6 % with a normal release explained in section 2.2.3. This is achieved with the smallest structures of 1.6 μm^3, most

likely because there have fewer defects than the larger structures of 23.3 µm^3 and 22.7 µm^3 which give a maximum strain of respectively 0.75 % and 0.91 %. Indeed, push to pull tests where the sample is only 2 µm long showed a very large strain up to 7 % as mentioned in section 1.2.4. Moreover, with the FIB cutting of the cursors, a strain up to 3.4 % is obtained, which has never been obtained before in the laboratory. The reason for such a difference probably comes from the loading rate which is not the same for the normal release and the release with the cursors cut by FIB. Finally, after relaxation, a strain of 4.7 % is achieved.

4.1.4 Plasticity

Thanks to the nanoindentation tests, a maximum elastic strain of 2.3 % is calculated. To remind, a relaxation process occurs and is described in the next section 4.2. Therefore, the maximum strain of 2.6 % reached with the usual release could be less important because of the relaxation of the material since the measurements are taken 1 hour after the release. On the other hand, for the FIB release, the measurements are taken only three minutes after the release, which is noteworthy since a normal release involves at least one hour between the beginning of the release and the SEM measurements of the cursors. Thus, the maximum strain of 3.4 % can be considered as plastic strain reached in the LOC tests.

4.1.5 Fracture

Based on the nanoindentation, the nanolaminate appears to deform plastically as no cracks are observed in the indent by SEM observations as Fig. 4.4 shows. On the other hand, lab on-chip tests show that the specimen beams break in a rather brittle manner as seen in Fig. 4.5. But it should be noted that these two techniques stress the material in two different ways. Finally, the cracks from the polymer tensile tests are very sharp as illustrated in Fig. 4.6 and their propagation is rapid.

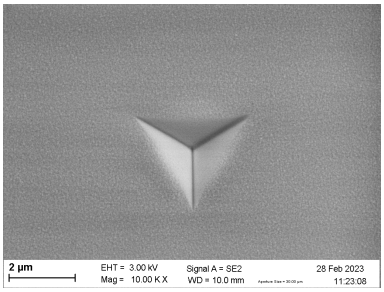

Figure 4.4: Shape of one indent from nanoindentation

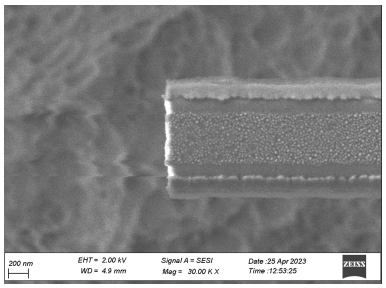

Figure 4.5: LOC : fracture of one specimen beam

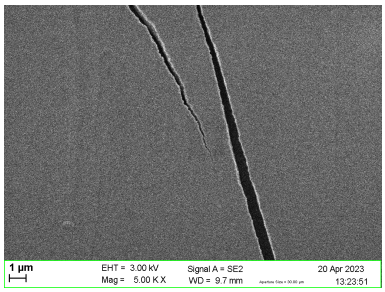

Figure 4.6: Sharp cracks from tensile test

4.1.6 Fracture toughness

Fracture toughness given by the tensile test on polymer can correspond to a brittle material but this is quite small for this kind of nanolaminate as mentioned in section 1.2. This value has to be taken with caution since the formula used to determine it does not take into account the fact that the substrate is no infinite, one should also have the size of initial crack before propagating to correct the calculated toughness, as mentioned in section 2.3.3.

4.2 Relaxation and strain rate sensitivity coefficient

Firstly, nanoindentation tests show a variation of the Young's modulus and of the hardness as a function of the imposed strain rate in the continuous stiffness measurement mode. This lead to deeper tests to analyse the strain rate sensitivity coefficient and relaxation phenomena. Fig. 4.7 presents the results about the strain rate sensitivity coefficients found by the nanoindentation tests, from the more reliable test with the CSR method and with Paul Baral's method. For the Paul Baral's method, the parameters that helped to improve the tests are the strain rate target, the stiffness stop, the stiffness hold, the surface approach and the maximum thermal drift allowed.

Concerning the nanoindentation tests, two different regimes are observed. At very low strain rates, the strain rate sensitivity coefficient is 0.24 while it is 0.04 at higher strain rates, obtained by the CSR method. According to a private communication by Paul Baral, alumina would have a strain rate sensitivity coefficient of 0.24 as shown in Fig. 4.8 while that of aluminium would be 0.05. Thus the question that is asked is whether the physical behaviour of the material specifically matches that of alumina at low strain rates and that of aluminium at high strain rates. This question can be answered by numerical simulations, not done in this work.

The relaxation measurements with lab on-chip structures give a coefficient between 0.01 to 0.03. This value is quite different from one of the two regimes observed in nanoindentation as written in Table 4.2. But as mentioned in the previous section 4.1, nanoindentation tests correspond more to an isostress configuration while LOC tensile tests are rather in isostrain configuration and this can lead to different results.

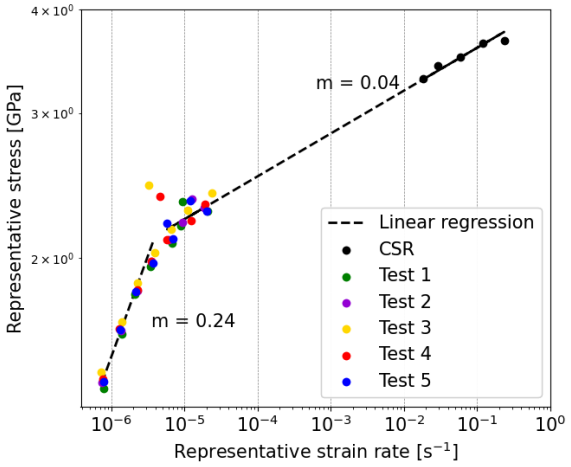

Figure 4.7: Baral's method on Al_2O_3-Al 138-16 nm x5: Representative stress versus representative strain rate curve in a log-log scale

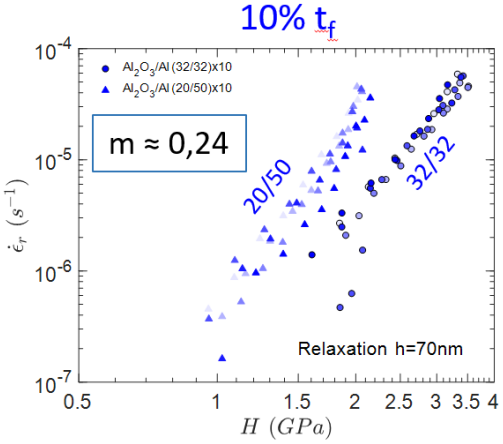

Figure 4.8: Representative strain rate as a function of the hardness (*Private communication - Paul Baral*)

Strain rate sensitivity coefficient	Results
At higher strain rate [-] (CSR method)	0.04
At lower strain rate [-] (Paul Baral's method)	0.24
LOC experiments [-]	0.01-0.03

Table 4.2: Strain rate sensitivity coefficients

4.3 Future research and improvements

First of all, lab on-chip tests are tests where sources of error can come from cross-section, mismatch and SEM measurements. To minimise them, a FIB cut would allow to have the true section.

In order to obtain larger strains without the sample fracture at the overlap, thinning the actuator at the overlap can be tested.

For both lab on-chip and tensile tests on polymer, DIC is a good tool to see the local deformation in the nanolaminate and better understand the deformation mechanism. Moreover, it allows to see if the deformation is homogeneous or heterogeneous.

Finally, a Stoney measurement is always interesting to know the internal stresses of the deposited material.

Conclusion

The objective of this thesis was to study the mechanical properties of nanolaminates such as alumina and aluminium.

Thin films are used in many fields such as electronics, MEMS or coatings to provide specific properties. And the importance of studying the mechanical behaviour of thin films lies in the fact that their properties can be different from bulk materials due to size effects. In recent years, UCLouvain has shown that nanolaminates composed of alumina with a thickness smaller than 100 nm and aluminium with a thickness between 10 nm and 20 nm exhibit remarkable properties such as strength, ductility and toughness. But this was only observed with the push-to-pull method and not with the lab on-chip. Thus, this thesis topic started.

First of all, nanoindentation tests allowed to determine the Young's modulus of the film of 145 GPa as well as its hardness of 7.5 GPa, but also a strain rate sensitivity coefficient of 0.24 for low strain rates and 0.04 for higher strain rates. Moreover, the nanoindentation tests deform the nanolaminate plastically without any cracks.

The lab on-chip tests gives a Young's modulus of between 100 GPa and 130 GPa and a strain rate sensitivity coefficient of between 0.01 and 0.03. These values are different from these obtained by nanoindentation, but it should be remembered that nanoindentation tests correspond more to an isostress configuration while LOC tests are rather in isostrain configuration and this can lead to different results. These LOC tests also show that a relaxation process occurs in these materials. Furthermore, a strain up to 3.4 % is reached, which has never been reached before in lab on-chip tests and after relaxation a strain up to 4.7 % is achieved. These levels of strain are obtained with the smallest specimen beams, which also corresponds to fewer defects. And the SEM observations show that the fracture seems to be brittle.

Finally, the tensile tests on polymer gave a Young's modulus of 145 GPa and a toughness of 3.2 J/m^2, corresponding to a brittle fracture; but this should be taken with caution. Also, the cracks from this test are sharp and propagate very fast.

For future work, DIC analysis can be carried out to better understand the deformation mechanisms, for lab on-chip as well as for tensile tests on polymer. Moreover, thinning the dogbone actuator would allow even larger strains to be obtained.

References

[1] A. Bagherpour et al. “Tailoring mechanical properties of a-C:H:Cr coatings”. In: (2022).
[2] A. Boé et al. “Internal stress relaxation based method for elastic stiffness characterization of very thin films”. In: (2009).
[3] B. Prorok et al. “Micro- and nanomechanics.” In: (2004).
[4] D. Kiener et al. “Fib damage of cu and possible consequences for miniaturized mechanical tests.” In: (2007).
[5] D. Read et al. “Tensile properties of free-standing aluminum thin films”. In: (2001).
[6] J. L. Loubet et al. “Nanoindentation with a surface force apparatus”. In: (1993).
[7] J. Wang et al. “Strength and plasticity of nanolaminated materials”. In: (2016).
[8] L. S. Schadler et al. “Experimental determination of the strain transfer across a flexible intermediate layer in thin-film structures.” In: (1992).
[9] M. Coulombier et al. “On-chip stress relaxation testing method for freestanding thin film materials”. In: (2012).
[10] M. Ghidelli et al. “Homogeneous flow and size dependent mechanical behavior in highly ductile $Zr_{65}Ni_{35}$ metallic glass films”. In: (2017).
[11] M.-S. Colla et al. “High strength-ductility of thin nanocrystalline palladium films with nanoscale twins: On-chip testing and grain aggregate model”. In: (2011).
[12] P. Baral et al. “Strong, ductile, ultra-tough thin Al/Al_2O_3 nanolaminates”. In: (2023).
[13] Paul Baral et al. “Indentation creep vs. indentation relaxation: A matter of strain rate definition?” In: (2020).
[14] Paul Baral et al. “Rheology of amorphous olivine thin films characterized by nanoindentation”. In: (2021).
[15] R. Huang et al. “Channel-cracking of thin films with the extended finite element method”. In: (2003).
[16] R. Vayrette et al. “On-chip fracture testing of freestanding nanoscale materials”. In: (2015).
[17] S. Jaddi et al. “Crack on a chip test method for thin freestanding films”. In: (2018).
[18] Sébastien Gravier et al. “New On-Chip Nanomechanical Testing Laboratory Applications to Aluminum and Polysilicon Thin Films”. In: (2009).
[19] T. Edward et al. “On the thinnest Al_2O_3 interlayers in Al-based nanolaminates to enhance strength, and the role of constraint”. In: (2022).
[20] T. Pardoen et al. “A versatile lab-on-chip test platform to characterize elementary deformation mechanisms and electromechanical couplings in nanoscopic objects”. In: (2015).
[21] T. Tsuchiya et al. “Tensile testing system for sub-micrometer thick films.” In: (2002).

[22] W. N. Sharpe et al. "A new technique for measuring the mechanical properties of thin films." In: (1997).
[23] W. Venstra et al. "Versatile wire configuration for independent actuation of bending and torsion displacements of microcantilevers." In: (2005).
[24] Solène Comby. "Développement et application d'un nanoindenteur in situ MEB couplé à des mesures électriques". In: (2018).
[25] Michael Coulombier. "Nanomechanical lab on-chip for testing thin film materials and application to Al and Al(Si)". In: (2012).
[26] MatWeb-Material property data. *Overview - Alumina, 98%*. https://www.matweb.com/search/DataSheet.aspx?MatGUID=38cd8590a98f457a8f4bea462fe91cfa. 2023.
[27] J. Hay and B. Crawford. "Measuring substrate-independent modulus of thin films". In: (2011).
[28] S. Jaddi. "Crack-on-chip: a nanomechanical test method to determine the fracture toughness of thin films and 2D materials". In: (2022).
[29] W. Oliver and G. Pharr. "An improved technique for determining hardness and elastic modulus using load and displacement sensing indentation experiments". In: (1992).
[30] Material Properties. *Aluminium – Strength – Hardness – Elasticity – Crystal Structure*. https://material-properties.org/aluminium-mechanical-properties-strength-hardness-crystal-structure/?utm_content=cmp-true. 2023.
[31] Astrid van der Rest et al. "Mechanical behavior of ultrathin sputter deposited porous amorphous Al2O3 films". In: (2016).
[32] Morgan Rusinowicz. "Mechanical and electrical properties of dielectric thin films: electrical-nanoindentation experiments and numerical simulations". In: (2022).
[33] Z. Suo. "Reliability of Interconnect Structures". In: (2002).
[34] J.J. Vlassak. "Channel cracking in thin films on substrates of finite thickness". In: (2003).

Appendices

A Correction of the contact depth

Starting from the raw data, the contact area is given by Eq. 4.1. Thanks to the calibration of the tip given by the software, it is possible to go back to the contract depth h_c and thus to the depth h by 2.6.

$$A_c = \pi * \left(\frac{S}{2E^*}\right)^2 \tag{4.1}$$

Here are the results obtained with this correction. For higher strain rates, the correction is minimal but for lower strain rates, it becomes more important. However, the studied strain rates are the highest because the lower ones do not stabilise well as a function of the penetration depth. The correction is therefore not necessary.

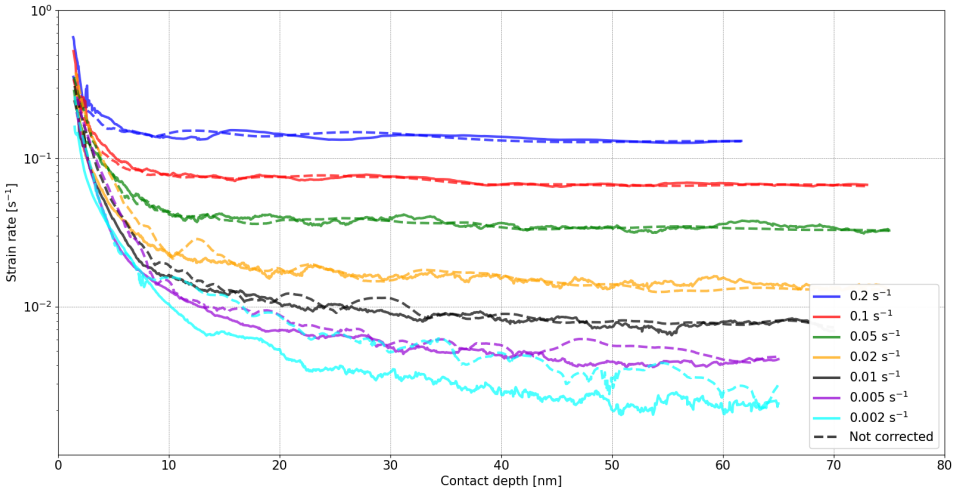

Figure 4.9: CSR test at different strain rates on Al_2O_3-Al 138-16 nm x5: Strain rate as a function of the contact depth

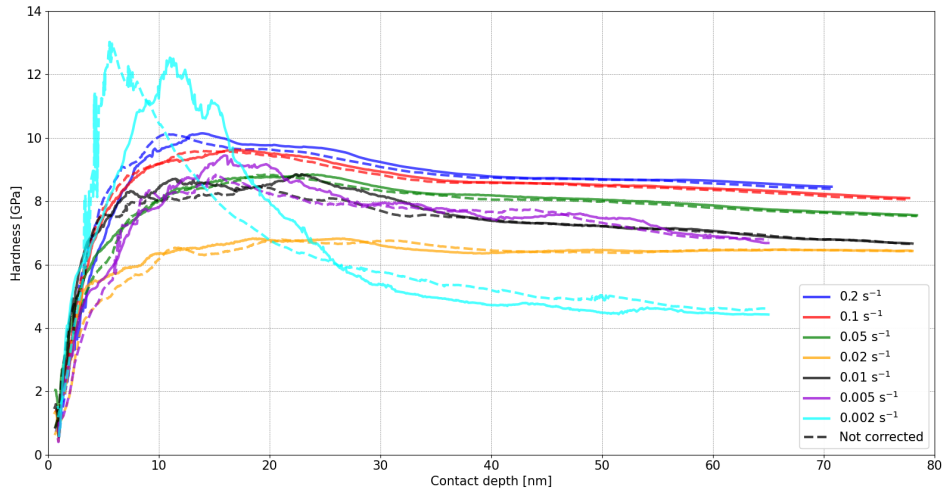

Figure 4.10: CSR test at different strain rates on Al_2O_3-Al 138-16 nm x5: Hardness as a function of the contact depth

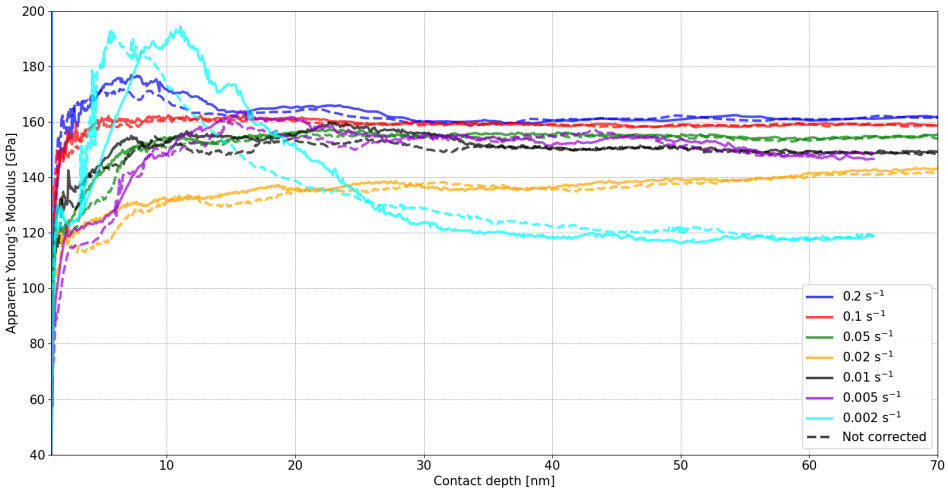

Figure 4.11: CSR test at different strain rates on Al_2O_3-Al 138-16 nm x5: Apparent Young's modulus as a function of the contact depth

B SEM : steps to follow to use the machine

- "Vent" on the machine
- Unscrew the support
- Stick the sample; screw the support
- "Store" on the machine
- "Exchange" on the keyboard
- Push cane, remove support, remove cane
- "Resume" on the keyboard
- Double click to position the sample in the center
- "Camera" on the keyboard
- Put the electron beam on
- Focus
- Take pictures
- Put the electron beam off
- "Exchange"
- "Resume"

C Standard cleaning and drying

Fill the pirhana baths (H_2SO_4 and H_2O_2) to the yellow bar, the reaction temperature is 110°C. Put sample in the first bath for 10 minutes then rinse with water for 10 minutes: rinse fill empty x5 and then add nitrogen for 5 minutes in the bath. Make the second bath and rinse again. To remove the oxide layer, HF bath for 15 seconds is necessary. Then 10 minutes in water. Then put the sample in the fountain with nitrogen. Then dry the sample with the dryer which rinses and dries.

D Aja Machine : Steps to follow to use the machine

Sample loading

- Check the vacuum level in the chamber (<5*10^{-7} Torr) (see green arrow on Fig. 4.12)

Figure 4.12: Vacuum level in the chamber (green arrow)

- Stop pumping the loadlock (blue arrow on Fig. 4.13) until 100 Hz and set "off" the loadlock pumping system (blue arrow on Fig. 4.14)

Figure 4.13: Venting/pumping button (blue arrow) and rotation buttons (green arrow)

Figure 4.14: Stopping the loadlock pumping system (blue arrow)

- Put the sample on the support upside down and put the support inside the loadlock

- Pump the loadlock by setting "on" the loadlock pumping system (blue arrow on Fig. 4.14 and by blue arrow on Fig. 4.13)
- When pressure in the loadlock is $< 10^{-5}$ Torr, open the valve between the loadlock and the chamber
- Put the chamber holder position to 30 mm (orange arrow on Fig. 4.15) and adjust the rotation of the holder manually

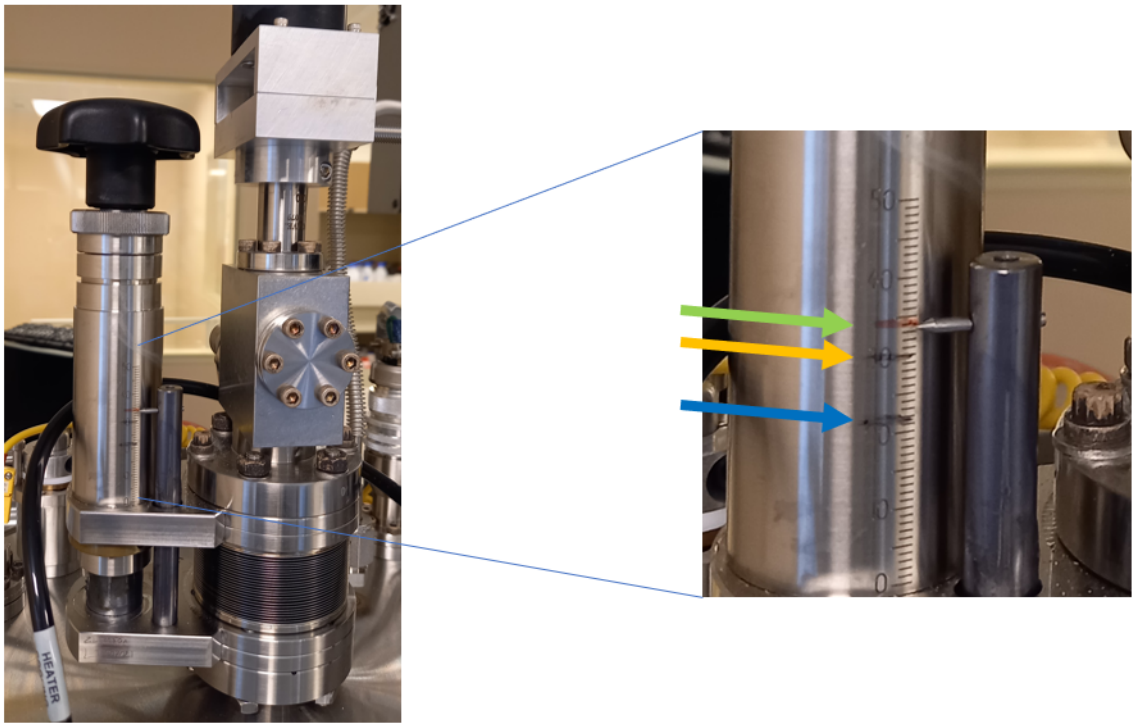

Figure 4.15: Levels of the chamber holder position

- Transfer the sample from the loadlock to the chamber slowly
- Set the chamber holder position to 21 mm (blue arrow on Fig. 4.15)
- Retract the transfer arm and close the transfer valve
- Set the chamber holder position to 34 mm (green arrow on Fig. 4.15)
- Start the sample rotation by the rotation button on Fig. 4.16 and the buttons shown by the green arrows on Fig. 4.13
- Close the window with the lamp

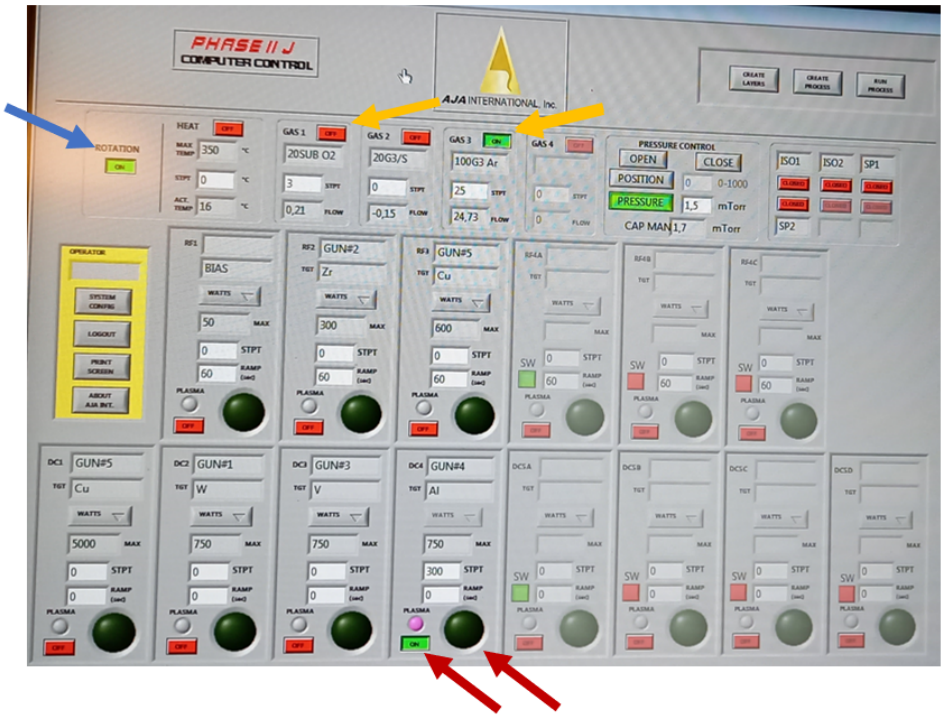

Figure 4.16: Interface to realise the deposition

Thin film deposition

- Set the gas flow values on the software : Ar 25 SCCM corresponding to Gas 3 colomn
- Start the Argon flow by setting "on" for the Gas 3 Ar (orange arrow on Fig. 4.16) on the software
- Set the pressure at 1.5 mTorr in the pressure control panel on the software
- Switch on the plasma source and set the plasma current to 300 mA (blue arrow on Fig. 4.17)

Figure 4.17: Interface to realise the deposition

- Start the plasma and wait 5 min to clean the sputtering target by setting "on" shown by the left red arrow on Fig. 4.16. (It gives a current of 712 mA and 430 V). If there is no current, one can go up to 10 mTorr in the pressure control panel.

Deposition of the NL alumina/aluminum

- Setting "3" SCCM for the Gas 1 O_2 shown by the left orange arrow and "on" and "22" SCMM for the Gas 3 Ar shown by the right orange arrow on Fig. 4.16
- Open the target shutter shown by the right red arrow on Fig. 4.16
- Stay 6 min for the deposition of alumina (11.3 nm/min for alumina and "we want" 68 nm)
- Close the target shutter, "off" the O_2 flow, set 25 SCCM for the Gas 3 Ar
- Wait 3 min for cleaning the target
- Open the target shutter for 1 min (7.7 nm/min for aluminum and "we want" 7.7 nm), then close it, set "3" for Gas 1 and "22" for Gas 3 and wait a few minutes to reach 3 SCCM
- Repeat this

Finishing the deposition

- Close the target shutter shown by the right red arrow on Fig. 4.16
- Stop the plasma power by setting "off" shown by the left red arrow on Fig. 4.16
- Open the APC (in the pressure control panel in the software)
- Stop the gas flows by setting "off" for the gas 1 and gas 3 shown by the orange arrows on Fig. 4.16
- Stop the sample rotation (green arrow on Fig. 4.13)
- Turn off the plasma power supply shown in Fig. 4.17

Unloading the sample

- Check that the vacuum in the loadlock and in the chamber are the same, open the valve
- Set the chamber holder position to 21 mm (blue arrow on Fig. 4.15) and adjust the rotation of the holder manually
- Move the transfer arm inside the chamber
- Set the chamber holder position to 30 mm (orange arrow on Fig. 4.15)
- Retract the transfer arm and close the valve
- Vent the loadlock by stopping the loadlock pumping system (first the blue arrow on Fig. 4.13 and then "off" on Fig. 4.14)
- Open the loadlock and take the sample
- Pump the loadlock by restarting the loadlock pumping system (first the "on" on Fig. 4.14 and then blue arrow on Fig. 4.13)

E XeF2 etching to release the structures

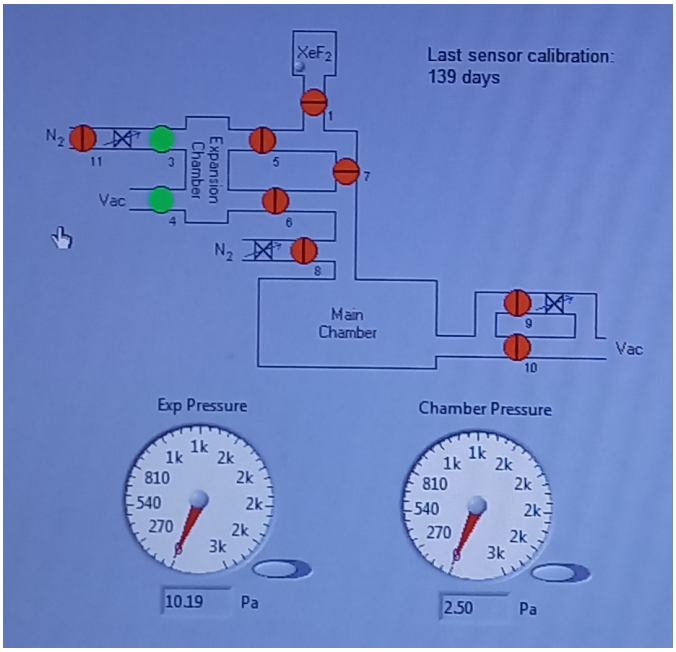

Figure 4.18: Xactix machine software

For the sake of readability, the letter "O" is used for "Open" and "C" for "Close".

Introduction of the sample into the machine

To put the sample in the chamber, it is necessary to make it wait for the atmospheric pressure (O8). Then, it is preferable not to place the sample just below a hole which is used for the arrival of XeF_2. Nitrogen purge (O8 to 4000 Pa -F8). Open the nitrogen valve behind the machine, then close it when the release is finished. Make the vacuum (O9-F9). Perform 3 nitrogen purges up to 4000 Pa (O8-F8 x3).

Release

First big pulse of XeF_2: pump (O10), open the XeF_2 valve and let 300 Pa pass (O1-O5-F5-F1). Then let the XeF_2 pass for about 10 seconds into the main chamber (O6-F6). When the etching starts, it becomes opaque on the screen because it looks rough when the Si is etched. It is now necessary to purge the chambers. Purge nitrogen (O8 up to 4000 Pa -F8 when 10 Pa is reached). Purge in the expansion chamber (O3-O4-O11 up to 5000 Pa - F11-F3-F4 when 5 Pa is reached).

Then, small pulses are performed while pumping (O10). Open the XeF_2 valve and let 150 Pa (O1-O5-F5-F1) pass into the expansion chamber and only 50 Pa into the main chamber (O6-F6). Purge nitrogen (O8 up to 4000 Pa -F8 when 10 Pa reached). Purge in the expansion chamber (O3-O4-O11 up to 5000 Pa - F11-F3-F4 when 5 Pa is reached). The new pulse can be carried out. To release a structure of Fig. 4.19, an average of 3 pulses is needed.

Remove the sample from the machine

3 nitrogen purges (O8 up to 4000 Pa -F8 when 10 Pa is reached) by pumping (O10). Then close the nitrogen valve behind the machine and purge again (O8) then stop pumping (F10) to return to atmospheric pressure 1 atm. Take out the sample, stop the extraction, pump again and evacuate the expansion chamber (O10-O4).

Thanks to the structures shown in Fig. 4.19, one can see when to stop the release in order not to etch too much or not enough. Indeed, if the structures with an 11 µm wide actuator must be released, one can check that the 12 µm wide structures are, as shown on the figure.

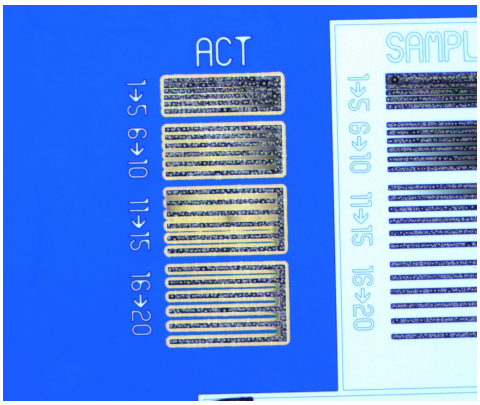

Figure 4.19: Actuator structures for the release

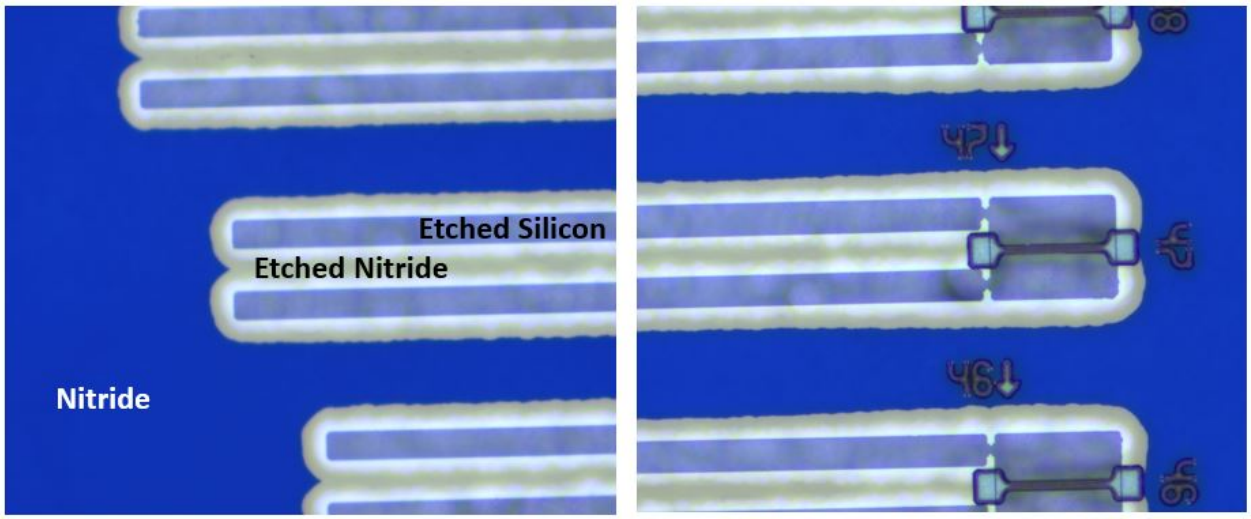

Figure 4.20: One structure after release

F Lab on-chip : Nanolaminates deposited by Sahar Jaddi

F.1 Lab on-chip : Sample 50-20 nm x3

Thickness of the nanolaminate and release

For this sample, the nanolaminate is already deposited and consists of 3 bilayers of 50-20 nm alumina and aluminium respectively. The release is carried out as indicated in the section 2.2.3. Table 4.3 gives the thicknesses of the silicon nitride and the nanolaminate.

Material	Thickness [nm]
Si_3N_4	83 (from 88)
Nanolaminate 2.5 µm Wide	130

Table 4.3: Thickness of the silicon nitride and the specimen beams

Observations and results

Fig. 4.21 shows that the rupture takes place at the overlap which can be a consequence of a non conform overlap as shown in Fig. 4.22. Fig. 4.23 gives a Young's modulus of 122 GPa.

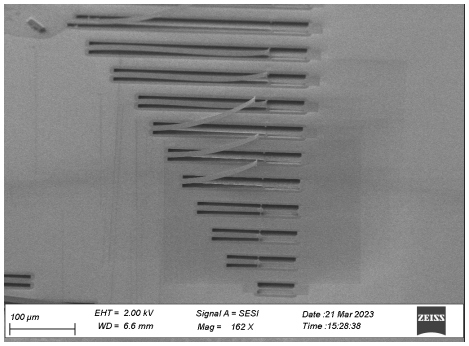

Figure 4.21: Broken at the overlap

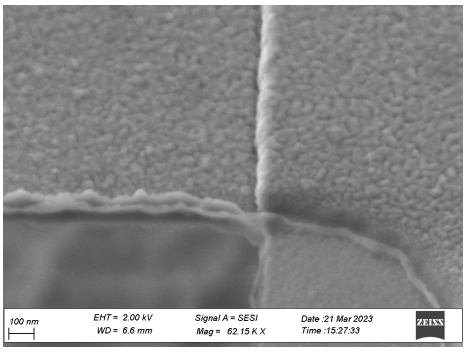

Figure 4.22: Overlap

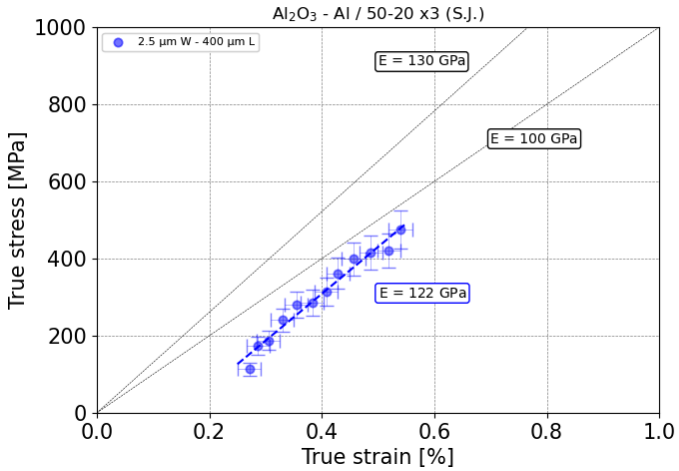

Figure 4.23: LOC test on Al_2O_3-Al 50-20 nm x3: True stress versus true strain curve

F.2 Lab on-chip : Sample 50-20 nm x5

Thickness of the nanolaminate and release

For this sample, the nanolaminate is already deposited and consists of 5 bilayers of 50-20 nm alumina and aluminium respectively. The release is carried out as indicated in the section 2.2.3. Table 4.4 gives the thicknesses of the silicon nitride and the nanolaminate.

Material	**Thickness [nm]**
Si_3N_4	93.5 (from 104)
Nanolaminate	274
Nanolaminate 2.5 µm Wide	250
Nanolaminate 1.5 µm Wide	225

Table 4.4: Thickness of the nitride and the specimen beams

Observations

This sample shows that the specimen beam appears to break in a brittle manner as shown in Fig. 4.24 and no structure breaks at the overlap.

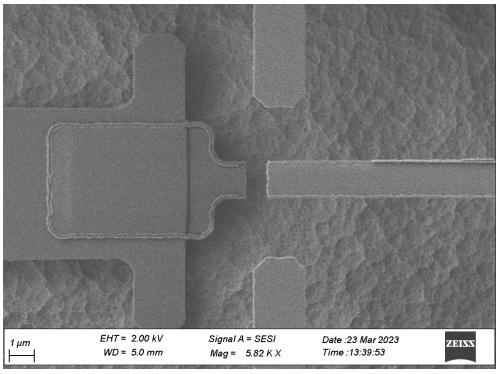

Figure 4.24: Broken specimen beam

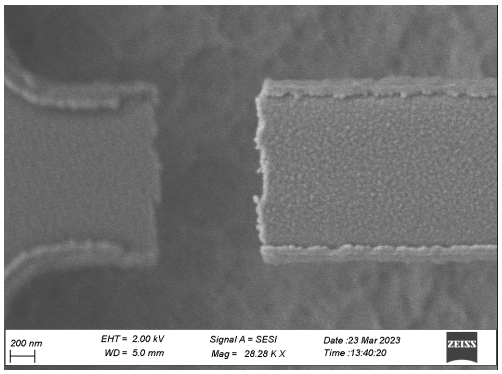

Figure 4.25: Zoom of the broken specimen beam

Results

Fig. 4.26 shows a maximum strain of 2.13 % and a Young's modulus of around 100 GPa considering that the 10 µm long structures are not precise enough.

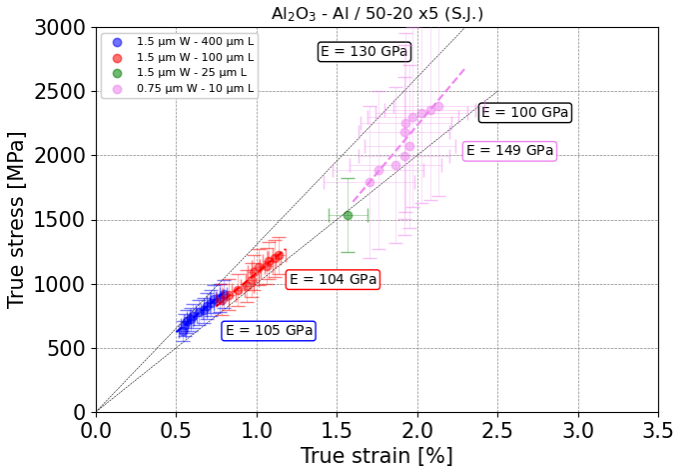

Figure 4.26: LOC test on Al_2O_3-Al 50-20 nm x5: True stress versus true strain curve

Regarding the relaxation, some of the most deformed structures are re-measured after 13 days, 19 days and 25 days as shown in Fig. 4.27 The sample relaxes well over time, so it is preferable to take SEM measurements just after release.

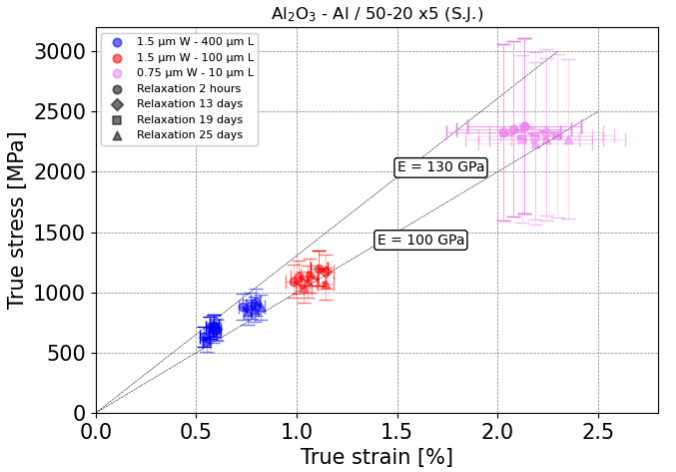

Figure 4.27: LOC test on Al_2O_3-Al 50-20 nm x5: True stress versus true strain curve - Relaxation 2 hours, 13 days, 19 days and 25 days

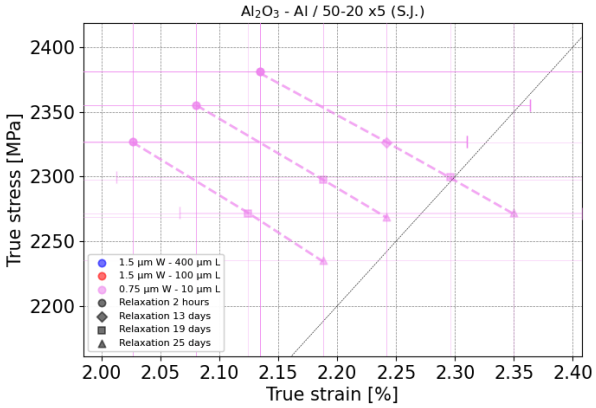

Figure 4.28: 0.75 µm W - 10 µm L structures

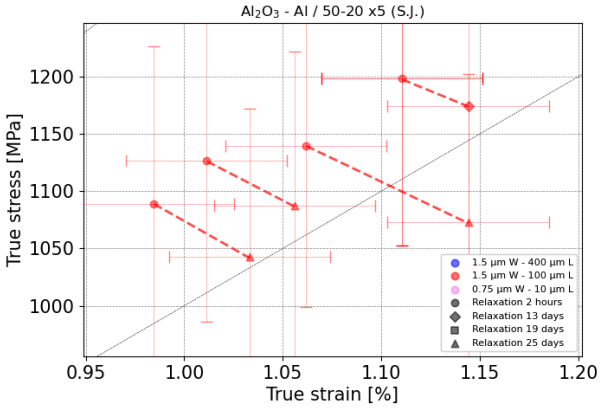

Figure 4.29: 1.5 µm W - 100 µm L structures

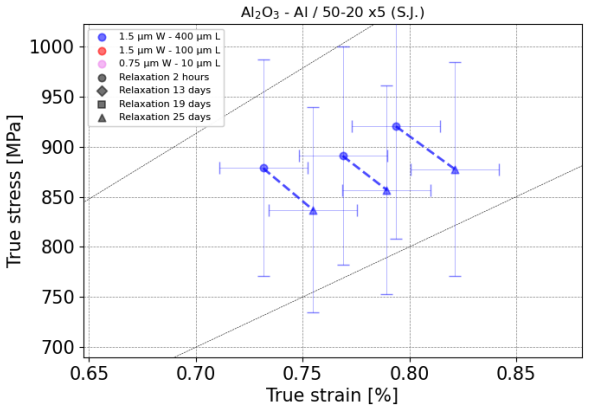

Figure 4.30: 1.5 µm W - 400 µm L structures

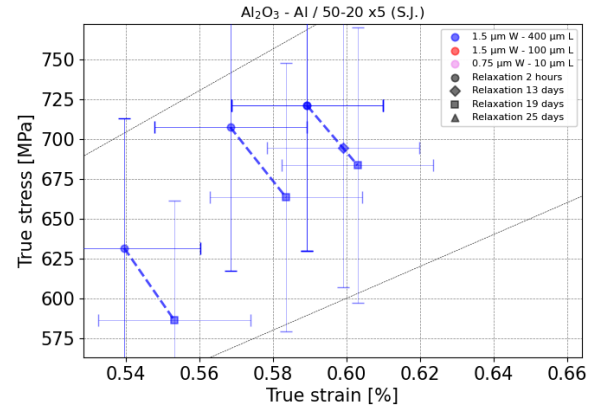

Figure 4.31: 1.5 µm W - 400 µm L structures

G Errors contribution

Here are the results for the three LOC samples with the errors on the SEM measurements represented by the error bars as well as that due to the error on the section represented by the coloured section.

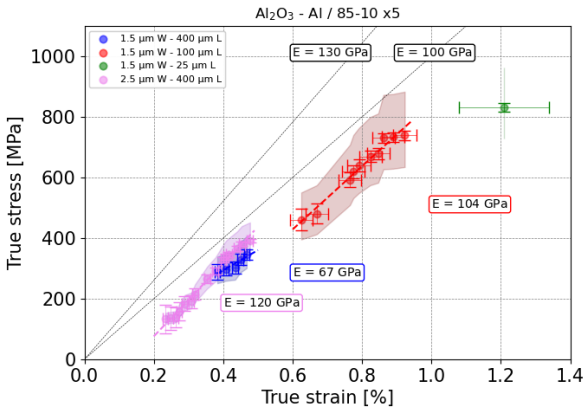

Figure 4.32: LOC test on Al_2O_3-Al 85-10 nm x5: True stress versus true strain curve

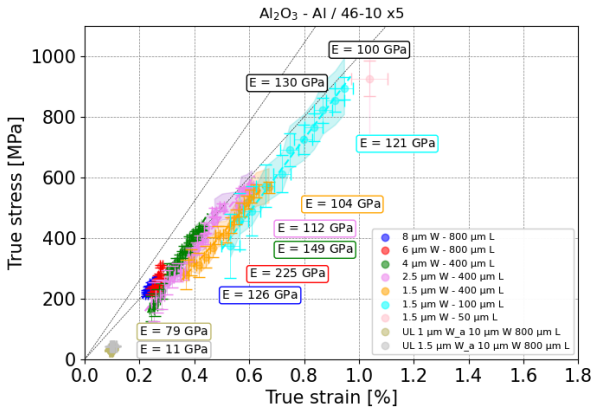

Figure 4.33: LOC test on Al_2O_3-Al 46-10 nm x5: True stress versus true strain curve

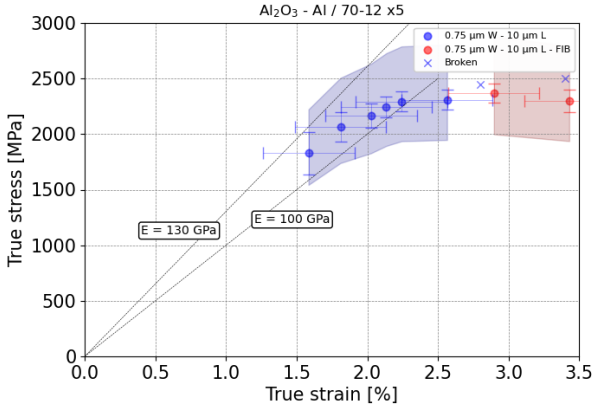

Figure 4.34: LOC test on Al_2O_3-Al 70-12 nm x5: True stress versus true strain curve

UNIVERSITÉ CATHOLIQUE DE LOUVAIN
École polytechnique de Louvain
Rue Archimède, 1 bte L6.11.01, 1348 Louvain-la-Neuve, Belgique | **www.uclouvain.be/epl**